Università degli Studi di Modena e Reggio Emilia

Dipartimento di Scienze Fisiche, Informatiche e Matematiche

Corso di Dottorato di Ricerca in "Physics and Nanosciences"

Tesi presentata per il conseguimento del titolo di Dottore di Ricerca in Fisica

---

Charged and nonlinear neutral excitations in low-dimensional and molecular systems by means of density-functional approaches

---

Candidato:
Alberto Guandalini

Relatori:
Prof. Alice Ruini
Dr. Stefano Pittalis

Coordinatore della Scuola di Dottorato:
Prof. Marco Affronte

XXXII ciclo

This work was made also under the supervision of Dr. Carlo A. Rozzi, who tutored Alberto Guandalini during his PhD. However, he is not appearing as co-tutor in the front page, as the internal regulation of the University of Modena and Reggio Emilia demands that only one co-tutor is formally mentioned therein.

Questo lavoro è stato prodotto anche sotto la guida del Dr. Carlo A. Rozzi, che, pur avendo co-tutorato Alberto Guandalini durante il suo dottorato, tuttavia, non puo' comparire come correlatore in quanto il regolamento dell'Università di Modena e Reggio Emilia impone che sia indicato un solo correlatore nel frontespizio.

Alberto Guandalini
Alice Ruini
Stefano Pittalis

Abstract

Electronic excitations play a prominent role in a large variety of physical properties of materials, e.g., quantum transport, heat transport, conductivity, and optical properties. Depending on the electric charge of the final state, charged and neutral excitations may be distinguished. In charged excitations, electrons are added or subtracted to the system. Direct or inverse photoemission experiments are a primary tool for the experimental observation of such processes. Instead, in neutral excitations, the total charge of the system is conserved during the excitation process. These can be probed through optical absorption measurements, both in the linear and nonlinear regimes.

Density functional theory (DFT) and its time-dependent extension (TDDFT) are often the theoretical framework of first choice in the first-principles description of excitation processes. However, it is well known that DFT and TDDFT show failures and limitations due to the functional approximations which are necessary in practice. Thus, the development of more accurate approximations and theoretical extensions is an interesting and intense field of research.

In this work, I develop new advances in the calculation of charged and neutral excitations. In the first part, it is shown that the fundamental gap of two-dimensional quantum dots can be accurately estimated at the effort of a standard ground-state calculation supplemented with a non-self-consistent step of negligible cost, all performed at the level of the local-density approximation. Yet, the procedure formally exploits the exchange discontinuity as expressed through the orbital-effective-potential method. In the second part, I derive an approximate potential that can capture non-vanishing exchange gaps both in finite and periodic two-dimensional systems. Although the procedure involves single-particle orbitals directly, the computational cost is comparable to standard DFT calculations. The potential approximation is applied to the artificial graphene, Kekulé distorted to open a gap at the Dirac points. In the third part of this work, nonlinear neutral excitations are investigated. In particular, I derive the optical cross section of a many-electron system subject to an *impulsive* electric field in the nonperturbative regime, i.e. for arbitrary values of the field strength, starting from the ground state. I show that the cross section includes absorptions from excited states for increasing intensities of the electric field – which are optical transitions that cannot be captured within the linear regime. As an example, I consider the case of a 1D two-electron model system. The analysis reveals that *gerade* excited states, which are dark in the linear regime, are populated in the nonlinear regime due to excited-state absorption. This analysis helps to interpret real-time TDDFT simulations which employ impulsive electric fields beyond the linear regime, as for studying processes in optical limiting phenomena.

The results obtained in this Ph.D. thesis contribute to the development of accurate and feasible methods to investigate electronic excitations in quantum systems, and, more generally, to the theory development of first-principles density-functional approaches.

Sommario

Le eccitazioni elettroniche assumono un ruolo di fondamentale importanza in diverse proprietà fisiche dei materiali, ad esempio nel trasporto quantistico, trasporto termico, conducibilità e proprietà ottiche. A seconda della carica elettrica dello stato finale, eccitazioni cariche e neutre possono essere distinte. Nelle eccitazioni cariche, gli elettroni vengono aggiunti o sottratti al sistema. Questi processi possono essere studiati tramite esperimenti di fotoemissione diretta o inversa. Invece, nelle eccitazioni neutre, la carica totale del sistema viene conservata durante il processo di eccitazione. Questo tipo di eccitazioni possono essere rilevate attraverso misure di assorbimento ottico, sia in regime lineare che non lineare.

La teoria del funzionale della densità (DFT) e la sua estensione dipendente dal tempo (TDDFT) sono spesso il primo quadro teorico di riferimento nella descrizione a primi principi dei processi di eccitazione. Tuttavia, è noto che la DFT e la TDDFT danno luogo ad errori e limiti di applicabilità a causa delle approssimazioni funzionali che devono essere necessariamente utilizzate in pratica. Pertanto, lo sviluppo di approssimazioni più accurate ed altre estensioni teoriche è un campo di ricerca interessante e attivo.

In questo lavoro, mi occupo dello sviluppo di nuovi metodi per il calcolo delle eccitazioni cariche e neutre. Nella prima parte, mostro come il gap fondamentale dei punti quantici bidimensionali può essere accuratamente stimato al costo computazionale di un calcolo di stato fondamentale, seguito da uno step non autoconsistente dal costo computazionale trascurabile, il tutto eseguito all'interno dell'approssimazione della densità locale. Nonostante ciò, la procedura include formalmente la discontinuità del potenziale di scambio espressa attraverso il metodo del potenziale effettivo orbitale. Nella seconda parte, ricavo un'approssimazione del potenziale che include esplicitamente un gap di scambio diverso da zero per sistemi bidimensionali sia finiti che periodici. Sebbene la forma funzionale utilizzata coinvolga direttamente gli orbitali a singola particella, il costo computazionale è paragonabile ai calcoli DFT standard. L'approssimazione del potenziale è applicata al grafene artificiale, in cui una distorsione di Kekulé è utilizzata per aprire un gap nei punti di Dirac. Nella terza parte di questo lavoro mi occupo di studiare le eccitazioni neutre non lineari. In particolare, derivo la sezione d'urto ottica per un sistema a più elettroni soggetto a un campo elettrico *impulsivo* nel regime non perturbativo, cioè per valori arbitrari dell'intensità del campo incidente, partendo dallo stato fondamentale. Successivamente mostro che la sezione d'urto include assorbimenti da stati eccitati all'aumentare dell'intensità del campo elettrico. Queste transizioni ottiche non sono possibili all'interno del regime lineare. Come esempio di applicazione, considero il caso di un sistema modello unidimensionale composto da due elettroni interagenti. L'analisi rivela che gli stati eccitati di tipo *gerade*, che non partecipano alle proprietà ottiche nel regime lineare, sono

popolati nel regime non lineare a causa dell'assorbimento da stato eccitato. Questa analisi aiuta a interpretare le simulazioni di TDDFT in tempo reale che impiegano campi elettrici impulsivi oltre il regime lineare, come per lo studio dei processi coinvolti nei fenomeni di limitazione ottica.

I risultati ottenuti in questa tesi di dottorato contribuiscono allo sviluppo di metodi accurati e praticabili per studiare le eccitazioni elettroniche nei sistemi quantistici e, in generale, allo sviluppo teorico nel campo degli approcci a principi primi basati sui funzionali della densità.

Contents

List of Figures

List of Tables

Chapter 1

Introduction

Most of the microscopic properties of materials have their origin in the electrons surrounding the nuclei. This is true for all kind of material, either solid, liquid or gas. In the last 60 years, the progress in the computation of electronic structures has brought an unprecedented level of power and efficiency to research. Quantum-mechanics ab-initio simulations are now able to make accurate quantitative predictions of the properties of (natural and man-made) materials and phenomena.

In principle, the electronic structure at equilibrium (at low temperature) is determined by the ground-state wavefunction, satisfying the time-independent Schrödinger equation. Similarly, dynamical electron properties are embedded in the time-dependent wavefunction, which is the solution of the time-dependent Schrödinger equation. Unfortunately, the exact calculation of the full many-body wavefunction (whether time dependent or independent) is not feasible except for few-electron systems and test models.

At present, several methods circumvent the calculation of the exact wavefunction and are able to give a quantitative (or at least qualitative) description of the electronic structure of matter. For example, explicit many-body methods [1], such as quantum Monte Carlo [2], many-body perturbation theory applied to Green's functions [3] and dynamical mean-field theory [4], can give very accurate results. However, in most cases explicit many-body methods are too expensive to be applied in real systems.

In this thesis, I am concerned with methodologies that can involve lower computational costs than the aforementioned ones. I will consider density functional theory (DFT) [5–9] in the Kohn-Sham (KS) formulation and its time-dependent extension (TDDFT) [10,11]. In particular, DFT allows the calculation of equilibrium geometries, potential energy surfaces, electron energy levels, and other ground-state properties. TDDFT is instead needed for the description of dynamical properties, such as quantum transport, chemical reactions and optical absorption.
Despite the remarkable results achived by DFT and TDDFT, some important failures and limitations have still to be fixed [12]. For this reason, the development of new functional approximations [13] or theory extensions [14] is still today an active and intense field of research. This is precisely the context of my thesis.

The excited-state properties of electrons play a fundamental role in a vast array of electrical, magnetic and optical properties of materials. Two types of excitations

may be distinguished. In charged excitations, an electron is added or removed from the system: assuming the initial state has N electrons, the final state has $N \pm 1$ electrons. In neutral excitations, the total number of electrons is conserved during the process.

A prototypical experimental setup to investigate charged excitations is photoemission spectroscopy (PES) [15], where photons are injected and absorbed by the system and the kinetic energy of the ejected electrons is measured. The minimum photon energy required to extract an electron (with zero kinetic energy) is called ionization potential $I = E_0(N-1) - E_0(N)$. The electron affinity instead measures the minimum energy gain if an electron is bound to the system $A = E_0(N) - E_0(N+1)$. This quantity can be measured through an inverse photoemission experiment (IPES) [16], where electrons are injected and absorbed by the system and the energy of the emitted photons is measured. The fundamental gap is defined as the difference between the ionization potential and electron affinity $E_{\text{gap}} = I - A$, and it plays an important role in a variety of applications. For example, in a transport measurement, E_{gap} is strictly related to the minimum voltage required to drive quantum transport. In the molecular case, E_{gap} can be experimentally determined via a combination of gas-phase ultraviolet photoelectron spectroscopy (UPS) [17] and electron attachment spectroscopy (EAS) [18]. In a quasiparticle picture, the ionization potential I is the minimum energy required to create a hole into the system, while the electron affinity A is the energy gain due to the creation of an electron. The fundamental gap thus represents the energy needed to create a non-interacting electron-hole pair.

Optical spectroscopy is perhaps the most widespread tool for studying neutral excitations. In this case, the system absorbs a photon (or more if the incoming field is intense) to create an electron-hole pair. The minimum energy required to create such pair is called optical gap $E_{\text{opt}} = E_1(N) - E_0(N)$, where $E_1(N)$ is the first optically-bright excited state. The optical gap derives its name from the fact that it corresponds to the energy onset of the optical absorption. The electrostatic electron-hole interaction is attractive, thus $E_{\text{opt}} \leq E_{\text{gap}}$ and $E_B = E_{\text{gap}} - E_{\text{opt}}$ is a measure of the electron-hole binding energy. In Fig. 1.1, a sketch summarizing the concepts described so far regarding electron excitations is shown.

Optical spectroscopies usually probe the optical properties in the linear-response regime. Under this assumption, spectroscopic observables can be linked to first-order response functions, e.g., the dielectric function $\epsilon(\omega)$. However, the recent improvement of laser sources, in terms of both quality and intensity, has pushed our ability to probe the optical response of matter to a higher level of sophistication. High-intensity ultrashort laser pulses (in the femtosecond/attosecond range) allow to reach coherent multi-photon absorption, i.e., to trigger highly nonlinear phenomena [19, 20]. But, how strong must be the laser electric field in order to trigger the nonlinear response? The natural scale of the field magnitude is the Coulomb electrostatic field between electrons and nuclei, that is in the order of $\mathcal{E}_0 \approx 5.14 \times 10^{11}$ V/m$=1$ atomic unit. Therefore, external perturbations with field magnitude close (or higher) to this value are considered strong enough to trigger the nonlinear response of the system. Nonlinear interactions between light and materials

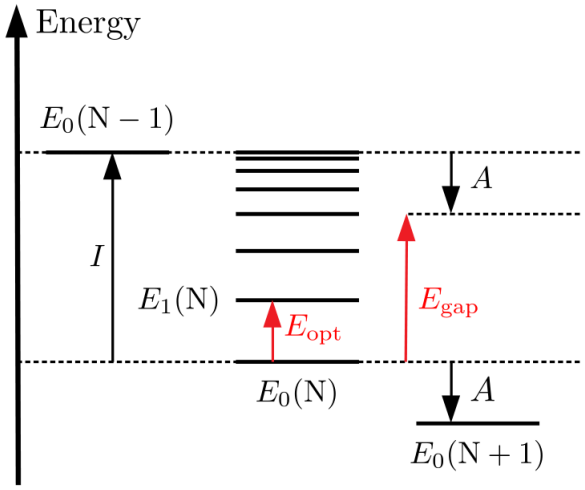

FIGURE 1.1: Sketch of gap energies related to excited-state properties of a quantum system. $E_0(N)$ indicates the ground-state energy of the N-electron system, while $E_1(N)$ is the first excited state accessible from an optical absorption measurement. Their energy difference denotes the optical gap E_{opt}. On the left side, the ground-state energy of the $N-1$ system is indicated with $E_0(N-1)$ (that is higher in energy with respect to the ground state of the N-electron system). The energy difference between the $E_0(N-1)$ and $E_0(N)$ is the ionization potential I. In the right side, at lower energies than $E_0(N)$, we have the ground-state energy of the $N+1$ system, $E_0(N+1)$. The energy difference between $E_0(N)$ and $E_0(N+1)$ is the electron affinity A. The difference between I and A is the fundamental gap E_{gap}, which is grater than E_{opt}. In fact, $E_{\mathrm{gap}} - E_{\mathrm{opt}}$ is a measure of the electron-hole binding energy, which is attractive.

give rise to a variety of optical phenomena. Among them, we may distinguish between second or high-order phenomena (linear or quadratic electro-optic effect, second or third harmonic generation, etc.) and purely nonperturbative phenomena (coherent ultrafast dynamics, high-order harmonic generation, multi-photon ionization, optical limiting, etc.) [21]. In order to complement the experimental studies, theoretical simulations are of fundamental importance. The development of theoretical frameworks and computational schemes able to reproduce accurately the previously described phenomena is still a matter of research [22].

The main goal of this work is to develop new methods for the calculation of both charged and neutral excited-state properties of quantum systems within the framework of DFT and TDDFT.

This thesis is organized as follows: in Chap. 2, I review the basics of DFT in the KS formalism. I then summarize some of the most common approximations of the exchange-correlation energy functional commonly employed in the literature. The basics of TDDFT are instead reviewed in Chap. 3, along with two other schemes for

the calculation of optical spectra and excited state properties.
Chaps. 4-6 report new advances and results completed within this thesis. In Chap. 4, I propose a new scheme to compute the fundamental gap of finite low-dimensional systems through the derivation of an explicit formula that approximates the exchange discontinuity of the KS potential, at the theory level of the local-density approximation. This method requires a computational effort similar to a simple self-consistent calculation. The proposed formalism is then applied in the calculation of the fundamental gap of a test case composed by two-dimensional harmonic quantum dots. In Chap. 5, I derive an exchange-correlation potential approximation suited for two-dimensional systems. Then, I show that the newly derived potential shows a non-vanishing exchange discontinuity both for finite and periodic two-dimensional systems, thus enabling the possibility to obtain the fundamental gap of periodic low-dimensional nanostructures in a reliable and efficient way. The proposed approximation is then applied to Kekulé-distorted artificial graphene, that shows a gap at the Dirac points. In Chap. 6, I show how to compute the non-perturbative response of a many-electron system subject to an impulsive high-intensity external field. Particular attention is given at the information included in the absorption cross section, that reveals important details about nonlinear neutral excitations. I apply the proposed scheme to a model 1D system composed by two interacting electrons trapped in a quantum well. General conclusions and possible outlooks are drawn in Chap. 7.

Unless explicitly stated otherwise, atomic units ($\hbar = m_e = e = 4\pi/\epsilon_0 = 1$) are used throughout this work.

Chapter 2

Density-functional theory

Density-functional theory (DFT) [5–9] is a reformulation of many-body quantum mechanics at equilibrium in which the electron density n_0 replaces the ground-state many-body wavefunction Ψ_0 as the basic variable. The advantage is clear: the ground-state density n_0 is easier to manage, as it depends on just three variables (the spatial coordinates), while Ψ_0 depends on $3N$ variables (three coordinates for each electron).
The first part of the Hohenberg-Kohn theorem demonstrates that the ground state density n_0 contains all information about the ground state of the system. The second part of the Hohenberg-Kohn theorem establishes a formal procedure to obtain n_0 through the minimization of the total energy functional $E[n]$. However, an exact expression of $E[n]$ that can be used in practice is not yet known, so we have to resort to approximations. DFT is often the method of choice for the calculation of electronic structures due to the Kohn-Sham (KS) formulation, which provides a way to make ground-state functional approximations that can be calculated in practice. Within the KS formulation, only the exchange-correlation part of the total energy, $E_{\text{xc}}[n]$, has to be approximated, while the other terms of the total energy have an explicit known expression in terms of the ground state density n_0 and the KS orbitals.
In this chapter, we review the basics of the KS formulation of DFT, and briefly discuss some of the approximations of $E_{\text{xc}}[n]$ employed in nowadays implementations.

2.1 The static many-body electron problem

In this section, we introduce the static electronic many-body problem, which is reformulated in the next sections.
We consider a system of N non-relativistic electrons interacting through the Coulomb repulsion and subject to an external local (multiplicative) potential $v(\mathbf{r})$. The Hamiltonian of such a system is

$$\hat{H} = \hat{T} + \hat{V} + \hat{W}, \tag{2.1}$$

where

$$\hat{T} = \sum_{i=1}^{N} -\frac{\nabla_i^2}{2} \tag{2.2}$$

is the kinetic energy operator,

$$\hat{V} = \sum_{i=1}^{N} v(\mathbf{r}_i) \tag{2.3}$$

is the external potential energy, and

$$\hat{W} = \frac{1}{2}\sum_{i,j\neq i}^{N} \frac{1}{|\mathbf{r}_i - \mathbf{r}_j|} \tag{2.4}$$

is the electron-electron interaction. $\mathbf{r}_i$ is the position vector of the i-th electron and ∇_i is the gradient operator with respect to $\mathbf{r}_i$.
The eigenstates of $\hat{H}$ are obtained from the solution of the time-independent Schrödinger equation

$$\hat{H}\Psi_k(\mathbf{x}_1, \mathbf{x}_2, \ldots, \mathbf{x}_N) = E_k\Psi_k(\mathbf{x}_1, \mathbf{x}_2, \ldots, \mathbf{x}_N), \tag{2.5}$$

where $\Psi_k(\mathbf{x}_1, \mathbf{x}_2, \ldots, \mathbf{x}_N)$ is the k-th eigenstate of $\hat{H}$ and E_k is the associated eigenvalue. We indicate with $\mathbf{x}_i \equiv (\mathbf{r}_i, \sigma_i)$ the spin-space coordinates of the i-th electron. We note that in Eq. (2.5) we have not included the nuclear degrees of freedom. The Born-Oppenheimer approximation is implicitly considered and the nuclei are treated as fixed point-like charges. The electron-nuclear interaction is included in the external potential $v(\mathbf{r})$. We suppose the system is in its ground state Ψ_0. The ground state wavefunction contains all the information about the system in equilibrium, as it allows the access to the expectation value of all physical observables. In fact, the expectation value of any physical observable $\hat{O}$ can be obtained from the bracket $O = \langle\Psi_0|\hat{O}|\Psi_0\rangle$. As an example, the ground state energy of the system is

$$E_0 = \langle\Psi_0|\hat{H}|\Psi_0\rangle\,. \tag{2.6}$$

However, as we pointed out in the introduction, the practical calculation of the exact Ψ_0 is an intractable numerical problem for all but a few exceptional cases. Over the years, many ingenious schemes have been devised to find approximate solutions of Eq. (2.5). Among these, we mention the Hartree-Fock method, configuration-interaction expansion, diagrammatic Green's function techniques, quantum Monte Carlo approaches, and, of course, density-functional theory.

2.1.1 The Hartree-Fock approximation

The Hartree-Fock approximation (HF) [23,24] is one of the cornerstones in electronic-structure theory. Here, we briefly review the key equations, that will be important to understand the exact-exchange approximation in Sec. 2.4.3.
The key of the HF approximation is that the many-body wavefunction is restricted to be an antisymmetrized uncorrelated product function that can be written as a single determinant which explicitly respects the exclusion principle,

$$\Phi_{\mathrm{HF}}(\mathbf{x}_1, \mathbf{x}_2, \ldots, \mathbf{x}_N) = \frac{1}{\sqrt{N!}}\begin{vmatrix} \varphi_1^{\mathrm{HF}}(\mathbf{x}_1) & \varphi_2^{\mathrm{HF}}(\mathbf{x}_1) & \ldots & \varphi_N^{\mathrm{HF}}(\mathbf{x}_1) \\ \varphi_1^{\mathrm{HF}}(\mathbf{x}_2) & \varphi_2^{\mathrm{HF}}(\mathbf{x}_2) & \ldots & \varphi_N^{\mathrm{HF}}(\mathbf{x}_2) \\ \vdots & \vdots & & \vdots \\ \varphi_1^{\mathrm{HF}}(\mathbf{x}_N) & \varphi_2^{\mathrm{HF}}(\mathbf{x}_N) & \ldots & \varphi_N^{\mathrm{HF}}(\mathbf{x}_N) \end{vmatrix}, \tag{2.7}$$

where $\{\varphi_i^{\mathrm{HF}}\}$ are the HF single-particle orbitals. This ansatz is plugged into Eq. (2.6) in order to obtain an approximation for the total energy of the system

$$E_{\mathrm{HF}} = \sum_{\sigma}\sum_{j=1}^{N_\sigma}\int d^3r\ \varphi_{j\sigma}^{\mathrm{HF}*}(\mathbf{r})\left(-\frac{\nabla^2}{2} + v(\mathbf{r})\right)\varphi_{j\sigma}^{\mathrm{HF}}(\mathbf{r}) + E_{\mathrm{H}} + E_{\mathrm{x}}, \tag{2.8}$$

where the first term in the right-hand side is the kinetic energy and the interaction with the external potential,

$$E_{\rm H} = \frac{1}{2}\int d^3r \int d^3r' \frac{n^{\rm HF}(\mathbf{r})n^{\rm HF}(\mathbf{r}')}{|\mathbf{r}-\mathbf{r}'|} \tag{2.9}$$

is the Hartree contribution of the total energy, and

$$E_{\rm x} = -\frac{1}{2}\sum_{\sigma}\sum_{i,j=1}^{N_\sigma}\int d^3r \int d^3r' \frac{\varphi_{i\sigma}^{\rm HF*}(\mathbf{r}')\varphi_{j\sigma}^{\rm HF}(\mathbf{r}')\varphi_{i\sigma}^{\rm HF}(\mathbf{r})\varphi_{j\sigma}^{\rm HF*}(\mathbf{r})}{|\mathbf{r}-\mathbf{r}'|} \tag{2.10}$$

is called Fock exchange energy. In Eq. (2.9), $n^{\rm HF}(\mathbf{r}) = \sum_\sigma \sum_{k=1}^{N_\sigma} |\varphi_{k\sigma}^{\rm HF}(\mathbf{r})|^2$ is the HF electron density.

The single-particle orbitals $\varphi_i^{\rm HF}$ are obtained by minimizing the total energy in Eq. (2.8) with respect to single-particle orbital variations, with the additional constraint that the square modulus of the single-particle orbitals is normalized to one

$$\frac{\delta}{\delta\varphi_{i\sigma}^{\rm HF*}(\mathbf{r})}\left\{E_{\rm HF} - \sum_\sigma\sum_{j=1}^{N_\sigma}\epsilon_{j\sigma}^{\rm HF}\int d^3r\ \varphi_{j\sigma}^{\rm HF*}(\mathbf{r})\varphi_{j\sigma}^{\rm HF}(\mathbf{r})\right\} = 0. \tag{2.11}$$

The Lagrangian multipliers are the orbital energies $\epsilon_{j\sigma}^{\rm HF}$. This procedure leads to the HF self-consistent equations

$$\left[-\frac{\nabla^2}{2} + v(\mathbf{r}) + v_{\rm H}(\mathbf{r})\right]\varphi_{i\sigma}^{\rm HF}(\mathbf{r}) - \sum_{j=1}^{N_\sigma}\int d^3r'\ \frac{\varphi_{j\sigma}^{\rm HF*}(\mathbf{r}')\varphi_{j\sigma}^{\rm HF}(\mathbf{r})}{|\mathbf{r}-\mathbf{r}'|}\varphi_{i\sigma}^{\rm HF}(\mathbf{r}') = \epsilon_{i\sigma}^{\rm HF}\varphi_{i\sigma}^{\rm HF}(\mathbf{r}), \tag{2.12}$$

where

$$v_{\rm H}(\mathbf{r}) = \int d^3r' \frac{n^{\rm HF}(\mathbf{r}')}{|\mathbf{r}-\mathbf{r}'|} \tag{2.13}$$

is the Hartree potential.

There are many similarities between the HF approximation and DFT in the KS formalism. They both rely on a single-particle framework, where the interaction between electrons is approximated by a self-consistent single-particle potential. However, there are also important differences. The self-consistent potential in HF theory [see Eq. (2.12)] is nonlocal, thus it is an operator acting on the orbital $\varphi_{i\sigma}^{\rm HF}$ in such a way that the result of its action at position $\mathbf{r}$ involves an integration of $\varphi_{i\sigma}^{\rm HF}$ over all $\mathbf{r}'$. As we will see in the following, the KS exchange-correlation potential is instead local, in the sense that its action on $\varphi_{j\sigma}^{\rm KS}$ is a simple multiplication at each $\mathbf{r}$. This feature makes the KS approach more attractive, as multiplicative potentials may be easier to manage.

It is worth noting that the Hartree-Fock total energy differ from the exact ground-state energy

$$E_0 = E_{\rm HF} + E_c'. \tag{2.14}$$

The missing piece, E_c', is called correlation energy. Since the HF method is variational, we know $E_c' < 0$. The correlation energy can be viewed as the relaxation energy due to the fact that the interacting many-body wavefunction is not restricted to be a single Slater determinant.

2.2 The Hohenberg-Kohn theorem

The proof that the ground state density n_0 contains all the information about the many-body system was provided by Hohenberg and Kohn in 1964 [25]. Here, we only enunciate the theorem and discuss the consequences.
We consider N interacting electrons described by the many-body Hamiltonian given by Eq. (2.1). For simplicity, we suppose that the ground state is non-degenerate as in the original formulation of Hohenberg and Kohn. The extension to degenerate ground states can be found, for example, in Ref. [5].
The time-independent Schrödinger equation [see Eq. (2.5)] formally defines a map by which each external potential v produces a ground-state wavefunction Ψ_0, and consequently a ground-state density n_0. This can be summarized by the following scheme:

$$v \xrightarrow{\hat{H}\Psi_0 = E_0\Psi_0} \Psi_0 \xrightarrow{\langle\Psi_0|\hat{n}|\Psi_0\rangle} n_0. \tag{2.15}$$

We may say that the ground state density n_0 is a functional of the external potential v, thus we may write $n_0 = n_0[v]$. The first part of the Hohenberg-Kohn theorem reverts the map (2.15), thus demonstrating that there is a one-to-one correspondence between the external potential v and the ground-state density n_0.

Hohenberg-Kohn theorem I. For a system of N interacting particles in an external potential v, the potential v is uniquely determined, except by a constant, by the ground state density n_0. In other words, the external potential is a unique functional of the ground state density, $v[n_0]$, up to an arbitrary additive constant.

For the demonstration, we refer to the original paper [25]. We note that the external potential v completely defines the quantum system, since $\hat{T}$ and $\hat{W}$ are the same for each N-electron system. Thus, also the Hamiltonian $\hat{H}$ is a functional of the ground state density $\hat{H} = \hat{H}[n_0]$. This means that also the ground state wavefunction is a functional of the density $\Psi_0 = \Psi_0[n_0]$ through the solution of the time-independent Schrödinger equation. Finally, we arrive at the conclusion that each ground state observable is a functional of the density as

$$O = \langle\Psi|\hat{O}|\Psi\rangle = \langle\Psi[n_0]|\hat{O}|\Psi[n_0]\rangle = O[n_0], \tag{2.16}$$

where O is a generic physical observable and $\hat{O}$ the correspondent quantum-mechanical operator. However, obtaining the exact $O[n_0]$ can be as difficult as solving the original problem.

The second part of the Hohenberg-Kohn theorem describes how to obtain the ground-state density n_0 encompassing the time-independent Schrödinger equation through a reformulation of the Ritz variational principle.

Hohenberg-Kohn theorem II. A universal functional for the energy $E_v[n]$ in terms of the density n can be defined, valid for any external potential v. For any particular v, the exact ground-state energy of the system is the global minimum value of this functional, and the density n that minimizes the functional is the exact ground-state density n_0.

The proof can be made through the construction of the total energy functional $E_v[n]$, defined as

$$\begin{aligned} E_v[n] &= \langle \Psi[n] | \hat{T} + \hat{V} + \hat{W} | \Psi[n] \rangle \\ &= F[n] + \int d^3r n(\mathbf{r}) v(\mathbf{r}). \end{aligned} \tag{2.17}$$

The functional $F[n]$, defined by Eq. (2.17), includes the kinetic and interaction energy terms

$$F[n] = \langle \Psi[n] | \hat{T} + \hat{W} | \Psi[n] \rangle = T[n] + W[n], \tag{2.18}$$

and it is a universal functional of the density, i.e., it does not depend explicitly on v. As a consequence of the Rayleigh-Ritz principle [26, 27], $E_v[n]$ has the following variational property

$$\begin{aligned} E_v[n] &> E_0 \quad \text{for} \quad n(\mathbf{r}) \neq n_0(\mathbf{r}), \\ E_v[n] &= E_0 \quad \text{for} \quad n(\mathbf{r}) = n_0(\mathbf{r}), \end{aligned} \tag{2.19}$$

where n_0 is the ground-state density belonging to v. The ground-state density may thus be found from the differentiation of $E_v[n]$, with the additional constrain that the density integrates to N electrons. We may thus write

$$\frac{\delta}{\delta n(\mathbf{r})} \left[E_v[n] - \mu \int d^3r' n(\mathbf{r}') \right] = 0. \tag{2.20}$$

where the Lagrange multiplier μ is the chemical potential. From Eq. (2.20), we arrive at the Euler equation

$$\frac{\delta F[n]}{\delta n(\mathbf{r})} + v(\mathbf{r}) = \mu. \tag{2.21}$$

Formally, solving Eq. (2.21) encompasses the need to deal with the many-body wavefunction and the time-independent Schrödinger equation.

$E_v[n']$ in Eq. (2.17) is formally defined only for those densities $n'(\mathbf{r})$ which are ground-state of a system with some external potential $v'(\mathbf{r})$. Such densities are called "v-representable". It is not easy to understand if a given n is v-representable, and there are examples in the literature of "reasonable densities" which are not [28]. This problem has been overcome by Levy [29] and Lieb [30] with the constrained search formulation, in which the minimization procedure is performed in two steps. In the first step, the minimum-energy search is restricted only for the class of many-body wavefunctions Ψ that have the same density n. Thus, the energy functional now assumes the form

$$E'_v[n] = \min_{\Psi \to n(\mathbf{r})} \langle \Psi | \hat{T} + \hat{W} | \Psi \rangle + \int d^3r n(\mathbf{r}) v(\mathbf{r}). \tag{2.22}$$

The kinetic energy and electron-electron interaction compose the following universal functional

$$F'[n] = \min_{\Psi \to n(\mathbf{r})} \langle \Psi | \hat{T} + \hat{W} | \Psi \rangle . \tag{2.23}$$

In the second step, the functional $E'_v[n]$ is minimized with respect to n to get the ground state energy

$$E_0 = \min_n E'_v[n]. \tag{2.24}$$

Note that now n and Ψ need not to be the density and eigenstate of any potential. Thus, the more difficult v-representability problem is replace by the N-representability problem, easier to manage [31].

Unfortunately, both the universal functionals $F[n]$ and $F'[n]$ are unknown, and much work has been carried out over the years to understand their properties and suitable approximations. In the next section, we show how to express the universal functional through the KS formalism.

2.3 The Kohn-Sham equations

The expression of the universal functional $F[n]$ given by the Hohenberg-Kohn theorem, or alternatively by the Levy-Lieb constrained search, is purely formal. In practice, $F[n]$ needs to be approximated. The success of DFT is due to the energy-functional reformulation made by Kohn and Sham [32]. The main idea is to extract from $F[n]$ the physically known contributions, and approximate the remainder. In particular, the total-energy functional $E_v[n]$ is rearranged as

$$E_{\rm KS}[n] = T_s[n] + \int d^3r\ v(\mathbf{r})n(\mathbf{r}) + E_{\rm H}[n] + E_{\rm xc}[n], \tag{2.25}$$

where T_s is the independent-particle kinetic energy (see below), $E_{\rm H}$ is the Hartree energy [see Eq. (2.9)], and

$$E_{\rm xc}[n] = (T[n] - T_s[n]) + (W[n] - E_{\rm H}[n]) \tag{2.26}$$

is the exchange-correlation (xc) energy. The xc energy is expressed as the difference between the exact and non-intercting kinetic energies, $T[n]$ and $T_s[n]$, plus the difference between the exact interaction energy $W[n]$ and the Hartree classical energy $E_{\rm H}[n]$.

The quantities in Eq. (2.25) are calculated by introducing the auxiliary KS system. This is defined as an independent-particle N-electron system, subject to an effective single-particle potential v_s, that shares the same ground-state density n_0 as the interacting one. If we suppose for a moment that v_s exists and is known, the KS single-particle orbitals $\{\varphi_j\}$ are solutions of the single-particle Schrödinger equation

$$\left(-\frac{\nabla^2}{2} + v_s(\mathbf{r})\right)\varphi_j(\mathbf{r}) = \epsilon_j\varphi_j(\mathbf{r}), \tag{2.27}$$

where ϵ_j are the single-particle KS energies.
The interacting ground-state density n_0 can be obtained from the KS orbitals as

$$n_0(\mathbf{r}) = \sum_{j=1}^{N} |\varphi_j(\mathbf{r})|^2, \tag{2.28}$$

as n_0 is also the ground state density of the KS system. In addition, the non-interacting kinetic energy also can be obtained from the KS orbitals as follows

$$T_s[n] = -\frac{1}{2}\sum_{j=1}^{N}\int d^3r\varphi_j^*(\mathbf{r})\nabla^2\varphi_j(\mathbf{r}). \tag{2.29}$$

Let us now find an expression for the effective potential v_s. The Hohenberg-Kohn theorem is valid also for the KS system, for which $F_s[n] \equiv T_s[n]$. Thus, the KS Euler equation reads as follows

$$\frac{\delta T_s[n]}{\delta n(\mathbf{r})} + v_s(\mathbf{r}) = \mu_s. \tag{2.30}$$

The Euler equation of the interacting system [see Eq. (2.21)], with the KS decomposition of the energy functional given by Eq. (2.25), can be written as

$$\frac{\delta T_s[n]}{\delta n(\mathbf{r})} + v(\mathbf{r}) + \int d^3r'\frac{n(\mathbf{r}')}{|\mathbf{r}-\mathbf{r}'|} + \frac{\delta E_{\rm xc}[n]}{\delta n(\mathbf{r})} = \mu. \tag{2.31}$$

As the KS potential v_s is defined up to a constant, we set without restrictions $\mu_s = \mu$. Thus, by comparing Eq. (2.30) with Eq. (2.31), we find

$$v_s(\mathbf{r}) = v(\mathbf{r}) + \int d^3r'\frac{n(\mathbf{r}')}{|\mathbf{r}-\mathbf{r}'|} + v_{\rm xc}(\mathbf{r}) \tag{2.32}$$

where the xc potential is defined as

$$v_{\rm xc}(\mathbf{r}) = \frac{\delta E_{\rm xc}[n]}{\delta n(\mathbf{r})}. \tag{2.33}$$

The xc potential $v_{\rm xc}(\mathbf{r})$ is the functional derivative of the exchange-correlation energy with respect to the density. Thus, it is a functional of the density itself, $v_{\rm xc} = v_{\rm xc}[n]$. Eqs. (2.27)-(2.28) and (2.32)-(2.33) are called KS equations. They must be solved self-consistently, as the effective potential v_s is a functional of the density n, which in turn depends on the KS orbitals. In practice, $E_{\rm xc}[n]$ cannot be computed through Eq. (2.26), as $T[n]$ and $W[n]$ are unknown. Thus, we must resort to approximate functionals. It is worth noting that $E_{\rm xc}[n]$ is the only quantity that must be approximated in the KS formalism. Ultimately, it is the accuracy of the xc functional which determines the accuracy of the results.

Finally, let us briefly discuss the existence conditions of the KS system. Whether or not a density n can be reproduced as the ground-state density of a non-interacting system is called *non interacting v-representability problem* [8,9]. Although it has been demonstrated the existence and unicity of the KS system under certain restrictions [33–35], it is important to point out that, for the most general case [30], the existence of the KS system is not yet demonstrated.

2.3.1 Spin-dependent extension

It is possible to introduce a spin-unrestricted version of the KS approach. Here, we just show the key equations. We consider a system of $N = N_\uparrow + N_\downarrow$ electrons. The

total ground-state density is now the sum of spin-up and spin-down densities

$$n_0(\mathbf{r}) = n_{0\uparrow} + n_{0\downarrow} = \sum_{\sigma=\uparrow,\downarrow} \sum_{j=1}^{N_\sigma} |\varphi_{j\sigma}(\mathbf{r})|^2, \tag{2.34}$$

where $\{\varphi_{j\sigma}(\mathbf{r})\}$ are the spin-dependent KS orbitals.
The Schrödinger-like equation of the KS system now assumes the form

$$\left[-\frac{\nabla^2}{2} + v_{s\sigma}[n_\uparrow, n_\downarrow](\mathbf{r})\right] \varphi_{j\sigma}(\mathbf{r}) = \epsilon_{j\sigma}\varphi_{j\sigma}(\mathbf{r}). \tag{2.35}$$

The KS effective potential may be decomposed as

$$v_{s\sigma}[n_\uparrow, n_\downarrow](\mathbf{r}) = v_\sigma(\mathbf{r}) + \int d^3r' \frac{n(\mathbf{r}')}{|\mathbf{r} - \mathbf{r}'|} + v_{\mathrm{xc}\sigma}[n_\uparrow, n_\downarrow](\mathbf{r}), \tag{2.36}$$

where $v_{\mathrm{xc}\sigma}[n_\uparrow, n_\downarrow]$ is a spin dependent potential, defined as

$$v_{\mathrm{xc}\sigma}[n_\uparrow, n_\downarrow](\mathbf{r}) = \frac{\delta E_{\mathrm{xc}}[n_\uparrow, n_\downarrow]}{\delta n_\sigma(\mathbf{r})}. \tag{2.37}$$

The spin-resolved KS formalism (2.34)-(2.37) is more general than the spin-independent version, since it includes the possibility to have spin-dependent external potentials $v_\sigma(\mathbf{r})$. When the external potential is spin-independent and the number of electrons for each spin is equal ($N_\uparrow = N_\downarrow$), the two formalisms are equivalent. The functional dependence of the spin-dependent xc functional $E_{\mathrm{xc}}[n_\uparrow, n_\downarrow]$ provides more flexibility, which may be useful for the construction of approximations. It is essential for computing (collinear) spin magnetization.

2.4 Density-functional approximations

The expression of the xc functional $E_{\mathrm{xc}}[n]$ in Eq. (2.26) is just a formal one, as $T[n]$ and $W[n]$ are unknown. Thus, in applications, we must resort to approximations. The reason why DFT is so successful lies in the fact that very simple approximations of E_{xc} can give remarkably accurate results. In this section, we briefly summarize some common approximations that are widely used in the literature.

2.4.1 The local density approximation (LDA)

The local density approximation (LDA) was introduced in the original work of Kohn and Sham [32]. The LDA is based on the uniform electron gas, where the effects of exchange and correlation are local in character. It reads as follows :

$$E_{\mathrm{xc}}^{\mathrm{LDA}}[n] = \int d^3r\ n(\mathbf{r})\epsilon_{\mathrm{xc}}^{\mathrm{LDA}}[n](\mathbf{r}), \tag{2.38}$$

where $\epsilon_{\mathrm{xc}}^{\mathrm{LDA}}[n] \equiv \epsilon_{\mathrm{xc}}^{\mathrm{UEG}}(n)$ is the xc energy density of the uniform electron gas (UEG) with density n. The LDA exchange-energy density can be expressed analytically as

$$\epsilon_{\mathrm{x}}^{\mathrm{LDA}}[n](\mathbf{r}) = -C_{\mathrm{x}} n^{1/3}(\mathbf{r}), \tag{2.39}$$

where $C_{\rm x} \approx 0.7386$. The correlation-energy density $\epsilon_c^{\rm LDA}[n]$ has been instead parameterized from accurate Monte Carlo calculations [36].
By construction, LDA is exact for the uniform electron gas, and accurate for slowly-varying densities such as crystalline simple metals. Surprisingly, it turns out that LDA is quite good also for inhomogeneous systems, such as atoms and molecules. The main reason is that LDA satisfies many correct features of the true xc energy functional. However, at the same time there are well known failures of the LDA. For example, the LDA potential shows a wrong long range behavior for $r \to +\infty$ with respect to the true KS potential in molecular systems. Some of the LDA drawbacks are solved by the use of the generalized gradient approximations, which will be described in the next section.

2.4.2 Generalized gradient appriximations (GGAs)

Generalized gradient approximations (GGAs) try to improve LDA by introducing a correction in the expression of the xc-energy density which depends on the first derivative of the electron density $|\nabla n|$. Such a correction, called enhancement factor $F_{\rm xc}^{\rm GGA}[n, \nabla n]$, is introduced in the expression of the xc energy in the following way

$$E_a^{\rm GGA}[n] = \int d^3r n(\mathbf{r}) \epsilon_a^{LDA}[n](\mathbf{r}) F_a^{\rm GGA}[n, \nabla n](\mathbf{r}) \ , \tag{2.40}$$

where $a = {\rm x}, {\rm c}, {\rm xc}$, depending on the energy type considered in the approximation.
Several forms of F_a have been proposed in the literature, each of them defining a different GGA functional [5,37]. Among them, the most widely used were introduced by Becke (B88) [38], Perdew and Wang (PW91) [39], and Perdew, Burke and Enzerhof (PBE) [40]. For each GGA, the enhancement factor is chosen in such a way that most of the exact properties satisfied by LDA are still valid, while other exact conditions (e.g. high density limit, long range tail etc.) are added.
GGAs have become popular in quantum chemistry due to the higher accuracy with respect to LDA at a comparable computational cost.
In order to give an example of a GGA functional, we consider the B88, that is an exchange functional approximation. Following the original paper [38], the spin-dependent form of the enhancement factor is defined as

$$F_{\rm x}^{\rm B88}[x_\sigma](\mathbf{r}) = 1 - \frac{\beta}{C_{\rm x}} \frac{x_\sigma^2(\mathbf{r})}{1 + 6\beta x_\sigma(\mathbf{r}) \sinh^{-1}[x_\sigma(\mathbf{r})]}, \tag{2.41}$$

where

$$x_\sigma = \frac{|\nabla n_\sigma(\mathbf{r})|}{n_\sigma^{4/3}(\mathbf{r})} \ . \tag{2.42}$$

This expression ensures the following exact conditions:

- it provides the exact uniform coordinate scaling $E_{\rm x}^{\rm B88}[n(\gamma\mathbf{r})] = \gamma E_{\rm x}^{\rm B88}[n(\mathbf{r})]$;
- it gives the proper long-range behavior of the x energy density for finite systems:

$$\epsilon_{\rm x}^{\rm B88}[n](\mathbf{r}) \xrightarrow[|\mathbf{r}|\to\infty]{} -\frac{1}{2r} \ ; \tag{2.43}$$

- it reproduces correctly both low and high gradient limits.

The parameter β has been determined by a least-squares fit to exact atomic Hartree-Fock data. In particular, Becke considered 6 noble gas atoms, from helium through radon. We remind that this energy functional is an important part of the B3LYP hybrid functional [41–43]. Finally, it is worth noting that LDA/GGA functionals show the self-interaction error, and they give a vanishing derivative discontinuity with respect to the change in particle number [9]. In order to resolve these problems, we may consider functionals which depend explicitly on the KS orbitals, thus that are implicit functionals of the electron density.

2.4.3 The exact-exchange approximation (EXX)

In the KS approach, the independent-particle kinetic energy $T_s[n]$ is an explicit functional of the KS orbitals $\{\varphi_i\}$, and it depends only implicitly on the electron density n. This is not problematic, since the KS orbitals can be viewed as density functionals $\varphi_i = \varphi_i[n]$ as shown by the Hohenberg-Kohn theorem: the density n uniquely determines the KS potential v_s, which then allows an unambiguous calculation of the KS orbitals $\{\varphi_i\}$ through the KS equations.
Following the same reasoning, it is possible to construct xc functionals which are explicitly dependent on the KS orbitals: $E_{\rm xc}[n] = E_{\rm xc}\{\varphi_i[n]\}$. In this section we consider one of such orbital functional approximation, the exact exchange approximation (EXX), in which $E_{\rm x}[n]$ is given by the Fock expression

$$E_{\rm x}[n] \equiv -\frac{1}{2}\sum_{i=1}^{N}\sum_{j=1}^{N}\int d^3r' \int d^3r'' \frac{\varphi_i^*(\mathbf{r}')\varphi_j^*(\mathbf{r}'')\varphi_j(\mathbf{r}')\varphi_i(\mathbf{r}'')}{|\mathbf{r}'-\mathbf{r}''|} \,, \tag{2.44}$$

and $E_c = 0$. It is worth noting that the EXX approximation is self-interaction free, as the self-interaction energy contained in the Hartree energy $E_H[n]$ [see Eq. (2.9)] is exactly canceled by the terms $i = j$ in Eq. (2.44). As we already pointed out, the self-interaction error is one of the drawbacks of the LDA and GGAs. Although HF theory and EXX share the same expression for the total energy, the two methods are different. In Eq. (2.44), the KS orbitals are used, which are the solution of the KS equations [see Eq. (2.27)], that are defined in terms of a local (multiplicative) potential. Instead, the HF orbitals are obtained from the solution of the HF equations [see Eq. (2.12)], in which a nonlocal potential is employed. Thus, the correlation energy as defined in DFT

$$E_c[n] \equiv E_{\rm xc}[n] - E_{\rm x}[n] \tag{2.45}$$

differs from the correlation energy $E_c'[n]$ which is defined in HF theory [see Eq. (2.14)].

Due to the implicit dependence with respect to the density in $E_{\rm x}[n]$, the calculation of $v_{\rm x}[n]$ is not straightforward. The corresponding potential can be derived within the optimized-effective-potential (OEP) equation [44–46], which is an integro-differential equation. A simple way to derive the OEP equation is to use the chain rule of

functional derivatives, as follows

$$v_{\rm x}^{\rm EXX}[n](\mathbf{r}) = \frac{\delta E_{\rm x}[n]}{\delta n(\mathbf{r})} = \int d^3r' \frac{\delta v_s[n](\mathbf{r}')}{\delta n(\mathbf{r})} \times \sum_k \int d^3r'' \left[\frac{\delta \varphi_k^*[v_s](\mathbf{r}'')}{\delta v_s(\mathbf{r}')} \frac{\delta E_{\rm x}[\varphi_i]}{\delta \varphi_k^*(\mathbf{r}'')} + c.c. \right] . \quad (2.46)$$

In Eq. (2.46), we used the fact that the KS orbitals $\{\varphi_i\}$ are functionals of the KS potential: $\{\varphi_i\} = \{\varphi_i[v_s]\}$. This is true since the solution of the KS equations is unique within the hypothesis of the Hohenberg-Kohn theorem. After some manipulations, Eq. (2.46) can be expressed in a more explicit way as

$$v_{\rm x}^{\rm EXX}(\mathbf{r}) = \frac{1}{2n(\mathbf{r})} \sum_{j=1}^{N} \left\{ |\varphi_j(\mathbf{r})|^2 \left[u_{{\rm x}j}(\mathbf{r}) + (\bar{v}_{{\rm x}j} - \bar{u}_{{\rm x}j}) \right] - \nabla \cdot \left[\psi_{{\rm x}j}^*(\mathbf{r}) \nabla \varphi_j(\mathbf{r}) \right] \right\} + c.c. . \quad (2.47)$$

In Eq. (2.47),

$$u_{{\rm x}j}(\mathbf{r}) = \frac{\delta E_{\rm x}[\varphi_i^*]}{\delta \varphi_j(\mathbf{r})} = -\sum_{k=1}^{N} \frac{\varphi_k^*(\mathbf{r})}{\varphi_j^*(\mathbf{r})} \int d^3r' \frac{\varphi_j^*(\mathbf{r}')\varphi_k(\mathbf{r})}{|\mathbf{r} - \mathbf{r}'|} \quad (2.48)$$

are the orbital-dependent potentials in the HF theory, and $\{\psi_{{\rm x}j}\}$ are the so-called orbital shifts, defined as

$$-\psi_{{\rm x}j}^*(\mathbf{r}) = \sum_{\substack{i=0 \\ i \neq j}}^{+\infty} \int d^3r' \varphi_j^*(\mathbf{r}) \frac{\varphi_i^*(\mathbf{r}')[u_{{\rm x}i}(\mathbf{r}') - v_{\rm x}(\mathbf{r}')]\varphi_i(\mathbf{r}')}{\epsilon_i - \epsilon_j} . \quad (2.49)$$

For the full derivation of Eq. (2.47), we refer to the original papers [44–46].
The OEP equation can be solved iteratively and simultaneously with the KS equations, in a self-consistent fashion. The full solution is non-trivial due to the virtual-orbital dependence of the orbital shifts.

In most cases the OEP equation is simplified by the Krieger-Li-Iafrate approximation (KLI) [47], in which the last term of Eq. (2.47) is neglected.
We note that the exchange potential in KLI approximation may be expressed as the sum of two terms

$$v_{\rm x}^{\rm KLI}(\mathbf{r}) = v_{\rm x}^{\rm resp/KLI}[n](\mathbf{r}) + v_{\rm x}^{\rm Slater}[n](\mathbf{r}) , \quad (2.50)$$

where $v_{\rm x}^{\rm Slater}$ is the exchange potential in the Slater approximation

$$v_{\rm x}^{\rm Slater}[n](\mathbf{r}) = \sum_{j}^{N} u_{{\rm x}j}(\mathbf{r}) \frac{|\varphi_j(\mathbf{r})|^2}{n(\mathbf{r})}, \quad (2.51)$$

and

$$v_{\rm x}^{\rm resp/KLI}(\mathbf{r}) = \sum_{i=1}^{N} w_i \frac{|\varphi_i(\mathbf{r})|^2}{n(\mathbf{r})}, \quad (2.52)$$

with

$$w_i = \int d^2r [v_{\rm x}^{\rm KLI}(\mathbf{r}) - u_{{\rm x}i}(\mathbf{r})] |\varphi_i(\mathbf{r})|^2 . \quad (2.53)$$

The Slater potential shows a smooth attractive form, with long-range behavior $v_{\mathrm{x}}^{Slater} \to -1/r$ as $r \to \infty$. The response potential is instead always repulsive and shows a shell-like structure for finite systems. Eq. 2.50 is defined up to a constant, fixed by setting the potential equal to zero at infinity with the additional condition $w_N = 0$.
The KLI approximation (Eqs. 2.50-2.53) transforms the OEP integral equation (Eq. 2.47) into an algebraic equation which is easier to solve in practical applications. The KLI approximation gives accurate results (very similar to the full OEP approach) for finite systems like atoms and small molecules [9, Chap. 2].

2.4.4 The GLLB potential approximation

Although the KLI equation is more affordable than the full OEP equation, the evaluation of the HF potentials $\{u_{\mathrm{x}i}\}$ makes the KLI equation more cumbersome than local and semi-local exchange approaches.
Computational cost, for example, can be reduced by considering an approximation, which was introduced by Gritsenko *et al.* (GLLB) directly for the x potential [48]. The idea at the base is to reproduce some basic features of the KLI without direct the evaluation of $\{u_{\mathrm{x}i}\}$.
GLLB keep the same form of the KLI response-potential, given by Eq. (2.52), but with different w_i coefficients

$$w_i^{\mathrm{GLLB}} = K_{\mathrm{x}}\sqrt{\mu - \epsilon_i}\ , \tag{2.54}$$

where μ is the chemical potential and ϵ_i are the KS eigenvalues. Due to this choice, the GLLB response potential preserves the short-ranged behavior and linear scaling under homogeneous scaling of the coordinates. $K_{\mathrm{x}} = 8\sqrt{2}/3\pi^2$ is a numerical constant determined by imposing the GLLB potential to be exact in the case of the uniform electron gas.
The Slater part is instead approximated by that of the B88 functional [38] (see Sec. 2.4.2)

$$v_{\mathrm{x}}^{\mathrm{Slater}}(\mathbf{r}) \approx v_{\mathrm{x}}^{\mathrm{Slater/B88}}(\mathbf{r}) = 2\epsilon_{\mathrm{x}}^{\mathrm{B88}}[n](\mathbf{r})\ , \tag{2.55}$$

where $\epsilon_{\mathrm{x}}^{\mathrm{B88}}$ is the exchange energy per particle. Among all possible local potentials, GLLB suggest to use the B88 because $v_{\mathrm{x}}^{\mathrm{Slater/B88}}$ has the correct asymptotic behavior $-1/r$ for $r \to \infty$. GLLB focused their construction on molecular systems, for which the long-range tail of the potential is known to be very important.

2.5 Ensemble density-functional theory and the derivative discontinuity

In this section, we briefly review the basics of Ensemble density-functional theory (EDFT) [49–51], which is an extension of DFT to treat ensembles of states with different particle numbers. Due to the ensemble mixing, the ground-state density may now integrate to non-integer electron numbers

$$\int d^3r\ n_M(\mathbf{r}) = M, \tag{2.56}$$

where $M = N + \omega$, with $N \in \mathbb{N}$ and $\omega \in [0, 1]$. To the end of the calculation of the fundamental gap, it is useful to consider an ensemble with two states for which

$$n_M(\mathbf{r}) = (1 - \omega)n_N(\mathbf{r}) + \omega n_{N+1}(\mathbf{r}), \tag{2.57}$$

where n_N and n_{N+1} are the ground-state densities of the N and $N+1$ particle systems, respectively. The ensemble energy is given by

$$E(M) = (1 - \omega)E(N) + \omega E(N + 1). \tag{2.58}$$

Eq. (2.58) shows the piecewise-linear behavior of $E(M)$ at fractional particle numbers [49]. We note $E(M)$ is a continuous function. Instead, the chemical potential, $\mu = \partial E(M)/\partial M$, is discontinuous at integer electron numbers. By using Eq. (2.58), the chemical potential is

$$\mu(M) = \frac{\partial E(M)}{\partial M} = \frac{\partial E(N + \omega)}{\partial \omega} = E(N + 1) - E(N). \tag{2.59}$$

In particular, we have

$$\mu(M) = \begin{cases} -I(N): & N - 1 < M < N \\ -A(N): & N < M < N + 1, \end{cases} \tag{2.60}$$

where $I(N) = E(N - 1) - E(N)$ is the first ionization potential and $A(N) = E(N) - E(N + 1)$ is the electron affinity of the N electron system.

The fundamental gap is defined as the difference between the first ionization energy $I(N)$ and the electron affinity $A(N)$

$$E_{\text{gap}}(N) = I(N) - A(N), \tag{2.61}$$

and it is the jump made by the chemical potential at N [see Eq. (2.60)]

$$E_{\text{gap}}(N) = \lim_{\omega \to 0} \left\{ \mu(M)|_{N+\omega} - \mu(M)|_{N-\omega} \right\}. \tag{2.62}$$

Using the Euler equation given by Eq. (2.21), the fundamental gap may be expressed as

$$E_{\text{gap}}(N) = \lim_{\omega \to 0} \left\{ \left. \frac{\delta E[n]}{\delta n(\mathbf{r})} \right|_{N+\omega} - \left. \frac{\delta E[n]}{\delta n(\mathbf{r})} \right|_{N-\omega} \right\}, \tag{2.63}$$

where the external single-particle potential is fixed to its given expression. Eq. (2.63) shows that the derivative discontinuity of the total-energy functional is identical to the fundamental gap. Thus, once computed the limit $\omega \to 0$, only N-particle quantities are required in principle to calculate the fundamental gap. A direct use of Eq. (2.61) would instead require the explicit knowledge of the ground-state energies of the systems with $N - 1$, N and $N + 1$ electrons. We will discuss this important point in more detail in Chap. 4.

Practical calculations with DFT usually employ the KS decomposition of the total energy functional, given by Eq. (2.25). The external energy and Hartree energy [see Eq. (2.9)] do not contribute to the derivative discontinuity in the right hand side

of Eq. (2.63), as they are explicit functionals of the electron density. Instead, the non-interacting kinetic energy T_s and the xc energy $E_{\rm xc}$ are discontinuous. Thus,

$$E_{\rm gap}(N) = \lim_{\omega\to 0}\left\{\left.\frac{\delta T_s[n]}{\delta n(\mathbf{r})}\right|_{N+\omega} - \left.\frac{\delta T_s[n]}{\delta n(\mathbf{r})}\right|_{N-\omega}\right\} + \lim_{\omega\to 0}\left\{\left.\frac{\delta E_{\rm xc}[n]}{\delta n(\mathbf{r})}\right|_{N+\omega} - \left.\frac{\delta E_{\rm xc}[n]}{\delta n(\mathbf{r})}\right|_{N-\omega}\right\} . \quad (2.64)$$

The first term on the right hand side of Eq. (2.64) is the KS gap

$$\Delta_{\rm KS}(N) = \lim_{\omega\to 0}\left\{\left.\frac{\delta T_s[n]}{\delta n(\mathbf{r})}\right|_{N+\omega} - \left.\frac{\delta T_s[n]}{\delta n(\mathbf{r})}\right|_{N-\omega}\right\} , \quad (2.65)$$

while the second term may be expressed as

$$\Delta_{\rm xc}(N) = \lim_{\omega\to 0}\left\{ v_{\rm xc}[n]|_{N+\omega} - v_{\rm xc}[n]|_{N-\omega}\right\} . \quad (2.66)$$

Therefore $\Delta_{\rm xc}$ is due to the contribution of the discontinuity of the xc potential at integer particle number. It is often refereed to as the contribution of the xc discontinuity to the fundamental gap. The use of EDFT is useful for the development of practical methods to obtain the fundamental gap at low computational cost, as discussed in Chap. 4.

We conclude this section with some remarks about modern approaches to EDFT. When we use the KS decomposition of the total energy, given by Eq. (2.25), in Eq. (2.63), we implicitly extended the domain of definition of the energy functional to fractional particle numbers in the following way

$$E[n_N] \to E[n_M], \quad (2.67)$$

where $N \in \mathbb{N}$ and $M \in \mathbb{R}$. As a consequence, the LDA and GGAs xc functionals have a vanishing derivative discontinuity, as they are explicit functional of the electron density and its gradients.
Kraisler et al. [52] proposed instead to use the following form of the Hartree and xc energy functional for fractional particle numbers:

$$E_{\rm Hxc}[n_M] = (1-\omega)E_{\rm Hxc}[n_N] + \omega E_{\rm Hxc}[n_{N+1}]. \quad (2.68)$$

This expression is obtained working consistently with expectation values of the energies and thus introducing state-dependent xc-contributions for the state in the ensemble. Within this approach, the LDA and GGAs functionals have a non-vanishing derivative discontinuity for finite systems. However, for periodic systems, LDA and GGAs functionals show a vanishing derivative discontinuity also in this case [52].
For a report on relevant and peculiar exact properties of the $E_{\rm Hx}$ functional defined through this latter approach, we refer to the recent work [73].

Chapter 3

Time-dependent density-functional theory

Time-dependent density-functional theory (TDDFT) [10,11] is an extension of static density-functional theory (DFT) to the time domain. In fact, TDDFT is a reformulation of time-dependent quantum mechanics, in which the time-dependent density $n(\mathbf{r},t)$ replaces the time-dependent many-body wavefunction $\Psi(\mathbf{x}_1,\mathbf{x}_2,\ldots,\mathbf{x}_N,t)$ as the basic variable.
There are many similarities between DFT and TDDFT, as we will point out during this chapter. However, there are other important differences. In ground state DFT, the Rayleigh-Ritz variational principle plays a dominant role in the second part of the Hohenberg-Kohn theorem (see Sec. 2.2). In addition, it provides a way to calculate the xc potential as the functional derivative of the xc energy $v^0_{\text{xc}}(\mathbf{r}) = \delta E_{\text{xc}}/\delta n(\mathbf{r})$. The extension of Rayleigh-Ritz variational principle to the time domain is not straightforward due to the initial-state dependence of the time-dependent wavefunction.

In this chapter we discuss the fundamentals of TDDFT. First, we introduce the many-body time-dependent electron problem. Then, we enunciate the Runge-Gross theorem, which is the time-dependent counterpart of the Hohenberg-Kohn theorem. Under restrictive assumptions, the van Leeuwen theorem ensures the unicity and existence of the time-dependent KS, that is shown in Sec. 3.4. As in the static case, the time-dependent xc potential is unknown, so we must resort to approximations. Here, we briefly review the adiabatic approximation, that is used in almost all practical cases. The adiabatic approximation allows the machinery of DFT approximations to be used in TDDFT. One of the main application of TDDFT is the calculation of optical spectra and excitation energies. In Sec. 3.6, we discuss two methods suitable for this purpose: the real-time propagation scheme, formulated in time domain, and the Casida equation, formulated in the frequency domain. The two methods are not always equivalents and we briefly describes the differences between the two methods in the last section.

3.1 The time-dependent many-body electron problem

In this section we introduce the time-dependent (TD) electronic many-body problem, which is reformulated in the following sections.

We consider a system of N non-relativistic electrons interacting through the Coulomb repulsion and subject to an external TD scalar potential $v(\mathbf{r}, t)$. This can be, for example, a time-dependent electric field. The Hamiltonian of such a system is

$$\hat{H}(t) = \hat{T} + \hat{V}(t) + \hat{W}, \tag{3.1}$$

where

$$\hat{T} = \sum_{j=1}^{N} -\frac{\nabla_j^2}{2} \tag{3.2}$$

is the kinetic energy operator,

$$\hat{V}(t) = \sum_{j=1}^{N} v(\mathbf{r}_j, t) \tag{3.3}$$

is the time-dependent external potential operator and

$$\hat{W} = \frac{1}{2} \sum_{i,j \neq i}^{N} \frac{1}{|\mathbf{r}_i - \mathbf{r}_j|} \tag{3.4}$$

is the electron-electron interaction. All the information about system dynamics is encoded in the TD wavefunction $\Psi(\mathbf{x}_1, \mathbf{x}_2, \ldots, \mathbf{x}_N, t)$, satisfying the TD Schrödinger equation

$$i\frac{\partial}{\partial t}\Psi(\mathbf{x}_1, \mathbf{x}_2, \ldots, \mathbf{x}_N, t) = \hat{H}(t)\Psi(\mathbf{x}_1, \mathbf{x}_2, \ldots, \mathbf{x}_N, t), \tag{3.5}$$

with initial condition $\Psi(t_0)$. In many cases of practical interest, the TD external potential is split into two parts

$$v(\mathbf{r}, t) = v_0(\mathbf{r}) + v_1(\mathbf{r}, t)\theta(t - t_0), \tag{3.6}$$

where v_0 is time-independent and v_1 is the interaction of the system with an external perturbation switched on at $t = t_0$. In this case, the system is usually supposed to be in the ground state of $\hat{H}_0$ for $t < t_0$, where $\hat{H}_0 = \hat{H}(t < t_0)$.
The nuclear degrees of freedom are not explicitly included in Eq. (3.1), as in the static many-body electron problem (see Sec. 2.1), since we consider the nuclei fixed at certain positions and their interaction with the electrons is included in v_0. It is worth noting that we are neglecting possible interactions with an external TD vector potential $\mathbf{A}(\mathbf{r}, t)$. Thus, the interaction with electromagnetic waves or TD magnetic fields is not included in this formalism.
Alternatively to Eq. (3.5), the TD many-body problem may be expressed in terms of the time-evolution operator as

$$\Psi(t) = \hat{U}(t, t_0)\Psi(t_0). \tag{3.7}$$

The time evolution operator $\hat{U}(t, t_0)$ acts on the initial state $\Psi(t_0)$ and yields the propagated wavefunction $\Psi(t)$ at time $t > t_0$. An important property of $\hat{U}(t, t_0)$ is the composition property

$$\hat{U}(t_2, t_0) = \hat{U}(t_2, t_1)\hat{U}(t_1, t_0), \quad t_2 \geq t_1 \geq t_0, \tag{3.8}$$

that allows to split the propagation from t_0 to t_2 into two steps: first from t_0 to t_1, then from t_1 to t_2. Another important property of $\hat{U}(t,t_0)$ is unitarity

$$\hat{U}^\dagger(t,t_0)\hat{U}(t,t_0) = 1, \quad \text{or} \quad \hat{U}^\dagger(t,t_0) = \hat{U}^{-1}(t,t_0), \tag{3.9}$$

where $\hat{U}^\dagger$ is the Hermitian conjugate of $\hat{U}$. Eq. (3.9) ensures that the norm of the TD wavefunction is conserved at each time.
In the case of a time-independent Hamiltonian $\hat{H}(t) \equiv \hat{H}_0$, the evolution operator is simply expressed as

$$\hat{U}(t,t_0) = e^{-i\hat{H}_0(t-t_0)}, \tag{3.10}$$

where we remind the exponential of an operator is defined through its Taylor expansion. For the general case, the time-evolution operator can be formally expressed as

$$\hat{U}(t,t_0) = \hat{\mathcal{T}} \exp\left[-i\int_{t_0}^{t} dt'\ \hat{H}(t')\right], \tag{3.11}$$

where $\hat{\mathcal{T}}$ is a time-ordering operator.
Time evolution written in terms of such operators is useful in the derivation of numerical methods for propagating the wavefunctions.

3.2 The Runge-Gross theorem

The fundamental existence theorem of TDDFT was formulated by Runge and Gross in 1984 [53]. Here, the theorem is enunciated and discussed. For the demonstration, we refer to TDDFT textbooks [10, 11].
We consider a system of N electrons described by the Hamiltonian in Eq. (3.1). We note the external potential $v(\mathbf{r},t)$ completely defines the Hamiltonian operator. We denote by $\Psi(t_0)$ the initial state of the system. By solving the TD Schrödinger equation, we have access to the TD wavefunction $\Psi(t)$ from which is possible to obtain the TD density $n(\mathbf{r},t) = \langle\Psi(t)|\hat{n}|\Psi(t)\rangle$. At fixed initial condition $\Psi(t_0)$, the solution of the Schrödinger equation is unique. Thus, for each external potential $v(\mathbf{r},t)$ there is one and only one TD electron density $n(\mathbf{r},t)$. This map can be summarized as

$$v(\mathbf{r},t) \xrightarrow[\text{fixed}\,\Psi(t_0)]{i\partial\Psi/\partial t=\hat{H}(t)\Psi} \Psi(t) \xrightarrow{\langle\Psi(t)|\hat{n}|\Psi(t)\rangle} n(\mathbf{r},t). \tag{3.12}$$

The Runge-Gross theorem inverts the map (3.12), thus demonstrating a one-to-one correspondence between $v(\mathbf{r},t)$ and $n(\mathbf{r},t)$ at fixed Ψt_0.

Runge-Gross theorem: two densities $n(\mathbf{r},t)$ and $n'(\mathbf{r},t)$, evolving from a common initial many-body state $\Psi(t_0)$ under the influence of two different potentials $v(\mathbf{r},t)$ and $v'(\mathbf{r},t)$ that differ by more than a time-dependent function $c(t)$ $[v(\mathbf{r},t) - v'(\mathbf{r},t) \neq c(t)]$, will start to become different infinitesimally later than t_0. Therefore, there is a one-to-one correspondence between density and potentials, for any fixed initial many-body state.

The proof of the Runge-Gross theorem requires the external potentials $v(\mathbf{r},t)$ and $v'(\mathbf{r},t)$ to be Taylor expandable in time around t_0. In addition, the original formulation of the Runge-Gross theorem is restricted to finite systems. The proof that the theorem holds also for periodic systems has been given by Botti *et al.* [54]. However, the case of a periodic system subject to a uniform electric field cannot instead be treated with TDDFT, since it involves a uniform current which is left undetermined by the time-dependent periodic density [55]. For such a case, TD-current-DFT (TDCDFT) [56] is required. Finally, we note the Runge-Gross theorem does not require that the initial state of the system is the ground state $\Psi(t_0) = \Psi_0$, thus the case of a sudden switching is included.

From the Runge-Gross theorem, it follows that the external potential $v(\mathbf{r},t)$ is a functional of the TD electron density $n(\mathbf{r},t)$ and the initial state of the system $\Psi(t_0)$: $v(\mathbf{r},t) = v[n,\Psi(t_0)](\mathbf{r},t)$. As the solution TD Schrödinger equation is unique at fixed $\Psi(t_0)$, the TD wavefunction $\Psi(t)$ is also a functional of the electron density $n(\mathbf{r},t)$ and the initial state $\Psi(t_0)$: $\Psi(t) = \Psi[n,\Psi(t_0)](t)$. Finally, we deduce that all physical observables can, in principle, be expressed as density functionals

$$O(t) = \langle\Psi[n,\Psi(t_0)]|\hat{O}(t)|\Psi[n,\Psi(t_0)]\rangle = O[n,\Psi(t_0)](t). \tag{3.13}$$

This provides the formal justification of the fact that the TD electron density $n(\mathbf{r},t)$ contains all the information about the system (under the hypothesis of the Runge-Gross theorem).

3.3 The van Leeuwen theorem

In the previous section, we have seen that the time-dependent density $n(\mathbf{r},t)$ contains all information about the system. However, we still do not have a procedure to obtain $n(\mathbf{r},t)$ without the use of the TD Schrödinger equation. In order to follow the same procedure already used for static DFT in Chap. 2 , we have to set up a TD KS auxiliary system, of which $n(\mathbf{r},t)$ is the solution of its single-particle equations. Unfortunately, the Runge-Gross theorem does not ensure neither that the TD KS system exists, nor its uniqueness. The existence and unicity of the TD KS system is ensured (within restrictive assumptions, however) by the van Leeuwen theorem instead [57].
In order to enunciate the theorem, we generalize the Hamiltonian given by Eq. (3.1) to systems with a generic two-body interaction

$$\hat{W} = \frac{1}{2}\sum_{i,j\neq i}^{N} w(|\mathbf{r}_i - \mathbf{r}_j|). \tag{3.14}$$

For interacting electrons, we have $w(|\mathbf{r}_i - \mathbf{r}_j|) = 1/|\mathbf{r}_i - \mathbf{r}_j|$, as in Eq. (3.4). The case $w = 0$ corresponds to an independent particle system. The theorem is stated as follows.

Van Leeuwen theorem: for a time-dependent density $n(\mathbf{r},t)$ associated with a many-body system with a given particle-particle interaction $w(|\mathbf{r} - \mathbf{r}'|)$,

external potential $v(\mathbf{r},t)$, and initial state $\Psi(t_0)$, there exists a different many-body system featuring an interaction $w'(|\mathbf{r}-\mathbf{r}'|)$ and a unique external potential $v'(\mathbf{r},t)$ [up to within a purely time-dependent function $c(t)$] which reproduces the same time-dependent density $n(\mathbf{r},t)$. The initial state $\Psi'(t_0)$ in this system must be chosen such that it correctly yields the given density and its time-derivative at the initial time.

For the proof, we refer to TDDFT textbooks [10, 11]. Let us consider the special case $w = 1/|\mathbf{r}_i - \mathbf{r}_j|$ and $w' = 0$. The unprimed system is the electronic many-body system of interest, while the primed system is composed by non-interacting particles. We suppose that there is a single-particle Slater determinant $\Psi'(t_0) \equiv \Phi_0$ that reproduces the density $n(\mathbf{r},t_0)$ and its first time derivative at the initial time t_0. In this case, the van Leeuwen theorem states that a unique single-particle potential $v'_s(\mathbf{r},t) \equiv v_s(\mathbf{r},t)$ exists [defined up to a time-dependent constant $c(t)$] such that the TD density of the non-interacting system is equal to the interacting one $n(\mathbf{r},t) = n'(\mathbf{r},t)$. Thus, the primed system is exactly the TD KS system. This provides the formal justification for the TD KS approach, that is formulated in the next section.

For completeness, we consider also a second special case, namely $w = w' = 1/|\mathbf{r}_i - \mathbf{r}_j|$, i.e. the two many-body systems present the same interaction. If we take $\Psi(t_0) = \Psi'(t_0)$, the van Leeuwen theorem ensures a unique potential $v(\mathbf{r},t)$ exists that gives the TD density $n(\mathbf{r},t)$. These are exactly the same conclusions of Runge-Gross theorem.

The proof of the van Leeuwen theorem relies on a Taylor expansion of the potential around the initial time t_0 and, in addition, requires the density to be analytic in time at t_0. It turns out that the analyticity of the TD density is a condition quite difficult to control. In fact, Maitra *et al.* [58] has demonstrated that non-analytic densities may originate from Taylor expandable external potentials. At present, intense efforts are under way to find alternative proofs which do not rely on the Taylor-expandability of the potential or the density. We refer to Ruggenthaler *et al.* [59] for a recent review about this topic.

3.4 The time-dependent Kohn-Sham scheme

We suppose the many-body electron system we are studying satisfies the van Leeuwen theorem. In the previous section, we have demonstrated that the TD density $n(\mathbf{r},t)$ of the many-body electron problem can be reproduced exactly by an auxiliary non-interacting system subject to the effective external potential

$$v_s[n,\Psi(t_0),\Phi_0](\mathbf{r},t), \tag{3.15}$$

called TD KS potential. In Eq. (3.15), we explicitly consider that v_s is a functional of the TD density $n(\mathbf{r},t)$, the initial state of the interacting system $\Psi(t_0)$ and the initial state of the KS system Φ_0.
We now suppose that the external potential $v(\mathbf{r},t)$ is given by Eq. (3.6) and that

the system is in its ground state Ψ_0 for $t < t_0$. This is the most common situation encountered in practical applications. In this case, the Hohenberg-Kohn theorem states that both the interacting and non-interacting ground states are functionals of the ground state density $n_0(\mathbf{r})$, i.e., $\Psi(t_0) = \Psi[n_0](t_0)$ and $\Phi_0 = \Phi_0[n_0]$. Due to this, the KS effective potential is a functional of the TD density only: $v_s(\mathbf{r}, t) = v_s[n](\mathbf{r}, t)$. This greatly simplifies the problem, as an exact or high quality $\Psi(t_0)$ often cannot be obtained in practice.
The non-interacting initial state Φ_0 is a Slater determinant of the N KS states $\varphi_i^0(\mathbf{r}, t)$ with lower energy. They satisfy the time-independent KS equations

$$\epsilon_j \varphi_j^0(\mathbf{r}) = \left[-\frac{\nabla^2}{2} + v_s^0[n_0](\mathbf{r}) \right] \varphi_j^0(\mathbf{r}). \tag{3.16}$$

The ground-state density is given by

$$n_0(\mathbf{r}) = \sum_{j=1}^{N} |\varphi_j^0(\mathbf{r})|^2. \tag{3.17}$$

More details about the static KS scheme can be found in Sec. 2.3. The density at $t > t_0$ can be obtained by propagating the occupied KS orbitals through the TD single-particle Schrödinger equation

$$\left[-\frac{\nabla^2}{2} + v_s[n](\mathbf{r}, t) \right] \varphi_j(\mathbf{r}, t) = i \frac{\partial}{\partial t} \varphi_j(\mathbf{r}, t), \tag{3.18}$$

with initial conditions $\varphi_j(\mathbf{r}, t_0) = \varphi_j^0(\mathbf{r})$, and computing the TD density as

$$n(\mathbf{r}, t) = \sum_{j=1}^{N} |\varphi_j(\mathbf{r}, t)|^2. \tag{3.19}$$

The TD KS potential is decomposed as

$$v_s[n](\mathbf{r}, t) = v(\mathbf{r}, t) + v_{\mathrm{H}}[n](\mathbf{r}, t) + v_{\mathrm{xc}}[n](\mathbf{r}, t), \tag{3.20}$$

where v_{H} is the TD Hartree potential

$$v_{\mathrm{H}}[n](\mathbf{r}, t) = \int d^3 r' \frac{n(\mathbf{r}', t)}{|\mathbf{r} - \mathbf{r}'|}, \tag{3.21}$$

and $v_{\mathrm{xc}}[n](\mathbf{r}, t)$ is the TD xc potential.
Up to now, we do not know how to construct the xc potential v_{xc}, implicitly defined by Eq. (3.20). The explicit form of v_{xc} is unknown, thus an approximation is needed. The vast majority of applications of TDDFT are carried out using the adiabatic approximation, that is described in Sec. 3.5.

Finally, we note that Eq.s (3.16)-(3.20) are valid also if the system starts from a generic state $\Psi(t_0)$ which is not the ground state (the state Φ_0 as usual can still be a Slater determinant). The only difference is that the xc potential v_{xc} would have been a functional of both the interacting and non-interacting initial states, $v_{\mathrm{xc}} = v_{\mathrm{xc}}[n, \Psi(t_0), \Phi_0]$.

3.4.1 Spin-dependent extension

It is possible to generalize the TD KS equations (3.16)-(3.20) to a spin-resolved form. In this section, we show just the key equations. The derivation follows straightforwardly the one presented for the spin-unresolved KS system.
We consider a system of $N = N_\uparrow + N_\downarrow$ electrons. The TD Schrödinger-like equation of the KS orbitals is

$$i\frac{\partial}{\partial t}\varphi_{j\sigma}(\mathbf{r},t) = \left[-\frac{\nabla^2}{2} + v_{s\sigma}[n_\uparrow, n_\downarrow](\mathbf{r},t)\right]\varphi_{j\sigma}(\mathbf{r},t), \tag{3.22}$$

where $\sigma = \uparrow, \downarrow$ is the spin index, and

$$v_{s\sigma}[n_\uparrow, n_\downarrow](\mathbf{r},t) = v_\sigma(\mathbf{r},t) + \int d^3r' \frac{n(\mathbf{r}',t)}{|\mathbf{r}-\mathbf{r}'|} + v_{\mathrm{xc},\sigma}[n_\uparrow, n_\downarrow](\mathbf{r},t). \tag{3.23}$$

The total TD density is expressed as

$$n(\mathbf{r},t) = n_\uparrow(\mathbf{r},t) + n_\downarrow(\mathbf{r},t) = \sum_\sigma \sum_{j=1}^{N_\sigma} |\varphi_{j\sigma}(\mathbf{r},t)|^2. \tag{3.24}$$

This spin-dependent KS equations are more general than their spin-independent version (3.16)-(3.20), as now we include the possibility for the external potential to be spin-dependent $v \to v_\sigma$. When the spin-up and spin-down electrons are paired $N_\uparrow = N_\downarrow$ and the external potential is spin independent, the two formulations are equivalent. However, if the spin-up and spin-down electrons are not paired, $N_\uparrow \neq N_\downarrow$, the spin-dependent version of the KS equations admits different relations from the ones obtained within the spin-restricted formulation even in the case of spin-independent potentials.

3.5 The adiabatic approximation

The main quantity to be approximated in the TD KS formalism is the xc potential $v_{\mathrm{xc}}[n](\mathbf{r},t)$, implicitly defined through Eq. (3.20).
In the adiabatic approximation, the xc potential at time t is given by the ground-state xc potential $v^0_{\mathrm{xc}}[n]$ evaluated at the density $n(\mathbf{r},t)$ at the same time t

$$v^{\mathrm{A}}_{\mathrm{xc}}(\mathbf{r},t) = v^0_{\mathrm{xc}}[n](\mathbf{r})\big|_{n_0(\mathbf{r})\to n(\mathbf{r},t)}, \tag{3.25}$$

where $v^0_{\mathrm{xc}}[n]$ is the static xc potential functional, given by Eq. (2.33). If the external time-dependence is very slow (adiabatic) and the system evolves from its ground-state, this approximation is justified. Unfortunately, this is usually not the case. Due to the fact that $v^{\mathrm{A}}_{\mathrm{xc}}(\mathbf{r},t)$ depends only on the density at the same time, there is no memory, which is instead included in the exact functional, that depends on the history of the density at previous times [60]. Due to the neglect of memory, the general applicability of the adiabatic approximation is still a matter of research. Although, it turns out that the adiabatic approximation often works surprisingly well in practice. The exact form of $v^0_{\mathrm{xc}}[n]$, of course, is unknown. Thus, static DFT approximations are used to approximate $v^0_{\mathrm{xc}}[n]$. We refer to Sec. 2.4 for some

examples about approximations of the static xc potential. The most widely used choice is LDA (see Sec. 2.4.1). The correspondent TD potential is called ALDA and is given by

$$v_{\mathrm{xc}}^{\mathrm{ALDA}}(\mathbf{r},t) = v_{\mathrm{xc}}^{0,\mathrm{LDA}}[n](\mathbf{r})\big|_{n_0(\mathbf{r})\to n(\mathbf{r},t)}\,, \tag{3.26}$$

where $v_{\mathrm{xc}}^{0,\mathrm{LDA}}$ is the xc potential in the LDA approximation. We note that in ADLDA there are two distinct approximations. First, the TD KS potential is approximated by the static one evaluated at the TD density $n(\mathbf{r},t)$. Second, LDA is used to approximate the static xc potential $v_{\mathrm{xc}}^{0}[n]$.

3.6 Optical spectra and excitation energies through TDDFT

One of the most important applications of TDDFT is the calculation of the optical absorption spectrum and excitation energies.
The optical absorption cross section $\sigma(\omega)$ is defined by the ratio between the energy absorbed from an incoming electro-magnetic field at frequency ω and its original intensity. If the wavelength of the incoming wave is very large compared to the characteristic length of the system, as in the case of light in the visible range with respect to molecules, magnetic interactions can be neglected, and optical properties are derived as the response to an external time-dependent electric field $\mathbf{E}(t)$ within the dipole approximation

$$v_1(\mathbf{r},t) = -\mathbf{r}\cdot\mathbf{E}(t). \tag{3.27}$$

We suppose the incoming field $\mathbf{E}(t)$ is small enough with respect to the static internal field such that only the linear response is triggered. In this case, the optical absorption spectrum may be extracted from the frequency-dependent first-order response function (see below). Alternatively, the same information may be obtained from real-time propagation techniques. In the following, we summarize how to obtain the linear absorption spectrum, first with the real-time propagation method [61], then with the frequency-dependent formulation of the Casida equation [62].

3.6.1 The real-time propagation

Let us suppose the system is in its ground state before the perturbation is applied. $\varphi_j^0(\mathbf{r})$ are the ground-state KS orbitals and $n_0(\mathbf{r})$ is the ground state density. We excite our system with an impulsive electric field at $t = 0$, $E^\mu(t) = K^\mu\delta(t)$, along a specific Cartesian direction μ. In the dipole-approximation [see Eq. (3.27)], the interaction term can be written as

$$v_1(\mathbf{r},t) = -x^\mu E^\mu(t) = -x^\mu K^\mu\delta(t), \tag{3.28}$$

where $x^\mu = x, y, z$. We note there is no summation over repeated indexes. Through this prescription, all frequencies of the system are excited with equal weight, as $E^\mu(\omega) = K^\mu$, where $E^\mu(\omega)$ is the Fourier transform of the incoming electric field. At

$t = 0^+$, the initial state for the time evolution reads

$$\varphi_j(\mathbf{r}, t = 0^+) = \exp\left\{ -i \int_{0^-}^{0^+} dt' \left[\hat{H}_{KS} - x^\mu K^\mu \delta(t) \right] \right\} \varphi_j^0(\mathbf{r}) = e^{i x^\mu K^\mu} \varphi_j^0(\mathbf{r}). \tag{3.29}$$

The net effect of the impulsive electric field is to add the same space-dependent phase factor to all initial Kohn-Sham orbitals. This does not alter the initial density, but produces an initial current along the x^μ direction:

$$j^\mu(\mathbf{r}, 0^+) = -K^\mu n_0(\mathbf{r}). \tag{3.30}$$

In other words, the impulsive electric field transfers a momentum K^μ along the direction x^μ to all electrons.
The KS orbitals are then freely propagated by solving the TD Kohn-Sham equations. Then, spectroscopic observables can be computed through the density $n(\mathbf{r}, t)$. For the case of the optical absorption, we are interested in the time-dependent dipole moment

$$d^\nu(t) = \int d^3 r x^\nu n(\mathbf{r}, t). \tag{3.31}$$

If the amplitude K^μ is small enough in order to trigger only the linear response, we may approximate the dipole moment up to first order in perturbation as $d^\nu(t) \approx d_0^\nu + d_1^\nu(t)$. The dipole moment $d_1^\nu(t)$ at first perturbative order is connected to the dynamical polarizability through

$$\alpha^{\nu\mu}(\omega) = \frac{1}{K^\mu} \int_0^{+\infty} dt d_1^\nu(t) e^{i\omega t}. \tag{3.32}$$

The quantity of interest, the absorption cross section $\sigma(\omega)$, is proportional to the imaginary part of the dynamical polarizability tensor averaged over the three spatial directions

$$\sigma(\omega) = \frac{4\pi\omega}{c} \frac{1}{3} \sum_{\mu=1}^{3} \mathrm{Im}\left[\alpha^{\mu\mu}(\omega)\right], \tag{3.33}$$

where c stands for the velocity of light.

The interaction with an external electro-magnetic field induces transitions between the ground to excited states. For this reason, optical absorption spectroscopy is commonly employed to get information about excited states. In fact, due to the Lehmann representation, the averaged dynamical polarizability is usually expressed as

$$\alpha^{\mu\nu}(\omega) = \sum_{i=1}^{+\infty} \left\{ \frac{|\langle \Psi_i | \hat{r}^\mu | \Psi_0 \rangle|^2}{\omega - \omega_{i0} + i\eta} - \frac{|\langle \Psi_i | \hat{r}^\nu | \Psi_0 \rangle|^2}{\omega + \omega_{i0} + i\eta} \right\}, \tag{3.34}$$

where $\omega_{i0} = E_i - E_0$ are the excitation frequencies of the system. The absorption cross section may be expressed as

$$\sigma(\omega) = \sum_{i}^{+\infty} \delta(\omega - \omega_{i0}) f_i, \tag{3.35}$$

where

$$f_i = \frac{2\omega_{i0}}{3} \sum_{\mu=1}^{3} |\langle \Psi_i | \hat{r}^\mu | \Psi_0 \rangle|^2 \tag{3.36}$$

are dimensionless quantities called oscillator strengths. As we can see from Eq. (3.35), the absorption cross section is composed by peaks at the excitation frequencies with amplitudes proportional to the square of the dipole matrix elements. Dipole matrix elements $\langle \Psi_i | \hat{r}^\mu | \Psi_0 \rangle$ determine if a transition $0 \to i$ is allowed or not. Of course, excited states which are not populated during the excitation process cannot be studied through the study of optical properties. We will see how to overcome this problem in Chap. 6 by studying the nonlinear optical response of a many-electron system due to an impulsive electric field. In fact, the nonlinear response shows different selection rules with respect to the linear case, enabling the study of excitations which are not induced in the linear regime.

3.6.2 Linear-response TDDFT and the Casida equation

We consider a system composed by N interacting electrons described by the Hamiltonian given by Eq. (3.1). We suppose the time-dependent external potential $v(\mathbf{r}, t)$ can be decoupled in a static term and a perturbation term as in Eq. (3.6), and that $v_1(\mathbf{r}, t)$ is small with respect to $v_0(\mathbf{r})$.
The difference between the time-dependent density $n(\mathbf{r}, t)$ and ground-state density $n_0(\mathbf{r})$ can be expanded in powers of the perturbation v_1

$$n(\mathbf{r}, t) - n_0(\mathbf{r}) = n_1(\mathbf{r}, t) + n_2(\mathbf{r}, t) + n_3(\mathbf{r}, t) + \dots \tag{3.37}$$

We are interested at the first-order response, given by

$$n_1(\mathbf{r}, t) = \int dt' \int d^3r' \chi(\mathbf{r}, t, \mathbf{r}', t') v_1(\mathbf{r}', t'), \tag{3.38}$$

where χ is the interacting density-density response function.
The first-order response can be written also for the KS system as

$$n_1(\mathbf{r}, t) = \int dt' \int d^3r' \chi_s(\mathbf{r}, t, \mathbf{r}', t') v_{s1}(\mathbf{r}', t'), \tag{3.39}$$

where χ_s is the KS response function. Of course, the first-order density variations $n_1(\mathbf{r}, t)$ are equal for the interacting and KS systems. In Eq. (3.39), v_{s1} is the first order variation of the effective potential due to the perturbation v_1. Due to the fact that the Hartree and xc potentials are density functionals, v_{s1} depends on n_1 through the following equation

$$v_{s1}[n](\mathbf{r}, t) = v_1(\mathbf{r}, t) + \int d^3r' \frac{n_1(\mathbf{r}', t)}{|\mathbf{r} - \mathbf{r}'|} + v_{\mathrm{xc1}}(\mathbf{r}, t), \tag{3.40}$$

where the first term is just the external perturbation v_1, the second term is the linearized Hartree potential and the third term the linearized xc potential. An explicit expression for it is obtained by functional Taylor expansion

$$v_{\mathrm{xc1}}(\mathbf{r}, t) = \int dt' \int d^3r' \left. \frac{\delta v_{\mathrm{xc}}[n](\mathbf{r}, t)}{\delta n(\mathbf{r}', t')} \right|_{n_0(\mathbf{r})} n_1(\mathbf{r}', t'). \tag{3.41}$$

The functional derivative of the xc potential with respect to the TD density is the xc kernel

$$f_{\rm xc}(\mathbf{r},t,\mathbf{r}',t') = \left.\frac{\delta v_{\rm xc}[n](\mathbf{r},t)}{\delta n(\mathbf{r}',t')}\right|_{n_0(\mathbf{r})}, \tag{3.42}$$

which is a functional of the ground-state density. The xc kernel is usually the key quantity to approximate in linear-response TDDFT. If we insert Eq. (3.40) into Eq. (3.39), we find

$$n_1(\mathbf{r},t) = \int dt' \int d^3r' \chi_s(\mathbf{r},t,\mathbf{r}',t') \Bigg[v_1(\mathbf{r}',t') + \int dt_1 \int d^3r_1 \left\{ \frac{\delta(t'-t_1)}{|\mathbf{r}'-\mathbf{r}_1|} + f_{\rm xc}(\mathbf{r}',t',\mathbf{r}_1,t_1) \right\} n_1(\mathbf{r}_1,t_1) \Bigg] \tag{3.43}$$

The self-consistent nature of the TD KS equations is reflected in Eq. (3.43), that must be solved self-consistently in order to obtain n_1. Eq. (3.43) is usually expressed in the frequency domain as

$$n_1(\mathbf{r},\omega) = \int d^3r' \chi_s(\mathbf{r},\mathbf{r}',\omega) \left[v_1(\mathbf{r}',\omega) + \int d^3r_1 \left\{ \frac{1}{|\mathbf{r}'-\mathbf{r}_1|} + f_{\rm xc}(\mathbf{r},\mathbf{r}_1,\omega) \right\} \right] n_1(\mathbf{r},\omega), \tag{3.44}$$

where $n_1(\mathbf{r},\omega)$, $\chi_s(\mathbf{r},\mathbf{r}',\omega)$, and $v_1(\mathbf{r}',\omega)$ are the Fourier transforms of $n_1(\mathbf{r},t)$, $\chi_s(\mathbf{r},\mathbf{r}',t)$, and $v_1(\mathbf{r}',t)$ respectively. In addition,

$$f_{\rm xc}(\mathbf{r},\mathbf{r}',\omega) = \int d(t-t') e^{i\omega(t-t')} \left.\frac{\delta v_{\rm xc}[n](\mathbf{r},t)}{\delta n(\mathbf{r}',t')}\right|_{n_0(\mathbf{r})}. \tag{3.45}$$

is the xc kernel in Fourier space. In Eq. (3.44), we used the fact that $f_{\rm xc}(\mathbf{r},t,\mathbf{r}',t')$ depends on the time difference $t-t'$ (as the KS response function). Thus, its Fourier transform depends on just one frequency.
Eq. (3.44) is the key linear-response TDDFT equation in the derivation of the Casida equation.

The excitation energies $\Omega_i = \omega_{i0}$ are given by the poles of the density-density response function in the frequency domain $\chi(\mathbf{r},\mathbf{r}',\omega)$. The density response diverges if the system is subject to any perturbation with the same frequency of the poles. An external perturbation is not even required: a system can sustain a finite response at its excitation frequencies without any external stimulus. Therefore, let us consider the linear response equation given by Eq. (3.44) setting $v_1(\mathbf{r},\omega) = 0$. We get

$$n_1(\mathbf{r},\Omega_i) = \int d^3r' \chi_s(\mathbf{r},\mathbf{r}',\Omega_i) \int d^3r'' f_{\rm Hxc}(\mathbf{r}',\mathbf{r}'',\Omega_i) n_1(\mathbf{r}'',\Omega_i) \tag{3.46}$$

where $f_{\rm Hxc}(\mathbf{r},\mathbf{r}',\omega) = 1/|\mathbf{r}-\mathbf{r}'| + f_{\rm xc}(\mathbf{r},\mathbf{r}',\omega)$ is the Hartree-exchange-correlation kernel. Formally, this equation can be viewed as an eigenvalue equation of a frequency-dependent integral operator acting on $n_1(\mathbf{r},\omega)$, with eigenvalues 1.
In the following, we label occupied states with i,i' and unoccupied states with a, a'. The Casida equation is a reformulation of Eq. (3.46), where the first order density variation $n_1(\mathbf{r},\omega)$ is projected into the particle-hole basis of the KS system

$$n_1(\mathbf{r},\omega) = \sum_{ia} \left[\Phi^*_{ia}(\mathbf{r}) X_{ia}(\omega) + \Phi_{ia}(\mathbf{r}) Y_{ia}(\omega) \right], \tag{3.47}$$

where

$$\Phi_{jk}(\mathbf{r}) = \varphi_j^{0*}(\mathbf{r})\varphi_k^0(\mathbf{r}) \tag{3.48}$$

are the particle-hole orbitals. We have labeled occupied states by i and unoccupied states by a.
As a result, the Casida equation can be written as follows

$$\begin{pmatrix} A & B \\ B & A \end{pmatrix}\begin{pmatrix} X \\ Y \end{pmatrix} = \Omega_i \begin{pmatrix} -1 & 0 \\ 0 & 1 \end{pmatrix}\begin{pmatrix} X \\ Y \end{pmatrix}, \tag{3.49}$$

where the sub matrices A and B are given by

$$A_{ia,i'a'}(\Omega_i) = \delta_{ii'}\delta_{aa'}\omega_{ai} + B_{ia,i'a'}(\Omega_i) \tag{3.50}$$

$$B_{ia,i'a'}(\Omega_i) = \int d^3r \int d^3r' \Phi_{ia}(\mathbf{r}) f_{\mathrm{Hxc}}(\mathbf{r},\mathbf{r}',\Omega_i)\Phi^*_{i'a'}. \tag{3.51}$$

Eq. (3.49) has the mathematical structure of an infinite-dimensional anti-hermitian eigenvalue problem.
It can be shown that $\Omega_i \in \mathrm{Re}$. From the solutions of the Casida equation [see Eq. (3.49)] it is possible to determine the excitation energies of the system. The oscillator strengths can be obtained from the eigenvectors as follows

$$f_n = \frac{2}{3}\sum_{\mu=1}^{3} \left|\mathbf{x}^{\mu T}(A-B)(\mathbf{X}-\mathbf{Y})\right|^2, \tag{3.52}$$

where

$$x_{ia}^{\mu} = \int d^3r x^{\mu} \Phi_{ia}(\mathbf{r}). \tag{3.53}$$

Finally, the absorption cross section $\sigma(\omega)$ can be evaluated by substituting the excitation frequencies Ω_i and oscillator strengths given by Eq. (3.52) into Eq. (3.35).

3.6.3 Comparison between the two methods

In this section, we briefly discuss the pros and cons of the Casida equation (or other linear-response methods) and the time-propagation scheme. Our considerations are limited to finite (e.g. molecular) systems.

The Casida method is generally more conveniently used to obtain low-lying, well separated excitations of small to medium molecules. The principal bottleneck of this method is that the Casida matrix requires to be converged with respect to the number of unoccupied states included in the calculation. For certain kind of systems, this convergence can be very slow, especially if high excitation energies are considered.
The problem of unoccupied-state convergence does not affect the time-propagation method, as only occupied states are involved in the solution of the TD KS equations. If combined with real-space representation of the KS orbitals, the real-time propagation method proves to be very robust, independent of both unoccupied-states convergence and basis set choice.
The real-time propagation method (in real-space representation) is also preferable

for metallic systems and clusters, which shows predominately collective excitations.

In practice, the numerical scaling when solving the Casida equation ranges from N^2 to N^3, depending on the implemented algorithm. The real-time propagation shows a better scaling with respect to the system size, ranging from N to N^2, being therefore better suited to compute the spectrum of large molecules. However, in practice very small time steps are usually required, which increases the prefactor of the numerical scaling.

Finally, we point out that one of the major advantage of the time-propagation method is that it is straightforward to extend to the nonlinear regime. This point is further discussed in Chap. 6.

Chapter 4

Fundamental gaps of quantum dots on the cheap

Quantum dots (QDs) are artificial nanostructures in which electrons (from a few to a few hundred) are confined in all the three spatial directions. They are also referred to as artificial atoms. Low-dimensional QDs [63, 64] are fabricated by restricting the two-dimensional electron gas of a semiconductor heterostructure laterally by electrostatic gates, or vertically by etching techniques. In both cases, they can be modeled as purely two-dimensional systems subject to an harmonic confinement. By playing with the heterostructure geometry or the strength of the external field, it is possible to explore a large spectrum of quantum effects. Transport properties of QDs are relevant for technological applications in the development of advanced nanoelectronic devices [63]. In particular, the fundamental gap plays a important role in the characterization of such nanostructures [65].

In this chapter, we show that the fundamental gaps of QDs can be accurately determined with the same computational effort of a standard ground-state calculation plus a non-self consistent step of negligible cost, all performed within density-functional theory at the local-density approximation level. In the exchange-only limit, a mean relative absolute error of 4% is obtained with respect to exact-exchange results in the Kriger-Lee-Iafrate approximation. A direct inclusion of the electronic correlation leads to a mean relative absolute error of 14% with respect to numerically exact diagonalization benchmark results.

The results of this work have been published in 2019 in Physical Review B [66]. In the following sections, the paper content is attached as an integral part of this Ph.D. thesis. The layout is slightly changed in order to make it coherent with the style of the present document.

4.1 Introduction

In single-electron transport through a semiconductor QD [63], an electron can pass from one reservoir (the source) to another (the drain) when a voltage is applied. In this process, an electron is first added to and then removed from the dot. Assuming a weak-coupling of the dots to the reservoirs, the addition of an electron requires to overcome the so-called charging energy. Coulomb-blockade resonances arise in

the conductance from the sequence of charging and discharging the QD [65]. The interval between two consecutive conductance peaks is the difference between the removal energy $E^r_{\rm N} = E_{\rm N-1} - E_{\rm N}$ and (the negative of) the addition energy $E^a_{\rm N} = E_{\rm N} - E_{\rm N+1}$, where $E_{\rm N}$ is the ground state energy of the QD with N electrons. Thus, the *fundamental gap* is defined as

$$\begin{aligned} G_{\rm E,N} :=& E^r_{\rm N} - E^a_{\rm N} \\ =& E_{\rm N-1} - 2E_{\rm N} + E_{\rm N+1}. \end{aligned} \tag{4.1}$$

This quantity is useful in the evaluation of the electronic properties of a QD, especially in the context of applying them in a circuit or in lattices such as QD cellular automata.

In Kohn-Sham (KS) density-functional theory (DFT) [5, 6, 9] – through the ionization potential theorem [49, 50, 67–70] – the fundamental gap can also be expressed as follows [51]

$$G_{\varepsilon,\rm N} = \varepsilon_{\rm H,N+1} - \varepsilon_{\rm H,N} \tag{4.2}$$

where $\varepsilon_{\rm H,N}$ is the energy of the highest (H) occupied KS level for the system with N electrons – hence the subscript N; the corresponding orbital may be referred to as the highest occupied "molecular" orbital (HOMO). Note that, throughout this work, we are primarily concerned with non-degenerate levels.

By mixing states with different integer electron numbers and, thus, switching from DFT to Ensemble-DFT (EDFT) [49–51], one finds that the fundamental gap can be expressed in terms of two contributions [70]

$$G_{\Delta,\rm N} = \Delta_{\rm KS,N} + \Delta_{\rm xc,N} \ , \tag{4.3}$$

where

$$\Delta_{\rm KS,N} = \varepsilon_{\rm L,N} - \varepsilon_{\rm H,N} \tag{4.4}$$

is the energy gap between the last occupied and the first unoccupied KS levels. In $\varepsilon_{\rm L,N}$, L refers to the lowest unoccupied "molecular" orbital (LUMO) and N to the fact that this is an eigenvalue of the KS system with N electrons; and

$$\Delta_{\rm xc,N} = \lim_{\delta N \to 0^+} \left\{ v_{\rm xc}(\mathbf{r})|_{\rm N+\delta N} - v_{\rm xc}(\mathbf{r})|_{\rm N-\delta N} \right\} \tag{4.5}$$

is the exchange-correlation (xc) contribution that can be obtained from the xc potential $v_{\rm xc}$ for ensemble particle densities. Thus, $\Delta_{\rm xc,N}$ is due to the discontinuities of $v_{\rm xc}$ that can occur at integer electron numbers [49, 71].

A few notes should be briefly made: (a) Eq. (4.3) is derived by borrowing the expression of the Hartree energy from regular DFT [see Eq. (4.9) below] by evaluating it on the ensemble particle density. The result is a smooth functional of N and, thus, the Hartree potential does not contribute to the fundamental gap. But generalizations of the Hartree-xc energy may also allow 'Hartree-like' contributions, with formal and practical advantages [52, 72, 73]. In a different framework, a similar expression to Eq. (4.3) is derived without invoking fractional electron numbers [74].

Moreover, in a recently derived framework, ensemble densities and corresponding xc-functionals are employed to tackle optical and fundamental gaps in a unified fashion [75]. In this work, however, we stay within the original EDFT formulation [49,50].

Finally, let us note that Eq. (4.2) together with Eq. (4.3) and Eq. (4.4) imply

$$\Delta_{\mathrm{xc,N}} = \varepsilon_{\mathrm{H,N+1}} - \varepsilon_{\mathrm{L,N}} \, . \tag{4.6}$$

Thus, it should be apparent that $\Delta_{\mathrm{xc,N}}$ yields in general a non-vanishing contribution. Artificially confined many-electron systems, such as QDs, can exhibit $\Delta_{\mathrm{xc,N}}$ of sizable magnitude [63, 76].

Although Eqs. (4.1), (4.2), and (4.3) give access to the same fundamental gap (i.e., $G_{\mathrm{E,N}} \equiv G_{\varepsilon,\mathrm{N}} \equiv G_{\Delta,\mathrm{N}}$), the procedures and corresponding computational efforts can differ substantially. Equation (4.1) entails *three* distinct self-consistent calculations performed for $N-1$, N and $N+1$, respectively. On the other hand, Eq. (4.2) requires *two* independent self-consistent calculations performed for N and $N+1$. Finally, Eq. (4.3) involves only one self-consistent calculation for N electrons, once the limit in Eq. (4.5) is expressed analytically. Below, we come back to this point when discussing the x-only contribution in detail. Next, let us briefly discuss approximate calculations.

It is well-known that the issue of getting vanishing $\Delta_{\mathrm{xc,N}}$ – when local-density approximation (LDA) or generalized-gradient approximation (GGA) is directly evaluated on the ensemble densities as in Eq. (4.5) – can be overcomed by adding many-body corrections as in the GW calculations [77–80]. Nevertheless, here we stick to computationally less expensive DFT-based approaches.

For finite systems, it has been shown that the LDA and GGA forms may become useful if they are properly upgraded to EDFT [52, 73, 81]. Here, instead, we proceed within a somewhat more traditional approach, to minimize both numerical and formal efforts.

A reason of inaccuracy ascribed to procedures based on LDA and GGA when computing fundamental gaps of atoms, molecules, and their arrays through Eq. (4.2), has been the over-damped tail of the xc potential, which does not bind the outer electrons sufficiently (if at all). *Non* Coulombic (e.g., harmonic) potentials can model effectively the confinement of electrons in artificial nanostructures (such as semiconductor interfaces). When such confinements are sufficiently strong, the over-damped tail of the LDA or GGA xc potentials may not have dramatic implications. Indeed, Capelle *et al.* [76] have demonstrated that LDA calculations of fundamental gaps based on Eq. (4.2) are equally accurate as those obtained from Eq. (4.1). In the same work, excellent agreement between LDA and full configuration interaction results [82] was also pointed out. We discuss these cases in more detail below.

For the calculation of the fundamental gaps, meta-GGAs (MGGAs) are promising alternatives but still with mixed results [83–85]. A class of models for the xc potential

(GGA-like and MGGA-like) have stimulated a surge of attention [86–92]. Due to their computational simplicity and reasonable accuracy, they may offer a suitable trade-off especially in (pre-)screening of large data sets [93].

Reaching a satisfactory accuracy in the calculation of fundamental gaps usually requires orbital-dependent functionals, e.g., in the form of hybrids. In this case, the *generalized* rather than the regular KS approach is adopted as a convenient computational procedure, and a part of $\Delta_{\mathrm{xc,N}}$ is absorbed in the corresponding *generalized* KS gap [94–99]. However, hybrid-based calculations can be rather expensive computationally.

In this work, we show that accurate estimations of the fundamental gap for QDs can be obtained by means of a computationally straightforward procedure, which requires a *single* set of self-consistent calculations supplied with a *non* self-consistent calculation of negligible computational burden – all at the LDA level. Our attention was drawn to such a procedure by earlier works [100, 101] that have considered atoms, molecules, and extended systems. Here, our focus is on two-dimensional QDs – for which, we will also analyze the case of x-only approximations extensively.

This chapter is organized as follows. Theoretical preliminaries illustrating the approach and the necessary computational steps are given in Sec. 4.2. Results of the applications are reported in Sec. 4.3. The chapter is summarized with an outlook in Sec. 4.4.

4.2 Theory

In the following, as in the typical calculations reported in the literature for QDs, we work within a spin-unrestricted formulation. Furthermore, we focus on electrons which are effectively confined to two-spatial dimensions, which is the case of main interest when considering semiconductor QDs. [63] In spin-DFT [102] (SDFT), under the restriction of collinear spin polarization, the total energy, E, of N interacting electrons in a given (local) external potential (i.e., the confinement), $v_{0\sigma}(\mathbf{r})$, can be expressed as a functional of the two spin densities $n_\sigma(\mathbf{r})$ (with $\sigma =\uparrow,\downarrow$)

$$\begin{aligned} E[\underline{n}] &= T_{\mathrm{KS}}[\underline{n}] + E_{\mathrm{H}}[n] + E_{\mathrm{xc}}[\underline{n}] \\ &+ \sum_{\sigma=\uparrow,\downarrow} \int d^2r\; v_{0\sigma}(\mathbf{r}) n_\sigma(\mathbf{r})\,, \end{aligned} \tag{4.7}$$

where d^2r is the infinitesimal volume in two dimensions, $\mathbf{r} = (x, y)$ is the position vector and x and y are the coordinates, $\underline{n}$ denotes the pair $(n_\uparrow, n_\downarrow)$, $n = n_\uparrow + n_\downarrow$ is the total particle density. $T_{\mathrm{KS}}[\underline{n}]$ is the kinetic energy of the Kohn-Sham systems, which is defined as

$$T_{\mathrm{KS}}[\underline{n}] = \sum_{\sigma=\uparrow,\downarrow} \sum_{j=1}^{N_\sigma} \int d^2r\; \varphi^*_{j\sigma}(\mathbf{r}) \left(-\frac{\nabla^2}{2}\right) \varphi_{j\sigma}(\mathbf{r})\,; \tag{4.8}$$

here the Lapalcian takes into account only two-dimensional partial derivatives, namely $\nabla^2 = \partial_x^2 + \partial_y^2$. N_σ is the number of electrons with spin σ, and $N = N_\uparrow + N_\downarrow$.

$E_{\rm H}[n]$ is the (Hartree) electrostatic interaction energy defined as

$$E_{\rm H}[n] = \frac{1}{2}\int d^2r \int d^2r' \, \frac{n(\mathbf{r})n(\mathbf{r}')}{|\mathbf{r}-\mathbf{r}'|} \, . \tag{4.9}$$

Finally, Exc$[\underline{n}]$ is the exchange-correlation energy functional that in practice needs to be approximated.
The KS single-particle orbitals are solutions of the equations [102]

$$-\frac{\nabla^2}{2}\varphi_{j\sigma}(\mathbf{r}) + v_{{\rm KS}\sigma}[\underline{n}](\mathbf{r})\varphi_{j\sigma}(\mathbf{r}) = \varepsilon_{j\sigma}\varphi_{j\sigma}(\mathbf{r}) \, . \tag{4.10}$$

The KS potential may be decomposed as

$$v_{{\rm KS}\sigma}[\underline{n}](\mathbf{r}) = v_{0\sigma}(\mathbf{r}) + v_{\rm H}[\underline{n}](\mathbf{r}) + v_{{\rm xc}\sigma}[\underline{n}](\mathbf{r}) \, , \tag{4.11}$$

where

$$v_{\rm H}(\mathbf{r})[n] = \int d^2r' \frac{n(\mathbf{r}')}{|\mathbf{r}-\mathbf{r}'|} \, , \tag{4.12}$$

and

$$v_{{\rm xc}\sigma}[\underline{n}](\mathbf{r}) = \frac{\delta E_{\rm xc}[\underline{n}]}{\delta n_\sigma(\mathbf{r})} \, . \tag{4.13}$$

The exact spin-densities can be calculated from the exact KS orbitals, in principle, by summing $n_{j\sigma}(\mathbf{r}) = |\varphi_{j\sigma}(\mathbf{r})|^2$ over the occupied single-particle states, $n_\sigma(\mathbf{r}) = \sum_{j=1}^{N_\sigma} n_{j\sigma}(\mathbf{r})$.

As mentioned in the introduction, the KS scheme provides us with all the ingredients to compute the fundamental gap either via differences of total energies [as in Eq. (4.1)] or KS eigenvalues [as in Eq. (4.2)]. In the next subsection, however, we are after the third (approximate) procedure, which is suggested by working with Eq. (4.3) at the level of the exchange-only approximation.

4.2.1 From exact to approximate x-only expressions

Ensemble-SDFT allows us to consider a fractional number of electrons, which are realized by mixing pure states with different integer numbers of electrons. The ensemble xc potential can jump by a well-defined (spin-dependent) constant, whenever the number of electrons passes through an integer value. This leads to an appealing way to compute the fundamental gap [49] [see Eq. (4.3)].

To conclude our analysis, however, we do not go into the details of ensemble-SDFT. It is sufficient to recall that through Eq. (4.5) we can isolate the exact x-contribution to the fundamental gap as follows [103, 104]:

$$\Delta_{\rm x,N} = \langle u_{{\rm xL}\sigma}[\underline{n}]\rangle_{{\rm L}\sigma} - \langle v_{{\rm x}\sigma}[\underline{n}]\rangle_{{\rm L}\sigma}, \tag{4.14}$$

where

$$u_{{\rm xj}\sigma}[n](\mathbf{r}) = -\sum_{i=1}^{N_\sigma} \frac{\varphi^*_{i\sigma}(\mathbf{r})}{\varphi^*_{j\sigma}(\mathbf{r})} \int d^2r' \frac{\varphi^*_{j\sigma}(\mathbf{r}')\varphi_{i\sigma}(\mathbf{r}')}{|\mathbf{r}-\mathbf{r}'|}, \tag{4.15}$$

$$\langle v_{\mathrm{x}\sigma}[\underline{n}]\rangle_{j\sigma} = \int d^2r\, \varphi^*_{j\sigma}(\mathbf{r}) v_{\mathrm{x}\sigma}[\underline{n}](\mathbf{r})\varphi_{j\sigma}(\mathbf{r})\,, \tag{4.16}$$

and

$$\langle u_{\mathrm{xj}\sigma}[\underline{n}]\rangle_{j\sigma} = \int d^2r\, \varphi^*_{j\sigma}(\mathbf{r}) u_{\mathrm{xj}\sigma}[\underline{n}](\mathbf{r})\varphi_{j\sigma}(\mathbf{r})\,. \tag{4.17}$$

For later convenience, we emphasize that the above quantities are well defined also for $j\sigma \neq \mathrm{L}\sigma$. Writing Eq. (4.14), we have assumed that the variation of the electron number occurs only within a given spin channel. For the sake of simplicity, we have also assumed that the considered states do not involve degeneracies.

So far, exchange and correlation were included and treated exactly. Next, we neglect the correlation and restrict ourselves to the exact-exchange approximation (EXX). Thus

$$E_{\mathrm{xc}} \to E_{\mathrm{x}} = -\frac{1}{2}\sum_{\sigma=\uparrow,\downarrow}\sum_{i,k=1}^{N_\sigma}\int d^2r' \int d^2r'' \frac{\varphi_{i\sigma}(\mathbf{r}'')\varphi^*_{i\sigma}(\mathbf{r}')\varphi^*_{k\sigma}(\mathbf{r}'')\varphi_{k\sigma}(\mathbf{r}')}{|\mathbf{r}'-\mathbf{r}''|}\,. \tag{4.18}$$

First we notice that E_{x} depends on $\underline{n}$ implicitly, i.e., through the KS orbitals $\{\varphi_{j\sigma}\} \equiv \{\varphi_{j\sigma}[\underline{n}]\}$. Thus, in the case of Eq. (4.18), the evaluation of the functional derivative as in Eq. (4.13) requires the solution of an integral equation for the EXX potential, to be used self-consistently in the solution of the KS equations [105–109]. In what follows, however, we simplify both our numerical efforts and analysis by adopting the Krieger, Li and Iafrate (KLI) approximation [110, 111].

The EXX potential in the KLI approximation is given by

$$v^{\mathrm{KLI}}_{\mathrm{x}\sigma}[\underline{n}](\mathbf{r}) \;=\; v_{\mathrm{Sl}\sigma}[\underline{n}](\mathbf{r}) + \Delta v^{\mathrm{KLI}}_{\mathrm{x}\sigma}[\underline{n}](\mathbf{r}), \tag{4.19}$$

where

$$v_{\mathrm{Sl}\sigma}[\underline{n}](\mathbf{r}) = \frac{1}{n_\sigma(\mathbf{r})}\sum_{j=1}^{N_\sigma} n_{j\sigma}(\mathbf{r}) u_{\mathrm{xj}\sigma}[\underline{n}](\mathbf{r}) \tag{4.20}$$

is the Slater (SL) potential and

$$\Delta v^{\mathrm{KLI}}_{\mathrm{x}\sigma}[\underline{n}](\mathbf{r}) = \frac{1}{n_\sigma(\mathbf{r})}\sum_{j=1}^{N_\sigma} n_{j\sigma}(\mathbf{r})\left[\langle v^{\mathrm{KLI}}_{\mathrm{x}\sigma}[\underline{n}]\rangle_{j\sigma} - \langle u_{\mathrm{xj}\sigma}[\underline{n}]\rangle_{j\sigma}\right] \tag{4.21}$$

can be regarded as a correction to the Slater potential.

As long as the particle density and the spin-polarization are preserved, the KS potential can be shifted, for each spin channel, by an arbitrary constant and thus the term with $j = N_\sigma$ in Eq. (4.21) can be set to zero. It may also be useful to remind that for strongly confined systems such as QDs – which are the systems of interest in this work – the Slater potential yields the leading contribution to the x-only potential and vanishes for $r \to +\infty$ (Refs. [112, 113]).

Next, we seek to further minimize our numerical efforts. As shown in Appx. 4.A, elementary but tedious algebraic steps allow us to define an *approximation* to $\Delta_{\mathrm{x,N}}$ in terms of the difference of single-particle energies, as follows

$$\Delta_{\mathrm{x,N}}^{\mathrm{KLI}} = \widetilde{\varepsilon}_{\mathrm{H}\sigma,\mathrm{N}+1}^{\mathrm{KLI}} - \varepsilon_{\mathrm{L}\sigma,\mathrm{N}}^{\mathrm{KLI}} \,. \tag{4.22}$$

In Eq. (4.22), $\widetilde{\varepsilon}_{\mathrm{H}\sigma,\mathrm{N}+1}^{\mathrm{KLI}}$ is a single-particle energy that refers to the system with $N+1$ electrons but it is obtained by using as an input the single-particle orbitals from the (self-consistent solution of) the corresponding N-electron problem – hence, the *tilde* is used here to stress that "frozen" orbitals are employed. $\widetilde{\varepsilon}_{\mathrm{H}\sigma,\mathrm{N}+1}^{\mathrm{KLI}}$ can be computed through a single iteration of the EXX-KLI procedure. In this step, the KS potential must be shifted – at most by a constant value – such that it goes to zero at large distance from the system. Thus, $\widetilde{\varepsilon}_{\mathrm{H}\sigma,\mathrm{N}+1}^{\mathrm{KLI}}$ may be related to an approximate ionization potential for the systems with $N+1$ electrons. $\varepsilon_{\mathrm{L}\sigma,\mathrm{N}}^{\mathrm{KLI}}$ is obtained as usual from the self-consistent solution for the system with N-electrons.

The importance of Eq. (4.22) is in the fact that it readily suggests us that a *non-vanishing* – albeit approximate – $\Delta_{\mathrm{x,N}}$ may be obtained by replacing the EXX-KLI quantities with quantities that do not necessarily entail orbital-dependent functionals. Especially for the systems considered in this work, it is compelling to try with the simplest approximation

$$\Delta_{\mathrm{x,N}}^{\mathrm{KLI}} \to \Delta_{\mathrm{x,N}}^{\mathrm{2DLDA}} := \widetilde{\varepsilon}_{\mathrm{H}\sigma,\mathrm{N}+1}^{\mathrm{x,2DLDA}} - \varepsilon_{\mathrm{L}\sigma,\mathrm{N}}^{\mathrm{x,2DLDA}} \,, \tag{4.23}$$

where 2DLDA, for brevity, stands for the 2D version of the local-spin-density approximation [114–116], and the notation emphasizes that eigenvalues are determined within *x-only* 2DLDA calculations. Eq. (4.23) requires no extra implementations, in codes that already implement regular calculations (including a restart procedure from given orbitals and the control of the number of iterations). Further details on the numerical procedure are reported in the section devoted to our applications (see below).

4.2.2 Inclusion of correlation

It is tempting to extend Eq. (4.23) to include the correlation as follows:

$$\Delta_{\mathrm{xc,N}}^{\mathrm{2DLDA}} := \widetilde{\varepsilon}_{\mathrm{H}\sigma,\mathrm{N}+1}^{\mathrm{2DLDA}} - \varepsilon_{\mathrm{L}\sigma,\mathrm{N}}^{\mathrm{2DLDA}} \,. \tag{4.24}$$

This equation expressed through the xc potential [see Eq. (4.A.4)] has been previously suggested in Ref. [100] and – with improved models for the xc potential [86,89] – also in Ref. [101]. Comparing Eq. (4.24) with Eq. (4.6), we see that Eq. (4.24) not only invokes an 'LDA replacement' but also makes use of frozen orbitals [similarly as in Eq. (4.23)]. In Ref. [100] it is shown that $\widetilde{\varepsilon}_{\mathrm{H}\sigma,\mathrm{N}+1}$ can be connected to $\varepsilon_{\mathrm{H}\sigma,\mathrm{N}+1}$ in a perturbative fashion – but we will not explore such corrections in this work. In Refs. [100, 101] neither electrons in artificial confinements nor the x-only limit were scrutinized. We carry out these analyses on QDs in the next section.

4.3 Applications

In this section, we show that the fundamental gaps of QDs computed up to exchange-only effects by using Eq. (4.23) compare very well with those obtained by using Eq. (4.22). More importantly, we show that the estimations including correlations through Eq. (4.24) are notable as well.

4.3.1 Quantum-dot model and numerical methods

We model electrons in a semiconductor QD with a two-dimensional harmonic external potential in effective atomic units [117] as

$$v_{0\sigma}(\mathbf{r}) = \frac{1}{2}\omega^2(x^2 + \alpha^2 y^2) \,, \tag{4.25}$$

where ω determines the strength of the confinement, and α defines the elliptical deformation. The harmonic confinement is the standard approximation for electrons in semiconductor QDs. [63] We use the material parameters of GaAs, $m^* = 0.067 m_e$ and $\epsilon = 12.4\epsilon_0$. In practice, the purpose of the ellipticity is to model more realistic QDs that are not perfectly symmetric due to deformations and impurities, etc. For the x-only calculations in Sec. 4.3.2, we set $\alpha = 1.05$ corresponding to an eccentricity of $e \approx 0.30$. These cases are free from degeneracies of the relevant single-particle levels. Whereas in Sec. 4.3.3, we set $\alpha = 1$ to compare with numerically exact results for conventional parabolic QDs – some of these cases include degeneracies. In all the cases, however, we could employ integer occupation numbers.

We carry out all our calculations with the OCTOPUS code [118–120] that solves the KS equations on a regular grid with Dirichlet boundary conditions. We select a grid spacing of $g = 0.1/\sqrt{\omega}$ eff. a.u. The simulation box containing the real-space domain is circular with a radius of $R = K/\sqrt{\omega}$, where $K = 5.0$ eff. a.u. is used for $N = 2, 4, 5$ and $K = \{6.0, 6.5, 7.0, 7.5, 8.0, 8.5\}$ eff. a.u. is used for $N = \{6, 12, 20, 30, 42, 56\}$, respectively. The self-consistent criteria for the solution of the KS equation is $\epsilon_{conv} = \int d\mathbf{r} \left| n^{old}(\mathbf{r}) - n^{new}(\mathbf{r}) \right| / N < 10^{-6}$. We verified numerically that these parameters are sufficient to get fundamental gaps converged within the fourth significant digit.

4.3.2 Exchange-only results

In Fig. 4.1 we show the fundamental gaps resulting from our EXX-KLI calculations for QDs with $N = 2, \ldots, 20$ electrons. The considered confinements are such $\alpha = 1.05$ and $\omega = 0.50$, 1.50, and 2.50, corresponding to the three sets of bars for each N in Fig. 4.1, respectively. We compare the results for the EXX-KLI fundamental gap obtained by means of three different procedures as suggested by Eqs. (4.1), (4.2), and (4.3). According to Fig. 4.1, the values for the gaps given by the aforementioned expressions are relatively close to each other in all cases. We stress that no deviations would be observed if the exact xc-energy functional could be used. These results support in particular the usefulness of Eq. (4.3), which corresponds to the simplest procedure [see also Eq. (4.22)].

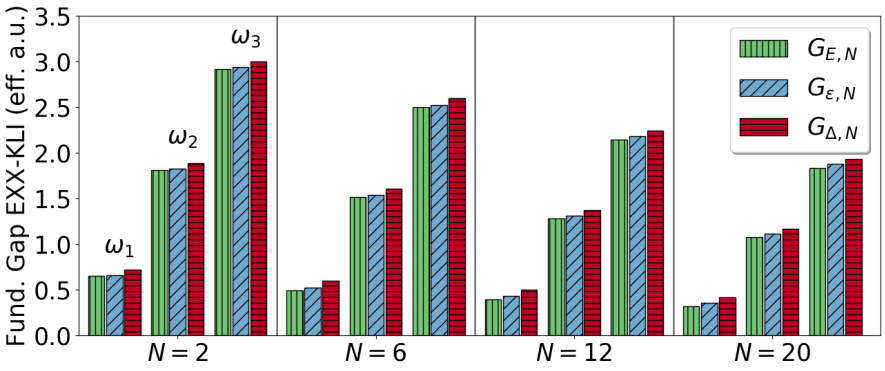

FIGURE 4.1: EXX-KLI results for the fundamental gaps computed according to $G_{\mathrm{E,N}}$ [Eq. (4.1)], $G_{\varepsilon,\mathrm{N}}$ [Eq. (4.2)], and $G_{\Delta,\mathrm{N}}$ [Eq. (4.3) together with Eq. (4.22)]. For each N, we have $\omega_1 = 0.50$, $\omega_2 = 1.50$, and $\omega_3 = 2.50$. In each case we set $\alpha = 1.05$ [see Eq. (4.25)].

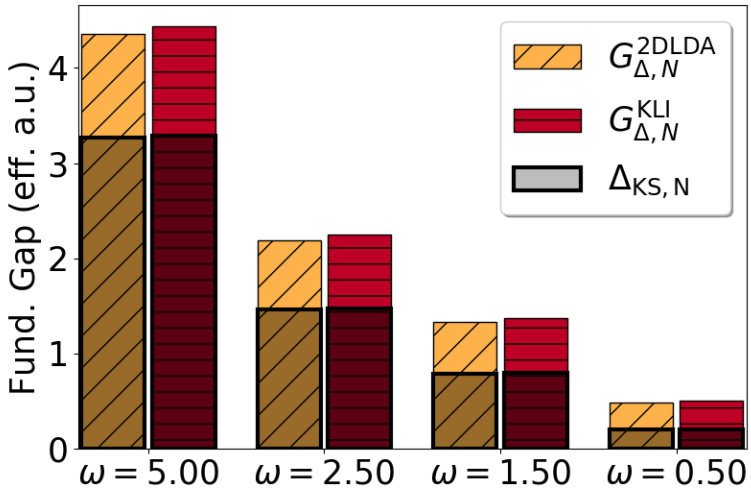

FIGURE 4.2: Fundamental gaps $G_{\Delta,N}$ obtained with the exchange-only KLI and 2DLDA approximations, respectively, for elliptic quantum dots [Eq. (4.25) with $\alpha = 1.05$] with $N = 12$ electrons and varying confinement strength ω. The contributions of the Kohn-Sham gap [Eq. (4.4)] are marked by shaded open boxes. The remaining part is given by the discontinuity, that is, Eq. (4.22) and Eq. (4.23) in the case of KLI and 2DLDA, respectively. All the numerical results are given in Tab. 4.1.

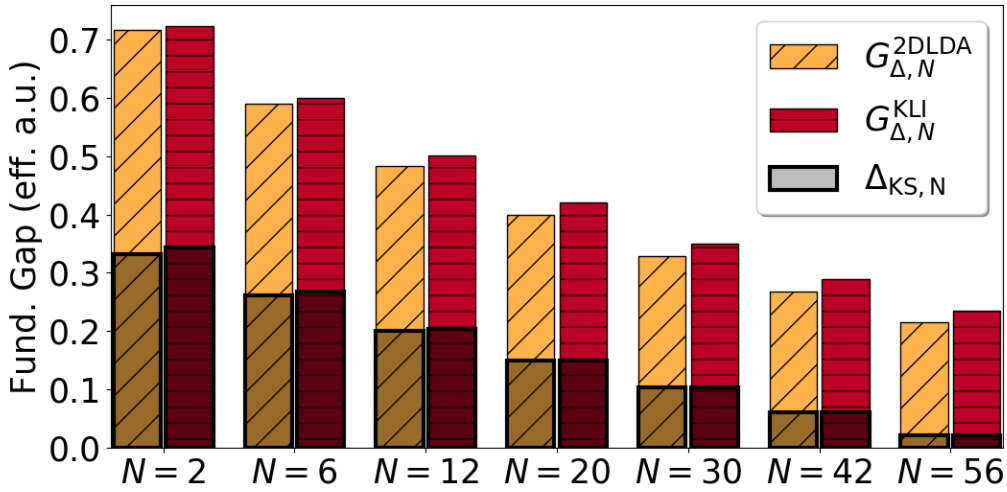

FIGURE 4.3: Same as Fig. (4.2) but for a fixed value of the confinement strength $\omega = 0.5$ and varying number of electrons N.

Next we compare our EXX-KLI results based on Eq. (4.22) with the simpler and numerically more efficient 2DLDA calculations as performed according to Eq. (4.23). The results are reported in Tab. 4.1 in the Appx. Some of the key results are visualized for fixed $N = 12$ and variable ω in Fig. 4.2, and for fixed $\omega = 0.5$ and variable N in Fig. 4.3. Generally, the 2DLDA values computed according to Eqs. (4.4) and (4.23) agree well with the EXX-KLI approximation: the mean relative absolute deviations being only 4%, with a maximum deviation of 8%. The 2DLDA errors in the fundamental gap are mostly due to Δ_x. This can be seen in the KS gaps (open boxes in Figs. 4.2 and 4.3) that are in most cases very close to each other. Equation (4.23) underestimates the EXX-KLI discontinuity but *only slightly* in most cases.

4.3.3 Results including correlations

Finally, we consider the full gaps when including correlations. We consider parabolic QDs by setting $\alpha = 1$ in Eq. (4.25) and compare our results against full configuration interaction results reported in Ref. [76]. Although alternative methodologies to direct exact diagonalization have been developed [121], large benchmark data sets are still challenging to be produced.

Fig. 4.4 shows the results for $\omega = 0.35$ and $N = 2 \ldots 6$. All the values – along with additional cases for different ω – can be found in Tab. 4.2 of the Appx. Since the values of the exact KS gaps are not available, KS gaps are not highlighted. The agreement between our scheme and the many-body (MB) results is reasonable with a mean absolute error of 14%.
We stress that our procedure exploits Eq. (4.24) as in $G^{2DLDA}_{\Delta,N} = \Delta^{2DLDA}_{KS,N} + \Delta^{2DLDA}_{xc,N} = \widetilde{\varepsilon}^{2DLDA}_{H\sigma,N+1} - \varepsilon^{2DLDA}_{H\sigma,N}$, while the 2DLDA procedure of Ref. [76] – for which data is also shown both Fig. (4.4) and in Tab. 4.2 of the Appx. – computes $G^{2DLDA}_{\varepsilon,N} = \varepsilon^{2DLDA}_{H\sigma,N+1} - \varepsilon^{2DLDA}_{H\sigma,N}$. Thus when comparing $G^{2DLDA}_{\Delta,N}$ with $G^{2DLDA}_{\varepsilon,N}$, the systematic overestimation

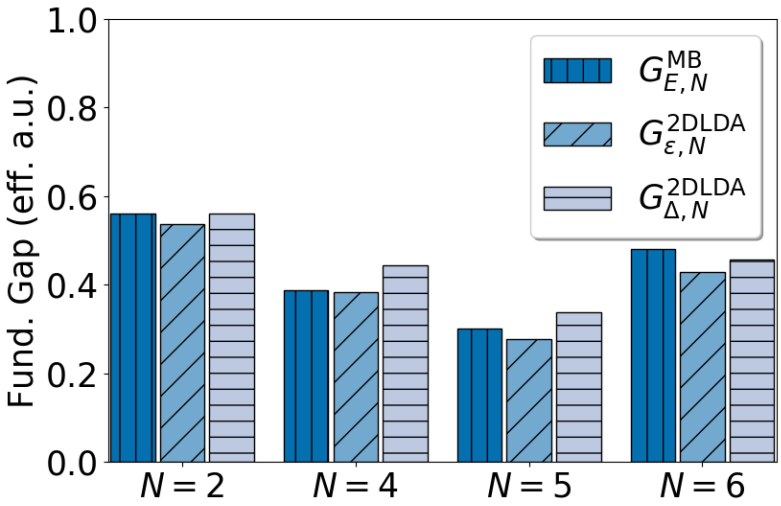

FIGURE 4.4: Fundamental gaps including correlations for parabolic quantum dots [Eq. (4.25) with $\alpha = 1$] with a fixed confinement strength of $\omega = 0.35$ and variable number of electrons N. $G^{\mathrm{MB}}_{E,N}$ is the full configuration interaction value from Ref. [76]; $G^{\mathrm{2DLDA}}_{\epsilon,N}$ is obtained from Eq. (4.2) at the 2DLDA level; $G^{\mathrm{2DLDA}}_{\Delta,N}$ from Eq. (4.24). See also Tab. 4.2.

$G^{\mathrm{2DLDA}}_{\Delta,\mathrm{N}} \geq G^{\mathrm{2DLDA}}_{\varepsilon,\mathrm{N}}$ may be explained in terms of the lack of relaxation of the frozen orbitals which are used in Eq. (4.24).

4.4 Conclusions and outlook

In this work, we have given evidence that the fundamental gaps of artificially confined systems such as semiconductor quantum dots can be accurately estimated by means of a simple procedure within a minimal computational effort: a regular Kohn-Sham calculation plus a straightforward non-self-consistent (one-shot) evaluation – all carried within the local-density approximation. Specifically, we have considered the case of quantum dots defined by parabolic and elliptical confinements.

It would be interesting to explore whether our conclusions can apply also to a larger variety of artificially confined nanoscale systems. Corrections in the form of the gradients of the particle-density may help to preserve accuracy without substantially increasing the numerical effort. But functional forms that explicitly depend only on the particle density and, possibly, gradients thereof, can still fail in the case of periodic systems [101] for which, an approach based on forms considered in Refs. [86, 89, 101] (if properly extended also to lower dimensions) appears to be the most promising.

4.A Derivation of Equation (4.22)

Let us start with the self-consistent EXX-KLI solution of a closed-shell N-electron system. As before, we assume non degeneracy for the relevant occupied and unoccupied single-particle levels (within each spin channel).
Next, let us add one electron to the system and keep the single-particle orbitals *frozen*; i.e., equal to the orbitals of the N-electron system. Let the 'additional' electron be in the spin channel σ. The spin density for the $(N+1)$-electron system is, thus, given by $\widetilde{n}_\sigma = n_\sigma + |\widetilde{\varphi}_{\mathrm{H}\sigma,\mathrm{N}+1}|^2$, where $\widetilde{\varphi}_{\mathrm{H}\sigma,\mathrm{N}+1} \equiv \varphi_{\mathrm{L}\sigma,\mathrm{N}}$ and n_σ is the spin-density of the N-electron system. No modification needs to be considered in the *other* spin channel. The corresponding x-potential, $v_{\mathrm{x}\sigma}[\underline{\widetilde{n}}]$, can be readily expressed in the EXX-KLI approximation [see Sec. 4.2.1]. We remind that $v_{\mathrm{x}\sigma}[\underline{\widetilde{n}}]$ may be shifted by a constant in such a way

$$\langle v_{\mathrm{x}\sigma}[\underline{\widetilde{n}}]\rangle_{\mathrm{H}\sigma} - \langle u_{\mathrm{xH}\sigma}[\underline{\widetilde{n}}]\rangle_{\mathrm{H}\sigma} \equiv 0\,. \tag{4.A.1}$$

Now, let us consider the single-particle energies

$$\widetilde{\varepsilon}^{\mathrm{KLI}}_{\mathrm{H}\sigma,\mathrm{N}+1} = \langle \hat{h}_{0\sigma} + v_{\mathrm{H}}[\widetilde{n}] + v^{\mathrm{KLI}}_{\mathrm{x}\sigma}[\underline{\widetilde{n}}]\rangle_{\mathrm{H}\sigma} \tag{4.A.2}$$

for the HOMO of the system with $N+1$ electrons, and

$$\varepsilon^{\mathrm{KLI}}_{\mathrm{L}\sigma,\mathrm{N}} = \langle \hat{h}_{0\sigma} + v_{\mathrm{H}}[n] + v^{\mathrm{KLI}}_{\mathrm{x}\sigma}[\underline{n}]\rangle_{\mathrm{L}\sigma} \tag{4.A.3}$$

for the LUMO of the system with N electrons. Note that $\hat{h}_{0\sigma}(\mathbf{r}) = -\nabla^2/2 + v_{0\sigma}(\mathbf{r})$ and $v_{\mathrm{H}}[\widetilde{n}] = v_{\mathrm{H}}[n] + v_{\mathrm{H}}[|\widetilde{\varphi}_{\mathrm{H}\sigma,\mathrm{N}+1}|^2]$. Thus the difference of Eq. (4.A.2) and Eq. (4.A.3) can be readily written as follows

$$\begin{aligned} \widetilde{\varepsilon}^{\mathrm{KLI}}_{\mathrm{H}\sigma,\mathrm{N}+1} - \varepsilon^{\mathrm{KLI}}_{\mathrm{L}\sigma,\mathrm{N}} &= \langle v^{\mathrm{KLI}}_{\mathrm{x}\sigma}[\underline{\widetilde{n}}]\rangle_{\mathrm{H}\sigma} - \langle v^{\mathrm{KLI}}_{\mathrm{x}\sigma}[\underline{n}]\rangle_{\mathrm{L}\sigma} \\ &+ \langle v_{\mathrm{H}}[|\varphi_{\mathrm{L}\sigma,\mathrm{N}}|^2]\rangle_{\mathrm{L}\sigma}. \end{aligned} \tag{4.A.4}$$

Next, Eq. (4.A.1) together with the identity

$$\langle u_{\mathrm{xH}\sigma}[\underline{\widetilde{n}}]\rangle_{\mathrm{H}\sigma} \equiv \langle u_{\mathrm{xL}\sigma}[\underline{n}]\rangle_{\mathrm{L}\sigma} - \langle v_{\mathrm{H}}[|\varphi_{\mathrm{L}\sigma,\mathrm{N}}|^2]\rangle_{\mathrm{L}\sigma}, \tag{4.A.5}$$

which can be derived from Eq. (4.15), allow us to rewrite Eq. (4.A.4) as follows

$$\widetilde{\varepsilon}^{\mathrm{KLI}}_{\mathrm{H}\sigma,\mathrm{N}+1} - \varepsilon^{\mathrm{KLI}}_{\mathrm{L}\sigma,\mathrm{N}} = \langle u_{\mathrm{xL}\sigma}[\underline{n}]\rangle_{\mathrm{L}\sigma} - \langle v^{\mathrm{KLI}}_{\mathrm{x}\sigma}[\underline{n}]\rangle_{\mathrm{L}\sigma}\,. \tag{4.A.6}$$

Note that in the steps above, we have repeatedly used $\widetilde{\varphi}_{\mathrm{H}\sigma,\mathrm{N}+1} \equiv \varphi_{\mathrm{L}\sigma,\mathrm{N}}$.

Evaluating Eq. (4.14) on EXX-KLI quantities and comparing with Eq. (4.A.6), we conclude that

$$\Delta^{\mathrm{KLI}}_{\mathrm{x,N}} \equiv \widetilde{\varepsilon}^{\mathrm{KLI}}_{\mathrm{H}\sigma,\mathrm{N}+1} - \varepsilon^{\mathrm{KLI}}_{\mathrm{L}\sigma,\mathrm{N}}\,. \tag{4.A.7}$$

Note, the KLI approximation is not essential – it is used here for simplicity. Correlation forms restricted to have an explicit dependence only on occupied orbitals may also be easily accommodated.

4.B Tables of the numerical results

		Δ_{KS}		$\Delta_{\mathrm{x}} := \widetilde{\varepsilon}_{\mathrm{H,N+1}} - \varepsilon_{\mathrm{L,N}}$		$\Delta_{\mathrm{KS}} + \Delta_{\mathrm{x}}$	
ω	N	2DLDA	KLI	2DLDA	KLI	2DLDA	KLI
5.00	2	4.31	4.37	1.30	1.33	5.61	5.70
5.00	6	3.77	3.81	1.19	1.23	4.96	5.03
5.00	12	3.27	3.29	1.09	1.15	4.36	4.44
5.00	20	2.82	2.82	0.99	1.07	3.80	3.90
5.00	30	2.38	2.38	0.90	1.01	3.28	3.39
5.00	42	1.95	1.95	0.84	0.95	2.79	2.90
5.00	56	1.54	1.53	0.79	0.90	2.32	2.43
2.50	2	2.04	2.08	0.91	0.92	2.95	3.00
2.50	6	1.73	1.76	0.82	0.84	2.55	2.59
2.50	12	1.46	1.47	0.73	0.77	2.19	2.25
2.50	20	1.21	1.22	0.66	0.72	1.87	1.93
2.50	30	0.98	0.98	0.60	0.67	1.58	1.65
2.50	42	0.75	0.75	0.55	0.63	1.31	1.38
2.50	56	0.54	0.53	0.52	0.59	1.06	1.13
1.50	2	1.16	1.19	0.69	0.70	1.85	1.89
1.50	6	0.97	0.98	0.62	0.63	1.58	1.61
1.50	12	0.79	0.80	0.54	0.58	1.33	1.37
1.50	20	0.64	0.64	0.48	0.53	1.12	1.17
1.50	30	0.49	0.49	0.44	0.49	0.93	0.98
1.50	42	0.36	0.35	0.41	0.46	0.76	0.81
1.50	56	0.23	0.23	0.38	0.43	0.61	0.65
0.50	2	0.33	0.34	0.38	0.38	0.72	0.72
0.50	6	0.26	0.27	0.33	0.33	0.59	0.60
0.50	12	0.20	0.20	0.28	0.30	0.48	0.50
0.50	20	0.15	0.15	0.25	0.27	0.40	0.42
0.50	30	0.10	0.10	0.23	0.25	0.33	0.35
0.50	42	0.06	0.06	0.21	0.23	0.27	0.29
0.50	56	0.02	0.02	0.19	0.21	0.21	0.23

TABLE 4.1: Fundamental gaps of elliptic quantum dots [Eq. (4.25) with $\alpha = 1.05$] are reported together with the the contributions of the corresponding Kohn-Sham (KS) gap and exchange-only (x) discontinuities within two procedure that employ either the KLI or the local-density approximation. For the x-discontinuities, the KLI calculations use Eq. (4.22) while the 2DLDA calculations use Eq. (4.23). Values in effective atomic units [117].

N	ω	$G^{\mathrm{2DLDA}}_{\Delta,N}$	$G^{\mathrm{2DLDA}}_{\varepsilon,N}$	$G^{\mathrm{MB}}_{E,N}$
2	0.35	0.56	0.53	0.56
4	0.15	0.26	0.22	0.22
4	0.25	0.36	0.31	0.32
4	0.35	0.44	0.38	0.39
5	0.15	0.21	0.17	0.20
5	0.25	0.28	0.23	0.24
5	0.35	0.34	0.28	0.30
6	0.15	0.23	0.21	0.25
6	0.25	0.35	0.32	0.38
6	0.35	0.46	0.43	0.48

TABLE 4.2: Fundamental gaps of parabolic quantum dots [Eq. (4.25) with $\alpha = 1$]. N. $G^{\mathrm{2DLDA}}_{\Delta,N}$ is obtained from Eq. (4.24); $G^{\mathrm{2DLDA}}_{\epsilon,N}$ from Eq. (4.2) at the 2DLDA level; $G^{\mathrm{MB}}_{E,N}$ is the full configuration interaction value from Ref. [76]. Values in effective atomic units [117].

Chapter 5

Potential approximation for two-dimensional systems with an explicit discontinuity at integer particle numbers

In density-functional theory (DFT), the accuracy and reliability of results strictly depend on the proper choice of the exchange-correlation (xc) functional approximation. Many advances have been achieved beyond the local-density approximation (LDA) by generalized-gradient approximations (GGAs), meta-GGAs (mGGAs), orbitals functionals and hybrid functionals [37]. Most of these functionals rely on three-dimensional (3D) reference systems, such as the 3D uniform electron gas.

Since 1970s, low-dimensional nanostructures have started to emerge. Prototypical two-dimensional (2D) systems are semiconductor layers and surfaces, quantum Hall systems, spintronic devices, quantum dots (QDs) [63], quantum rings and artificial graphene (AG) [122]. These systems are usually referred as "purely" 2D, i.e. their electrons are treated as 2D fermionic particles. The physical reason for this is that the confinement along one direction (say z) is typically much stronger than along the other two spatial dimensions. This results in a quantum-mechanical suppression of the degrees of freedom along the z direction and the system becomes effectively 2D.

Conventional 3D functional approximations perform poorly or breakdown when applied to 2D systems, as confirmed by previous studies [123, 124]. This is because the 3D electron gas is not an appropriate starting point for the study of 2D systems. The exact-exchange approximation (EXX) – that is not based on a particular reference system – automatically conforms to various dimensionalities. However, a proper approximation for the correlation energy compatible with EXX and computationally feasible is still a challenge. These considerations encouraged the development of xc-functional approximations based on 2D reference systems, such as the 2DLDA [114–116]. After that, several other 2D functionals have been proposed in the literature [112, 113, 125–142]. 2D functional approximations are usually derived by properly converting a "regular" 3D functional to the 2D world. This is the case, for example, of the 2DB88 [135] approximation, that is the 2D counterpart of B88 [38] approximation.

For 3D solids, much effort has been spent to develop functional approximations able to accurately describe the band gap without explicitly carrying out many-body perturbation theory calculations. Among different proposals [143], the GLLB-SC potential [144] has received great attention in the literature. In fact, it can predict the band gap of 3D semiconductors at a level of accuracy comparable to the one of benchmark GW calculations, while requiring the same computational effort of a standard semi-local approximation [144].

In this chapter, we construct a new potential approximation for 2D systems derived in the spirit of the GLLB-SC potential [144] and its precursor made by Gritsenko *et al.* [145] (GLLB). To be consistent with previous functional nomenclature, we refer to the new approximation as the 2DGLLB potential. In Sec. 5.1, the 2DGLLB potential is derived. Particular attention is given to the discontinuity of the 2DGLLB potential at integer electron numbers, as it plays a central role in the determination of the fundamental gap. Next, in Sec. 5.2, we test the accuracy of the 2DGLLB potential in the evaluation of the fundamental gap of both finite and periodic 2D nanostructures. Computational details are given in Sec. 5.3. Finally, conclusions are summarized in Sec. 5.4.

5.1 Theory

Following the original derivation of GLLB and GLLB-SC approximations, the derivation of the 2DGLLB potential is done within the spin-restricted formalism of DFT. The extension to the spin-unrestricted case is straightforward. In DFT, the total energy functional E of a 2D system composed by N interacting electrons is

$$E[n] = T_{\mathrm{KS}}[n] + \int d^2r v_0(\mathbf{r})n(\mathbf{r}) + E_{\mathrm{H}}[n] + E_{\mathrm{xc}}[n], \tag{5.1.1}$$

where v_0 is the external potential, $T_{\mathrm{KS}}[n]$ is the kinetic energy of the Kohn-Sham (KS) system

$$T_{\mathrm{KS}}[n] = \sum_{j=1}^{N} \int d^2r \varphi_j^*(\mathbf{r}) \left(-\frac{\nabla^2}{2}\right) \varphi_j(\mathbf{r}), \tag{5.1.2}$$

$E_{\mathrm{H}}[n]$ is the Hartree energy

$$E_{\mathrm{H}}[n] = \frac{1}{2} \int d^2r \int d^2r' \frac{n(\mathbf{r})n(\mathbf{r}')}{|\mathbf{r}-\mathbf{r}'|} \tag{5.1.3}$$

and $E_{\mathrm{xc}}[n]$ is the exchange-correlation (xc) energy.
The position operator is defined in two dimensions, $\mathbf{r} = (x, y)$. Thus, the Laplacian in Eq. (5.1.2) is $\nabla^2 = \partial_x^2 + \partial_y^2$.
The single-particle KS orbitals $\{\varphi_j\}$ satisfy the KS equations

$$\left[-\frac{\nabla^2}{2} + v_0(\mathbf{r}) + v_{\mathrm{H}}[n](\mathbf{r}) + v_{\mathrm{xc}}[n](\mathbf{r})\right] \varphi_j(\mathbf{r}) = \epsilon_j \varphi_j(\mathbf{r}), \tag{5.1.4}$$

where v_{H} is the Hartree potential

$$v_{\mathrm{H}}[n](\mathbf{r}) = \int d^2r' \frac{n(\mathbf{r}')}{|\mathbf{r}-\mathbf{r}'|} \tag{5.1.5}$$

and $v_{\rm xc}[n]$ is the xc potential

$$v_{\rm xc}[n](\mathbf{r}) = \frac{\delta E_{\rm xc}[n]}{\delta n(\mathbf{r})}. \tag{5.1.6}$$

The electron density n is obtained from the KS orbitals as

$$n(\mathbf{r}) = \sum_{j=1}^{N} |\varphi_j(\mathbf{r})|^2. \tag{5.1.7}$$

The starting point of the derivation of the 2DGLLB potential is the exchange-correlation energy functional $E_{\rm xc}[n]$ expressed in terms of the xc hole as

$$E_{\rm xc}[n] = \frac{1}{2}\int d^2r' \int d^2r'' n(\mathbf{r}')n(\mathbf{r}'')\frac{[\bar{g}_{\rm xc}[n](\mathbf{r}',\mathbf{r}'')-1]}{|\mathbf{r}'-\mathbf{r}''|}, \tag{5.1.8}$$

where $\bar{g}_{\rm xc}$ is the xc hole function averaged over the coupling-constant integration [37]. If we perform the functional derivative of Eq. (5.1.8), in order to get the xc potential $v_{\rm xc}$ through Eq. (5.1.6), we may distinguish two terms

$$v_{\rm xc}[n](\mathbf{r}) = v_{\rm xc,scr}[n](\mathbf{r}) + v_{\rm xc,resp}[n](\mathbf{r}), \tag{5.1.9}$$

where the first is called screening potential

$$v_{\rm xc,scr}[n](\mathbf{r}) = \int d^2r' n(\mathbf{r}')\frac{[\bar{g}_{\rm xc}[n](\mathbf{r},\mathbf{r}')-1]}{|\mathbf{r}-\mathbf{r}'|} \tag{5.1.10}$$

and the second is called response potential

$$v_{\rm xc,resp}[n](\mathbf{r}) = \frac{1}{2}\int d^2r' \int d^2r'' \frac{n(\mathbf{r}')n(\mathbf{r}'')}{|\mathbf{r}'-\mathbf{r}''|}\frac{\delta \bar{g}_{\rm xc}[n](\mathbf{r}',\mathbf{r}'')}{\delta n(\mathbf{r})}. \tag{5.1.11}$$

$v_{\rm xc,scr}$ has a smooth attractive form, with long-range behavior $v_{\rm xc,scr} \to -1/r$ as $r \to +\infty$. Instead, the response part of the potential $v_{\rm xc,resp}$ originates from the first order response of the xc hole $\delta\bar{g}_{\rm xc}$ due to the infinitesimal density variation δn. $v_{\rm xc,resp}$ is repulsive, short-ranged and it shows a stepped structure induced by the steps in the pair-correlation function.
The idea of GLLB was to approximate separately the screening and response parts of the x potential in order to better reproduce their different behaviors. Here, we follow the same strategy. In addition, we include a correlation term in order to construct an xc potential. Thus, the potential is split into four parts: $v_{\rm x,scr}$, $v_{\rm x,resp}$, $v_{\rm c,scr}$ and $v_{\rm c,resp}$.

5.1.1 Exchange potential

We start by constructing the exchange part of the potential. Following GLLB [145], we use the Krieger-Li-Iafrate (KLI) approximation [47] as a reference

$$v_{\rm x}^{\rm KLI}[n](\mathbf{r}) = v_{\rm x,scr}^{\rm KLI}[n](\mathbf{r}) + v_{\rm x,resp}^{\rm KLI}[n](\mathbf{r}), \tag{5.1.12}$$

where $v_{\mathrm{x,scr}}^{\mathrm{KLI}}[n](\mathbf{r}) \equiv v_{\mathrm{x}}^{\mathrm{Slater}}[n](\mathbf{r})$ is the Slater potential. Instead, the response part is

$$v_{\mathrm{x,resp}}^{\mathrm{KLI}}[n](\mathbf{r}) = \sum_{i=1}^{N} w_i \frac{|\varphi_i(\mathbf{r})|^2}{n(\mathbf{r})}, \tag{5.1.13}$$

where

$$w_i = \int d^2r \left[v_{\mathrm{x}}^{\mathrm{KLI}}[n](\mathbf{r}) - u_{\mathrm{x}i}[n](\mathbf{r})\right] |\varphi_i(\mathbf{r})|^2 \tag{5.1.14}$$

are computed self-consistently with Eq. (5.1.12). In Eq. (5.1.14), we have

$$u_{\mathrm{x}i}[n](\mathbf{r}) = -\sum_{j=1}^{N} \frac{\varphi_j(\mathbf{r})}{\varphi_i^*(\mathbf{r})} \int d^2r' \frac{\varphi_i^*(\mathbf{r}')\varphi_j(\mathbf{r}')}{|\mathbf{r}-\mathbf{r}'|}. \tag{5.1.15}$$

We model the response exchange potential using the KLI expression

$$v_{\mathrm{x,resp}}^{\mathrm{2DGLLB}}[n](\mathbf{r}) \equiv \sum_{i=1}^{N} w_i^{\mathrm{2DGLLB}} \frac{|\varphi_i(\mathbf{r})|^2}{n(\mathbf{r})}, \tag{5.1.16}$$

but with approximate coefficients

$$w_i^{\mathrm{2DGLLB}} = K_{\mathrm{x}}^{\mathrm{2D}} \sqrt{\mu - \epsilon_i}, \tag{5.1.17}$$

where μ is the chemical potential and $K_{\mathrm{x}}^{\mathrm{2D}}$ is a numerical constant. In this section, we consider a finite system, thus the chemical potential $\mu \equiv \epsilon_{\mathrm{H}}$ is the energy of the highest occupied molecular orbital (HOMO). The value $K_{\mathrm{x}}^{\mathrm{2D}} = \sqrt{2}/\pi \approx 0.4502$ is fixed by imposing Eq. (5.1.16) exact for the 2D uniform electron gas. We refer to Appx. 5.A for the derivation of $K_{\mathrm{x}}^{\mathrm{2D}}$.
Eq. (5.1.16) reproduces some of the exact conditions of the response part of the exchange potential: (i) it vanishes asymptotically (since $w_N^{\mathrm{2DGLLB}} = 0$); (ii) it scales linearly under uniform coordinate scaling; (iii) it shows a stepped structure; (iv) it has a non-vanishing discontinuity at integer electron number (see below).

The 2DB88 approximation [135] offers an ideal simplification for $v_{\mathrm{x,scr}}$ as it reproduces the correct asymptotic behavior $v_{\mathrm{x,scr}} \to -1/r$ for $r \to +\infty$ and accurate total exchange energies. Therefore, we write

$$v_{\mathrm{x,scr}}^{\mathrm{2DGLLB}}[n](\mathbf{r}) \equiv v_{\mathrm{x,scr}}^{\mathrm{2DB88}}[n](\mathbf{r}) = 2\epsilon_{\mathrm{x}}^{\mathrm{2DB88}}[n](\mathbf{r}), \tag{5.1.18}$$

where $\epsilon_{\mathrm{x}}^{\mathrm{2DB88}}[n](\mathbf{r})$ is the exchange energy density of the 2DB88 approximation.

5.1.2 Correlation potential

In the original paper of GLLB, only the exchange part of the potential is discussed. By following instead the derivation of the GLLB-SC potential, we consider a correlation term that is local or semi-local in the density. By invoking the 2DLDA [114–116], we have

$$v_{\mathrm{c,scr}}^{\mathrm{2DGLLB}}[n](\mathbf{r}) \equiv v_{\mathrm{c,scr}}^{\mathrm{2DLDA}}[n](\mathbf{r}) = 2\epsilon_{\mathrm{c}}^{\mathrm{2DLDA}}[n](\mathbf{r}), \tag{5.1.19}$$

where $\epsilon_{\mathrm{c}}^{\mathrm{2DLDA}}$ is the correlation energy density of the 2DLDA approximation, and

$$v_{\mathrm{c,resp}}^{\mathrm{2DGLLB}}[n](\mathbf{r}) \equiv v_{\mathrm{c,resp}}^{\mathrm{2DLDA}}[n](\mathbf{r}) = v_{\mathrm{c}}^{\mathrm{2DLDA}}[n](\mathbf{r}) - v_{\mathrm{c,scr}}^{\mathrm{2DLDA}}[n](\mathbf{r}). \tag{5.1.20}$$

5.1.3 Model xc potential

By combining all the different terms of the 2DGLLB potential [Eqs. (5.1.16), (5.1.18), (5.1.19), (5.1.20)], we finally write

$$v_{\mathrm{xc}}^{\mathrm{2DGLLB}}[n](\mathbf{r}) = \sum_{i=1}^{N} K_{\mathrm{x}}^{\mathrm{2D}} \sqrt{\mu - \epsilon_i} \frac{|\varphi_i(\mathbf{r})|^2}{n(\mathbf{r})} + 2\epsilon_{\mathrm{x}}^{\mathrm{2DB88}}[n](\mathbf{r}) + v_{\mathrm{c}}^{\mathrm{2DLDA}}[n](\mathbf{r}). \quad (5.1.21)$$

In summary, the proposed 2DGLLB approximation is a simplification of the KLI approximation for exchange. For correlation, we use the correlation term of the 2DLDA, which is consistent with the screening exchange part of the potential.

5.1.4 Discontinuity of the xc potential

By invoking Ensemble-DFT (EDFT) [49–51], the fundamental gap can be expressed as the sum of two contributions

$$G_\Delta = \Delta_{\mathrm{KS}} + \Delta_{\mathrm{xc}}, \quad (5.1.22)$$

where $\Delta_{\mathrm{KS}} = \epsilon_{\mathrm{L}} - \epsilon_{\mathrm{H}}$ is the KS gap, and

$$\Delta_{\mathrm{xc}} = \lim_{\delta N \to 0^+} \left\{ v_{\mathrm{xc}}(\mathbf{r})|_{N+\delta N} - v_{\mathrm{xc}}(\mathbf{r})|_{N-\delta N} \right\} \quad (5.1.23)$$

is called discontinuity of the xc potential. We refer to Sec. 4.1 for a more detailed description of the possible ways to obtain the fundamental gap within DFT.

The 2DGLLB potential shows a non-vanishing discontinuity at integer electron numbers due to the response part of the exchange potential $v_{\mathrm{x,resp}}^{\mathrm{2DGLLB}}$ given by Eq. (5.1.16). In fact, by adding a small fraction of electrons δN, the chemical potential μ changes abruptly from ϵ_{H} to ϵ_{L}, where L stands for Lowest Unoccupied Molecular Orbital (LUMO). Thus,

$$\begin{aligned} \Delta_{\mathrm{xc}}^{\mathrm{2DGLLB}}(\mathbf{r}) &= \lim_{\delta N \to 0^+} \left\{ v_{\mathrm{xc}}^{\mathrm{2DGLLB}}(\mathbf{r})\big|_{N+\delta N} - v_{\mathrm{xc}}^{\mathrm{2DGLLB}}(\mathbf{r})\big|_{N-\delta N} \right\} \\ &= \sum_{i=1}^{N} K_{\mathrm{x}}^{\mathrm{2D}} \left(\sqrt{\epsilon_{\mathrm{L}} - \epsilon_i} - \sqrt{\epsilon_{\mathrm{H}} - \epsilon_i} \right) \frac{|\varphi_i(\mathbf{r})|^2}{n(\mathbf{r})}. \end{aligned} \quad (5.1.24)$$

The discontinuity of the 2DGLLB potential depends on the space coordinates, thus affecting the wavefunctions. It is not clear how to correct the KS gap with the help of Eq. (5.1.24), since the true discontinuity should be a constant term independent on the space coordinates.
In the paper where the GLLB-SC approximation is derived [144], first order perturbation theory is applied to the LUMO orbital in order to obtain a correction which is independent on the space coordinates. In our case, this would imply

$$\bar{\Delta}_{\mathrm{xc}}^{\mathrm{2DGLLB}} \equiv \langle \varphi_{\mathrm{L}} | \Delta_{\mathrm{xc}}^{\mathrm{2DGLLB}}(\mathbf{r}) | \varphi_{\mathrm{L}} \rangle \,. \quad (5.1.25)$$

We propose instead to correct the KS gap in Eq. (5.1.22) by evaluating Δ_{xc} with the method discussed in Chap. 4, published in 2019 [66]. Within this framework, which was inspired by the works in Refs. [100, 101], Δ_{xc} assumes the form

$$\Delta_{\mathrm{xc}}^{\mathrm{2DGLLB}} = \tilde{\epsilon}_{\mathrm{H},N+1}^{\mathrm{2DGLLB}} - \epsilon_{\mathrm{L},N}^{\mathrm{2DGLLB}}, \quad (5.1.26)$$

where we remember the tilde superscript ($\sim$) refers to the frozen orbital approximation.
Let us write an equivalent expression to Eq. (5.1.26). The KS energies may be written explicitly in the bracket notation as

$$\epsilon_i = \langle\varphi_i|-\frac{\nabla^2}{2} + v_0 + v_{\mathrm{H}}[n] + v_{\mathrm{xc}}[n]|\varphi_i\rangle\,. \tag{5.1.27}$$

By using Eq. (5.1.27) to express the KS energies in Eq. (5.1.26), we find

$$\begin{aligned}\Delta_{\mathrm{xc}}^{\mathrm{2DGLLB}} = {} & \langle\varphi_{\mathrm{L}}|v_{\mathrm{H}}[n+n_{\mathrm{L}}] - v_{\mathrm{H}}[n]|\varphi_{\mathrm{L}}\rangle \\ & + \langle\varphi_{\mathrm{L}}|v_{\mathrm{xc}}^{\mathrm{2DGLLB}}[n+n_{\mathrm{L}}] - v_{\mathrm{xc}}^{\mathrm{2DGLLB}}[n]|\varphi_{\mathrm{L}}\rangle\end{aligned} \tag{5.1.28}$$

where we used the fact that $\tilde{\varphi}_{\mathrm{H},N+1}^{\mathrm{2DGLLB}} \equiv \varphi_{\mathrm{L},N}^{\mathrm{2DGLLB}}$, i.e. the HOMO of the $N+1$ electron system in the frozen orbital approximation is equal to the LUMO of the N electron system. In Eq. (5.1.28), $n_{\mathrm{L}} = |\varphi_{\mathrm{L}}|^2$.

5.1.5 The case of periodic systems

Here, we discuss the extension of the 2DGLLB potential to periodic systems. The screened-exchange and correlation parts of the potential are taken from local and semilocal approximations, thus their generalization for periodic systems is straightforward. However, the evaluation of $v_{\mathrm{x,resp}}^{\mathrm{2DGLLB}}$ and $\Delta_{\mathrm{xc}}^{\mathrm{2DGLLB}}$ need some cautions. For simplicity, we suppose the system has a finite band gap. The limit case of a semimetal is included. In Eq. (5.1.16), the sum over states i must be considered as a double sum over k points and the occupied bands n

$$v_{\mathrm{x,resp}}^{\mathrm{2DGLLB}}[n](\mathbf{r}) = \sum_{n,\mathbf{k}}^{\mathrm{occ.}} K_{\mathrm{x}}^{\mathrm{2D}} \sqrt{\mu - \epsilon_{n\mathbf{k}}} \frac{|\varphi_{n\mathbf{k}}(\mathbf{r})|^2}{n(\mathbf{r})}, \tag{5.1.29}$$

where $\mu = \epsilon_{\mathrm{H}}$ must be interpreted as the top of the valence band.
The discontinuity of the potential is given by Eq. (5.1.28). In this case, the LUMO of a periodic system must be understood as the bottom of the conduction band.
We now suppose an electron is added to the crystal. As described by Baerends [101, Fig. 3], since the added electron is spread over the all crystal we have $n(N+1) \approx n(N)$, $v_{\mathrm{H}}[n(N+1)] \approx v_{\mathrm{H}}[n(N)]$ and $\varphi_i(N+1) \approx \varphi_i(N)$. At the same time, the chemical potential μ passes from ϵ_{H} (the top of the valence band) to ϵ_{L} (the bottom of the conduction band). By substituting the limit expressions in Eq. (5.1.28), we find

$$\Delta_{\mathrm{xc}}^{\mathrm{2DGLLB}} = \langle\varphi_{\mathrm{L}}|\sum_{n,\mathbf{k}}^{\mathrm{occ}} K_{\mathrm{x}}^{\mathrm{2D}} \left(\sqrt{\epsilon_{\mathrm{L}} - \epsilon_{n\mathbf{k}}} - \sqrt{\epsilon_{\mathrm{H}} - \epsilon_{n\mathbf{k}}}\right) \frac{|\varphi_{n\mathbf{k}}|^2}{n}|\varphi_{\mathrm{L}}\rangle \tag{5.1.30}$$

that is exactly Eq. (5.1.25), i.e. $\Delta_{\mathrm{xc}}^{\mathrm{2DGLLB}} = \bar{\Delta}_{\mathrm{xc}}^{\mathrm{2DGLLB}}$ for periodic systems [101]. We have already shown that the formulation of Δ_{xc} derived in Chap. 4 is appropriate to correct the KS gap for *finite* 2D nanostructures. The similarity between our method (Δ_{xc}) and expressions previously reported in the literature ($\bar{\Delta}_{\mathrm{xc}}$) for 3D periodic systems further justify our approach.

We now consider $\Delta_{\rm xc}^{\rm 2DLDA}$, given by Eq. (4.24) of Chap. 4, in the limit of a periodic system. By substituting the limiting expression to Eq. (4.24), we find

$$\Delta_{\rm xc}^{\rm 2DLDA} = 0. \tag{5.1.31}$$

Thus, the 2DLDA gives a non-vanishing correction only for finite systems, while the 2DGLLB approximation gives a non-vanishing correction also for periodic systems. It is worth noting that the non-vanishing discontinuity of the 2DGLLB potential in Eq. (5.1.30) originates from the response part of the *exchange* potential. As $v_{\rm c}^{\rm 2DGLLB} = v_{\rm c}^{\rm 2DLDA}$ [as can be seen from Eq. (5.1.21)], the correlation part of the discontinuity is zero in both the 2DLDA and 2DGLLB approximations. The use of Eq. (5.1.26) for finite systems and Eq. (5.1.30) for periodic systems results in a unified theoretical framework for the evaluation of $\Delta_{\rm xc}$, thus G_Δ, for low-dimensional nanostructures.
Following Kuisma *et al.* [144], we propose to extend Eq. (5.1.30) for the correction of a generic state in a conduction band n at a given k point as

$$\Delta_{{\rm xc},n\mathbf{k}}^{\rm 2DGLLB} = \langle\varphi_{n\mathbf{k}}|\sum_{n',\mathbf{k}'}^{\rm occ} K_{\rm x}^{\rm 2D}\left(\sqrt{\epsilon_{\rm L}-\epsilon_{n'\mathbf{k}'}}-\sqrt{\epsilon_{\rm H}-\epsilon_{n'\mathbf{k}'}}\right)\frac{|\varphi_{n'\mathbf{k}'}|^2}{n}|\varphi_{n\mathbf{k}}\rangle\ . \tag{5.1.32}$$

5.2 Applications

In this section, we report the first numerical tests of the 2DGLLB potential. In particular, the analysis is focused in the evaluation of the fundamental gap of both finite and periodic nanostructures. First, we consider the same set of QDs in the exchange-only limit already discussed in Sec. 4.3.1. Then, we consider the case of AG. A Kekulé distortion is applied in order to open a gap at the Dirac points.

5.2.1 Quantum dots in the exchange-only limit

As we have done in Sec. 4.3.1, we model the N electrons in a semiconductor QD as 2D fermionic particles confined by an harmonic external potential in the effective atomic units (eff. a.u.) as

$$v_0(\mathbf{r}) = \frac{1}{2}\omega^2(x^2+\alpha^2y^2), \tag{5.2.1}$$

where ω determines the strength of the confinement and α defines the elliptical deformation. The elliptical deformation models the symmetry breaking of a realistic QD due to deformation, impurities, etc. If $\alpha \neq 1$, the degeneracy of the single-particle levels is removed. We use the parameters of GaAs, $m^* = 0.067m_e$ and $\epsilon = 12.4\epsilon_0$. In order to compare the fundamental gaps obtained within the 2DGLLB approximation with the results presented in Sec. 4.3.1, we consider the exchange-only limit, i.e. we set $v_{\rm c}^{\rm 2DGLLB} = 0$.

Before discussing the values obtained for the gaps, it is illustrative to discuss the potentials. In Fig. 5.1, we show the response (left) and screening (right) parts of the 2DGLLB exchange potential of a parabolic QD described by Eq. (5.2.1)

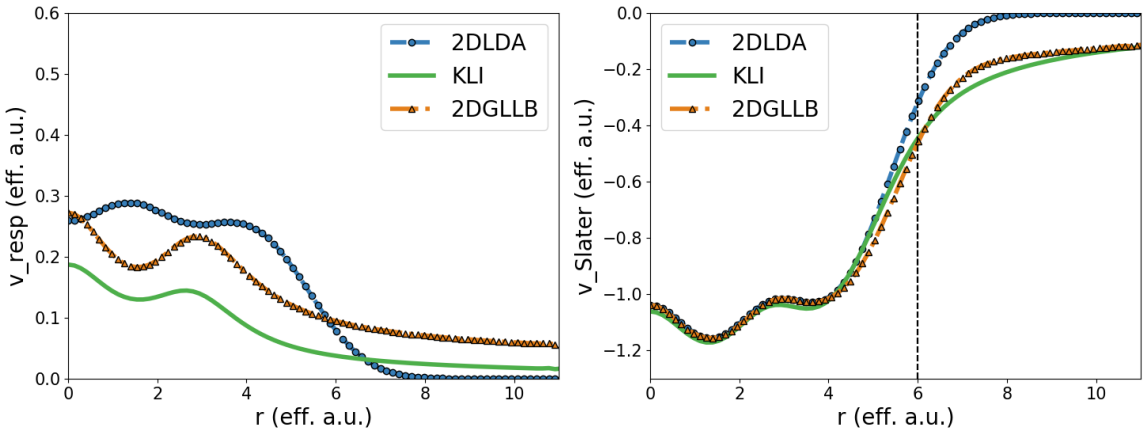

FIGURE 5.1: Non-self-consistent exchange-potential components (left: response part, right: screening part) of a parabolic quantum dot [Eq. (5.2.1) with $\alpha = 1$] with $N = 20$ electrons and strength of confinement $\omega = 0.50$ eff. a.u. obtained at different levels of approximation. We indicate the potentials of the 2DLDA with (circled) blue lines, of 2DGLLB with (triangled) orange lines, and the KLI benchmark with (solid) green lines.

with $\alpha = 1$, $N = 20$ and $\omega = 0.50$. The 2DLDA and KLI potentials are shown for comparison. The potentials are computed non self-consistently starting from the accurate ground state density of the KLI benchmark. $v_{\mathrm{x,resp}}^{\mathrm{2DLDA}}$ is qualitatively wrong, as it shows displaced positions of the maxima and the minima with respect to KLI, e.g., at $r \approx 0$, $v_{\mathrm{x,resp}}^{\mathrm{2DLDA}}$ shows a minimum, while $v_{\mathrm{x,resp}}^{\mathrm{KLI}}$ shows a maximum. Instead, $v_{\mathrm{x,resp}}^{\mathrm{2DGLLB}}$ reproduces the qualitative behavior of $v_{\mathrm{x,resp}}^{\mathrm{KLI}}$. This is due to the fact that $v_{\mathrm{x,resp}}^{\mathrm{2DGLLB}}$, given by Eq. (5.1.16), has the same formal expression as $v_{\mathrm{x,resp}}^{\mathrm{KLI}}$, given by Eq. (5.1.13). The 2DGLLB coefficients w_i^{2DGLLB} overestimate those of KLI, $w_i^{\mathrm{2DGLLB}} > w_i$, thus $v_{\mathrm{x}}^{\mathrm{2DGLLB}} > v_{\mathrm{x}}^{\mathrm{KLI}}$. It seems that a rigid shift of the GLLB potential would increase the accuracy of the KS energies.
The screening part of the KLI potential in the internal region ($r \leq 4$ eff. a.u.) is well reproduced both by the 2DLDA and the 2DGLLB approximation. As expected, the 2DGLLB approximation reproduces the long-range tail of the KLI screening potential, in contrast with 2DLDA. As discussed in the theory section, this is why we choose to approximate the screening part of the potential with that of the 2DB88 [135]. However, the long-range behavior of $v_{\mathrm{x}}^{\mathrm{scr/2DLDA}}$ should not be relevant for energetic calculations, as more of the 98% of the electronic charge is included within 6 eff. a.u. of the dot (dashed vertical line in the plot).

The exchange potentials $v_{\mathrm{x}} = v_{\mathrm{x}}^{\mathrm{resp}} + v_{\mathrm{x}}^{\mathrm{scr}}$ of 2DGLLB, 2DLDA and KLI are compared in Fig. 5.2. Again, the potentials are evaluated non self-consistently at the KLI ground-state density. The 2DLDA generally overestimates the KLI potential for all r, as confirmed by previous results (see e.g. [135, Fig. 5b]). Also the 2DGLLB approximation overestimates the KLI potential due to the fact that $v_{\mathrm{x,resp}}^{\mathrm{2DGLLB}} > v_{\mathrm{x,resp}}^{\mathrm{KLI}}$, as discussed above, but by a lower amount with respect to 2DLDA. Thus, the 2DGLLB potential ranges in between from the 2DLDA and the KLI. The shell structure is also better reproduced by the 2DGLLB approximation with respect

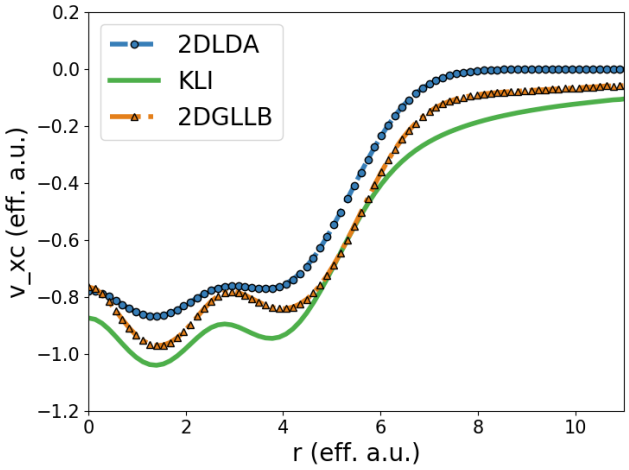

FIGURE 5.2: Non-self-consistent exchange potential of a parabolic quantum dot [Eq. (5.2.1) with $\alpha = 1$] with $N = 20$ electrons and strength of confinement $\omega = 0.50$ eff. a.u. obtained at different levels of approximation. We indicate the potentials of 2DLDA with a (circled) blue line, of 2DGLLB with a (triangled) orange line, and the KLI benchmark with a (solid) green line.

to 2DLDA.

Now, we discuss the performance of the 2DGLLB approximation in the evaluation of the fundamental gap through Eq. (5.1.22) combined with Eq. (5.1.26) on the same set of elliptically confined QDs [Eq. (5.2.1) with $\alpha = 1.05$] given in Tab. 4.1. Some of the key results are summarized in Fig. 5.3 ($N = 12$ and variable ω), and in Fig. 5.4 ($\omega = 0.5$ and variable N). 2DLDA and KLI results, summarized Tab. 4.1, are shown for comparison. Generally, both 2DLDA and 2DGLLB approximation yield accurate results in the whole range considered. This is true also for the KS gap Δ_{KS} (open boxes in Fig. 5.3 and Fig. 5.4) and the discontinuity correction Δ_{x} (remaining part) taken separately. We note the 2DLDA always underestimate the KLI values. Instead, 2DGLLB results slightly overestimate the gap at low N, while it slightly underestimates the gap at high N. In particular, 2DLDA performs slightly better at low N, while the 2DGLLB approximation performs slightly better at high N. With respect to KLI values, we found a mean relative absolute error of 3% for the 2DGLLB gaps and 4% for the 2DLDA gaps. Thus, we conclude that the 2DGLLB potential gives more accurate results than the 2DLDA for the test case considered. However, since the differences are small, we conclude that both the 2DLDA and the 2DGLLB approximation estimate the fundamental gap of low-dimensional QDs in the exchange limit at a good level of accuracy.

5.2.2 Artificial graphene with Kekule distortion

AG refers to any physical system composed by quantum elements arranged in a (man-made) honeycomb lattice [122, 146–148]. For what concerns this section, we consider AG realized with nanopatterned two-dimensional electron gas in GaAs

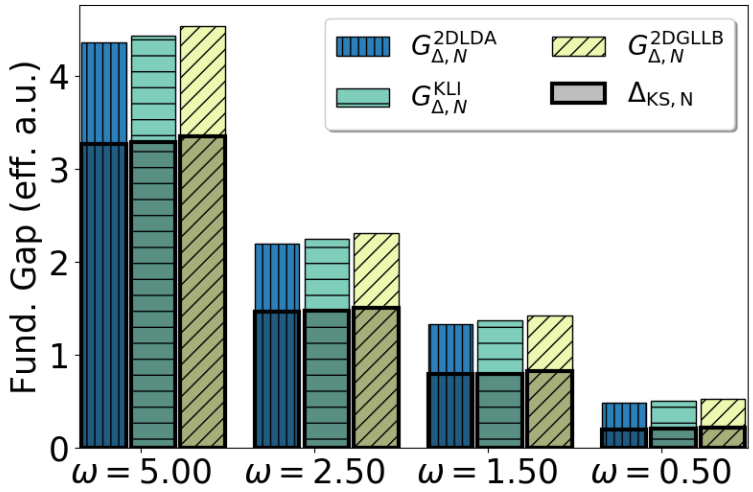

FIGURE 5.3: Fundamental gaps G_Δ of elliptic quantum dots [Eq. (4.25) with $\alpha = 1.05$] with $N = 12$ electrons and varying confinement strength ω obtained at different levels of approximation. The blue bars (vertical lines) indicate the fundamental gaps obtained within 2DLDA, the yellow bars (oblique lines) refer to the 2DGLLB approximation, and the green bars (horizontal lines) to the KLI benchmark. The contributions of the KS gaps are marked by shaded boxes. The remaining parts are the discontinuity contributions, given by Eq. (4.23), Eq. (5.1.26), and Eq. (4.22) in the case of LDA, GLLB and KLI, respectively.

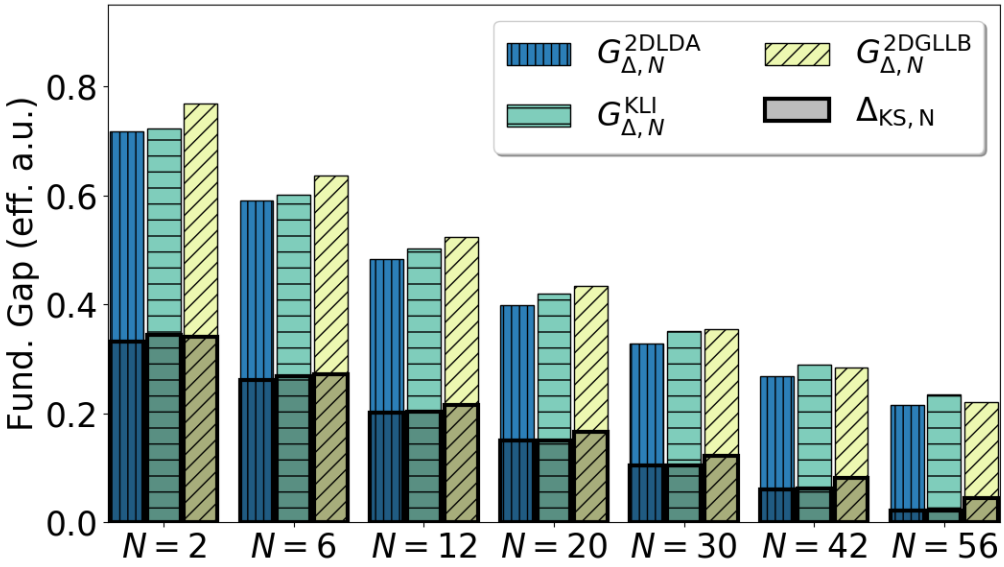

FIGURE 5.4: Same as Fig. (5.3) but for a fixed value of the confinement strength $\omega = 0.5$ and varying number of electrons N.

heterostructures [149–152]. As the topology is the same of graphene, Dirac cones can emerge in the band structures.
The geometry of AG can be easily modified, leading to tunable band structures that can be used to design new materials with specific electronic properties. Kekulé distortion is a possible way to tune the electronic structure of AG and open a band gap at the Dirac points [122].
As a test of our 2DGLLB potential, we study the fundamental gap at the Dirac points of AG Kekulé distorted. 2DLDA results are shown for comparison.

We model semiconductor AG with DFT in the spin-restricted framework in the same way as previous studies in the literature [152, 153]. The electrons are described as 2D particles in the effective mass approximation (as we have done in the previous section and Chap. 4). We select $m^* = 0.067m_0$ and $\epsilon = 12.4\epsilon_0$, which are the numerical parameters of GaAs. In the left side of Fig. 5.5, we show the rectangular unit cell composed by four QDs. Since we are not considering the primitive cell, that in AG is composed by two QDs, the bands have to be unfolded as explained in Ref. [152, Fig. 2]. The lattice constant is $a = 150$ nm. Each of the four QD is modeled by a cylindrical hard-wall potential with radius $R = 52.5$ nm and $V_0 = 0.60$ meV. It is shown in the literature that the softening of the potential from a hard-wall to a Gaussian shape does not affect qualitatively the results [153]. We consider $N = 1$ electrons per dot. These are realistic values that can be reproduced experimentally [154–156], and are similar to tight-binding studied shown in Ref. [150]. The Kekulé distortion is shown in the right side of Fig. 5.5. The height of the potential of two of the four QDs is decreased by $\Delta V_0 = 0.00$-0.40 meV, where $\Delta V_0 = 0$ meV corresponds to AG. The inclusion of the Kekulé distortion results in a triangular lattice.

In the previous section and in Chap 4, the results have been presented in effective atomic units (eff. a.u.). Here, we will show energies in meV and lengths in nm. This choice is justified by the fact that in literature AG results are commonly expressed with this system of units [150, 152, 153].

In Fig. 5.6, we show the energy bands of AG without Kekulé distortion ($\Delta V_0 = 0$) obtained with the 2DLDA (left side) and the 2DGLLB approximation (right side). We indicate the valence band in blue and the conduction band in orange. The Fermi energy is set to zero. As expected, we note the presence of Dirac cones with linear dispersion relation at the K point. As AG is a periodic system, $\Delta_{\rm xc}^{\rm LDA} = 0$ as shown in Eq. (5.1.31). In addition, as AG is a semi-metal, the top of the valence band and the bottom of the conduction band have the same energy, i.e. $\epsilon_{\rm L} = \epsilon_{\rm H}$. Thus, also $\Delta_{\rm xc}^{\rm 2DGLLB} = 0$, due to Eq. (5.1.30). The discontinuity corrections will be important for the Kekulé distorted AG, i.e., when $\Delta V_0 \neq 0$. 2DLDA results are consistent with previous studies in the literature [152, 153]. 2DGLLB results give qualitatively similar but less dispersive bands than the 2DLDA counterparts due to the increased electron localization originated from the 2DGLLB potential. The tendency of the 2DGLLB potential to increase electron localization in AG can be seen from the plot of the electron density difference $n^{\rm 2DGLLB}(\mathbf{r}) - n^{\rm 2DLDA}(\mathbf{r})$ in Fig. 5.7.a (upper panel). The electron localization originates from the xc potential (Fig. 5.7) that is deeper in

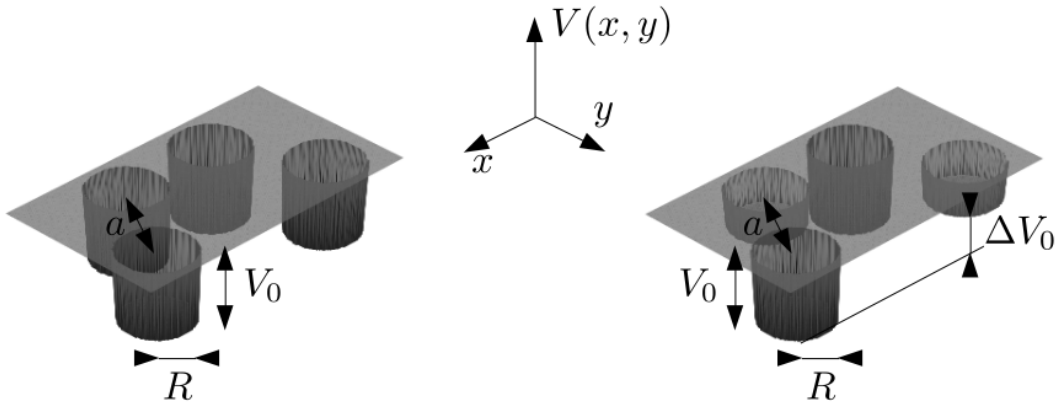

FIGURE 5.5: Left: rectangular unit cell of artificial graphene in real space. Right: rectangular unit cell of artificial graphene with Kekulé distortion, modeled as a difference in the height of the muffin-tin potentials of the QDs ΔV_0. The numerical parameters we used in our calculations are $a = 150$ nm, $V_0 = 0.60$ meV, $R = 52.5$ nm and $\Delta V_0 = 0.0$-0.40 meV.

the 2DGLLB case.

In Fig. 5.8, we show the energy bands of AG with Kekulé distortion ($\Delta V_0 = 0.30$ meV) obtained with 2DLDA (left side) and 2DGLLB (right side). Again, we indicate the valence band in blue and the conduction band in orange. The Fermi energy is set to zero. As expected, the Kekulé distortion opens a gap at the K points, where the Dirac cones were found for AG. 2DGLLB and 2DLDA valence bands are qualitatively similar. Again, the 2DGLLB band is less dispersive due to electron localization as shown in the upper panel of Fig. 5.7.b, in which we plot the difference of the electron densities $n^{\text{2DGLLB}}(\mathbf{r}) - n^{\text{2DLDA}}(\mathbf{r})$ for the Kekulé distorted structure. As can be seen from the lower panel of Fig. 5.7.b, the 2DGLLB potential is deeper than the 2DLDA, leading to a pronounced localization. Instead, the conduction bands of the 2DGLLB and 2DLDA are very different. We have $\Delta_{\text{xc}}^{\text{2DLDA}} = 0$, while the 2DGLLB correction given by Eq. (5.1.32) significantly affects the position of the conduction band. Although the correction of the 2DGLLB potential given by Eq. (5.1.32) is $\mathbf{k}$ dependent, the net effect is a rigid shift of the conduction band.

Finally, in Fig. 5.9 we plot the fundamental gaps $G_{\Delta}^{\text{2DGLLB}}$ and $G_{\Delta}^{\text{2DLDA}}$ of AG with Kekulé distortion as a function of the distortion parameter ΔV_0. For both the 2DLDA and the 2DGLLB approximation, we found a direct gap at the K point for all the considered range of $\Delta V_0 = 0.00$-0.40 meV. G_{Δ} is obtained from Eq. (5.1.22). For 2DLDA, we have $\Delta_{\text{xc}}^{\text{2DLDA}} = 0$, thus $G_{\Delta}^{\text{2DLDA}} = \Delta_{\text{KS}}^{\text{2DLDA}}$. The 2DGLLB discontinuity given by Eq. (5.1.30) is instead non-vanishing, $\Delta_{\text{xc}}^{\text{2DGLLB}} \neq 0$. We plot also $\Delta_{\text{KS}}^{\text{2DGLLB}}$ for comparison. The fundamental gap increases monotonically as the distortion parameter ΔV_0 increases. At $\Delta V_0 = 0$ meV, we recover the Dirac cones of AG, thus $G_{\Delta}^{\text{2DGLLB}} = G_{\Delta}^{\text{2DLDA}} = 0$. The KS gaps Δ_{KS} of the 2DLDA and the 2DGLLB approximation are quite similar at low ΔV_0, while $\Delta_{\text{KS}}^{\text{2DGLLB}} \approx 2\Delta_{\text{KS}}^{\text{2DLDA}}$ at the maximum

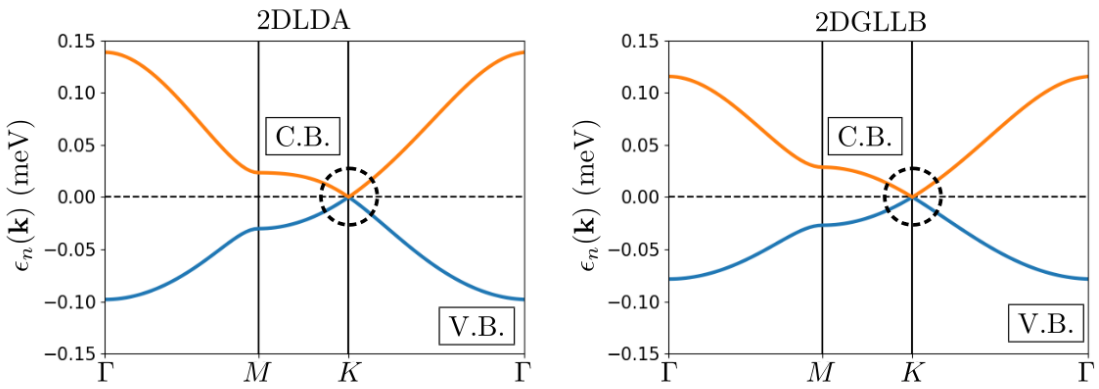

FIGURE 5.6: Energy bands of artificial graphene along the symmetry path Γ-M-K-Γ obtained with the 2DLDA (left side) and the 2DGLLB approximation (right side). We note the presence of Dirac cones at the K points (dashed circle). Valence bands are in blue and conduction bands in orange. Fermi energy is set to zero (dashed line).

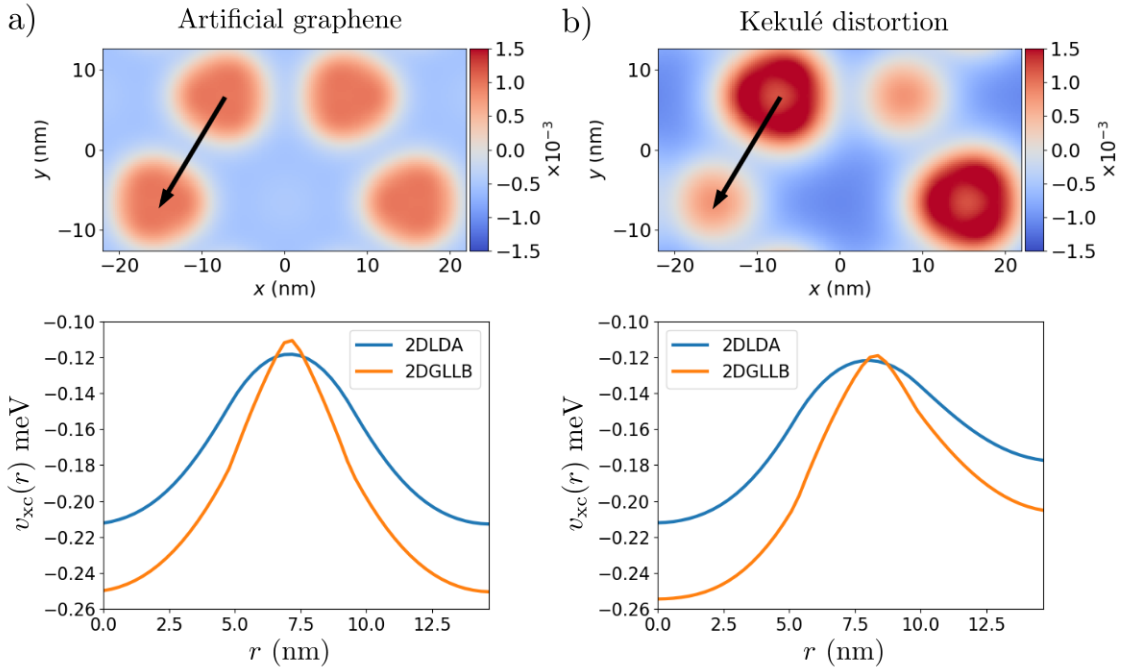

FIGURE 5.7: a) Upper panel: Difference of the electron density obtained with the 2DGLLB and 2DLDA approximations, $n^{\mathrm{2DGLLB}}(\mathbf{r}) - n^{\mathrm{2DLDA}}(\mathbf{r})$, in artificial graphene without Kekulé distortion ($\Delta V_0 = 0$). Lower panel: xc potential obtained with 2DGLLB and 2DLDA approximations along the line indicated by the black arrow in the upper panel. b) Same as a), but in artificial graphene with Kekulé distortion ($\Delta V_0 = 0.30$ meV).

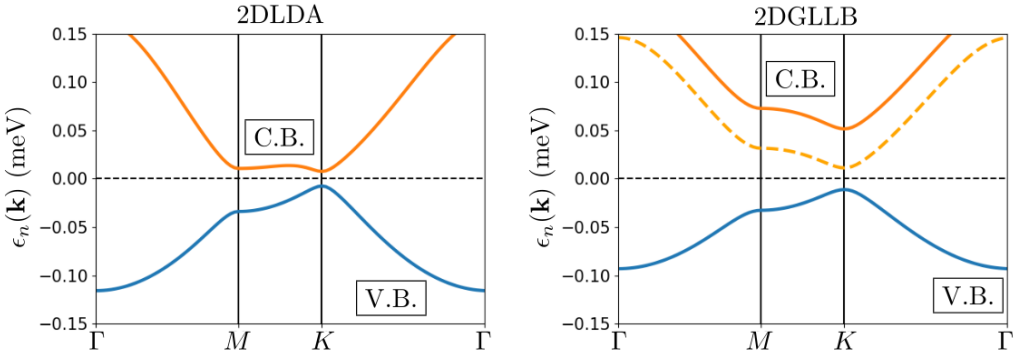

FIGURE 5.8: Energy bands of artificial graphene Kekulé distorted ($\Delta V_0 = 0.30$ meV) along the symmetry path Γ-M-K-Γ obtained with the 2DLDA (left side) and the 2DGLLB approximation (right side). Valence bands are in blue and conduction bands in orange. In the plot on the right panel, the continuous orange line corresponds to the conduction band with the correction given by Eq. (5.1.32), the dashed orange line the conduction band without correction. Although the $\Delta_{\rm xc}$ correction is $\mathbf{k}$ dependent, the net effect is a rigid shift of the conduction band. Fermi energy is set to zero (dashed line).

distortion $\Delta V_0 = 0.40$ meV. Again,the 2DGLLB potential provides higher values of $\Delta_{\rm KS}$ due to the increased electron localization around the dot (see Fig. 5.7.b).
The xc discontinuity $\Delta_{\rm xc}^{\rm 2DGLLB}$ is a very important contribution to $G_{\Delta}^{\rm 2DGLLB}$, as it contributes by at least 50%. The combined effects of the electron localization and non-vanishing $\Delta_{\rm xc}$ make the fundamental gap obtained using the 2DGLLB approximation about 4 times larger than that of the 2DLDA. The same trend is found for 3D semiconductors, e.g. silicon, for which the GLLB-SC fundamental gap is at least 2 times larger than that of the LDA [144]. This analysis suggests that the non-vanishing contribution $\Delta_{\rm xc}^{\rm 2DGLLB}$ is of fundamental importance for the study of the fundamental gap in 2D periodic nanostructures in a similar way as for 3D semiconductors.

5.3 Computational details

We have implemented the 2DGLLB potential both in the spin restricted and unrestricted framework in a local version of the software package OCTOPUS [118–120], that solves the Kohn-Sham equations on a regular space grid, with either Dirichlet or periodic boundary conditions. In this way, results are not bounded to any particular choice of the basis set.
For the case of finite QDs, we use the spin unrestricted framework to be consistent with previous calculations and use the same numerical parameters already discussed in Sec. 4.3.1. We select a grid spacing $g = 0.1/\sqrt{\omega}$ eff. a.u.. The simulation box containing the real-space domain is circular with radius $R = K/\sqrt{\omega}$ eff. a.u., where $K = \{5.0,6.0,6.5,7.0,7.5,8.0,8.5\}$ is used for $N = \{2,6,12,20,30,42,56\}$ respectively.
For the case of AG, we select a grid spacing $g \approx 2.45$ nm. The irreducible Brillouin zone was sampled with a 12×12 regular grid according to a modified version of the Monkhorst-Pack scheme [157]. In order to compute the bands given by Fig.

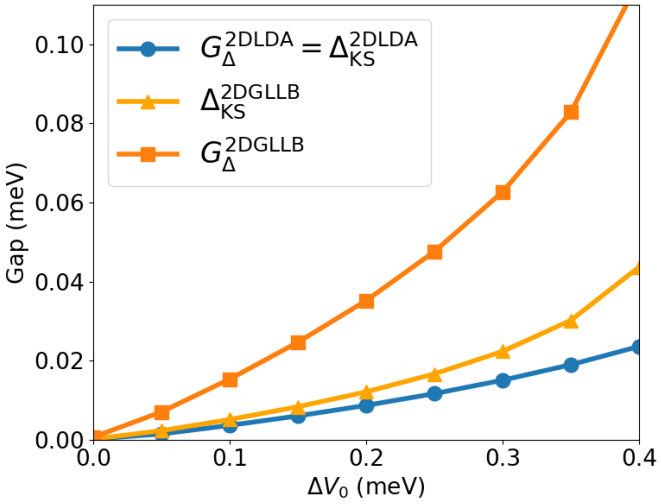

FIGURE 5.9: Fundamental gap (G_Δ) and KS gap (Δ_{KS}) at the K point in artificial graphene with Kekulé distortion as a function of ΔV_0 (see Fig. 5.5) obtained within the 2DLDA and 2DGLLB approximations. As the discontinuity of 2DLDA vanishes for periodic systems, we have $G_\Delta^{\mathrm{2DLDA}} = \Delta_{\mathrm{KS}}^{\mathrm{2DLDA}}$. The discontinuity of the 2DGLLB potential is obtained by (5.1.30).

5.6 and Fig. 5.8, we sampled 100 equally spaced k points along the path Γ-M-K-Γ. We verified numerically that these parameters are sufficient to get fundamental gaps converged within the fourth significant digit.

5.4 Conclusions and outlooks

We have constructed a new potential approximation for 2D systems in the spirit of the GLLB [145] and GLLB-SC [144] potentials. To be consistent with previous notation of 2D functionals, we have referred to the new approximation as the 2DGLLB potential.

We have tested the 2DGLLB potential in the calculation of the fundamental gap of both finite harmonic QDs in the exchange-only limit and periodic AG with Kekulé distortion.

The 2DGLLB potential gives accurate fundamental gaps of QDs with a mean relative absolute error of 3%.

Next, we have considered the case of AG. We have applied a Kekulé distortion in order to open a gap at the Dirac points. The correction to the KS gap given by the 2DGLLB approximation greatly affects the conduction band with respect to 2DLDA results – 2DLDA shows instead a vanishing gap correction. The 2DGLLB fundamental gap is approximately 4 times larger than that of the 2DLDA. The same trend is found for 3D semiconductors, e.g. silicon, for which the GLLB-SC fundamental gap is at least 2 times larger than that of the LDA [144].

It would be interesting to compare the fundamental gap obtained with the 2DGLLB approximation with accurate many-body calculations using, for example, the GW method [77–80]. To the best of our knowledge, however, GW calculations have not yet been performed for this type of systems.

5.A $K_{\mathrm{x}}^{\mathrm{2D}}$ from the uniform electron gas

We consider a two-dimensional uniform electron gas (2DUEG) with density n. The exchange potential for such a system is [114]

$$v_{\mathrm{x}}^{\mathrm{2DUEG}} = -\frac{2}{\pi}\sqrt{2\pi n}, \tag{5.A.1}$$

and

$$v_{\mathrm{x,scr}}^{\mathrm{2DUEG}} = 2\epsilon_{\mathrm{x}}^{\mathrm{2DUEG}} = \frac{4}{3}v_{\mathrm{x}}^{\mathrm{2DUEG}}. \tag{5.A.2}$$

By combining Eq. (5.A.1) and (5.A.2), the response part of the potential is

$$v_{\mathrm{x,resp}}^{\mathrm{2DUEG}} = v_{\mathrm{x}}^{\mathrm{2DUEG}} - v_{\mathrm{x,scr}}^{\mathrm{2DUEG}} = \frac{2}{3\pi}\sqrt{2\pi n}. \tag{5.A.3}$$

The KS orbitals of the 2DUEG are

$$\varphi_k(\mathbf{r}) = \frac{1}{\sqrt{A}}e^{i\mathbf{k}\cdot\mathbf{r}}, \tag{5.A.4}$$

where A is the area of the system. The correspondent KS eigenvalues are

$$\epsilon_k = \frac{k^2}{2} + v_{\mathrm{x}}[n] + v_{\mathrm{c}}[n]. \tag{5.A.5}$$

For the case of the HOMO we have

$$\epsilon_H = \frac{k_{\mathrm{F}}^2}{2} + v_{\mathrm{x}}[n] + v_{\mathrm{c}}[n]. \tag{5.A.6}$$

By substituting Eqs. (5.A.4)-(5.A.6) into the expression of the 2DGLLB response potential [see Eq. (5.1.29)], we obtain

$$v_{\mathrm{x,resp}}^{\mathrm{2DGLLB}} = \frac{K_{\mathrm{x}}^{\mathrm{2D}}}{\sqrt{2}nA}\sum_{|\mathbf{k}|\leq k_{\mathrm{F}}}\sqrt{k_{\mathrm{F}}^2 - k^2}. \tag{5.A.7}$$

The sum over occupied states can be transformed into an integral

$$\sum_{|\mathbf{k}|\leq k_{\mathrm{F}}} \approx \frac{2A}{(2\pi)^2}\int d\Omega \int_0^{k_{\mathrm{F}}} dk\ k. \tag{5.A.8}$$

By substituting Eq. (5.A.8) into Eq. (5.A.7), we get

$$\begin{aligned} v_{\mathrm{x,resp}}^{\mathrm{2DGLLB}} &= \frac{K_{\mathrm{x}}^{\mathrm{2D}}}{\sqrt{2}nA}\frac{2A}{(2\pi)^2}\int d\Omega \int_0^{k_{\mathrm{F}}} dk\ k\sqrt{k_{\mathrm{F}}^2 - k^2} \\ &= \frac{2K_{\mathrm{x}}^{\mathrm{2D}}\sqrt{\pi}}{3}n^{1/2}, \end{aligned} \tag{5.A.9}$$

where we used the following expression for the 2D Fermi momentum: $k_{\mathrm{F}} = \sqrt{2\pi n}$. By equating Eq. (5.A.3) with Eq. (5.A.9), we obtain

$$K_{\mathrm{x}}^{\mathrm{2D}} = \frac{\sqrt{2}}{\pi} \approx 0.4502, \tag{5.A.10}$$

that is the result we have shown in Sec. 5.1.1.

Chapter 6

Non-perturbative optical properties of a many-electron system probed by impulsive fields

Real-time propagation schemes based on TDDFT are considered successful among the methods for investigating time-dependent responses and electron dynamics [158]. In Sec. 3.6.1, we described how to obtain the absorption spectrum and excitation energies from the linear response to an impulsive electric field. Within this scheme, the linear optical properties of different kinds of materials, ranging from molecules, solids and nanostructures are nowadays routinely calculated [10, 11].

The main advantage of real-time TDDFT approaches is that they are able to account for dynamical non-linearities in a natural way. In fact, the time-dependent density $n(\mathbf{r}, t)$ is obtained from the full solution of the time-dependent KS equations, thus, $n(\mathbf{r}, t)$ automatically contains all the terms of the perturbation expansion compatible with the xc functional.

Real-time computational approaches have been developed and applied to describe and predict several nonlinear optical properties. For example, by combining the response generated to applied electric fields of different shapes, it is possible to extract second and higher-order frequency-dependent response functions [159–161]. High-order harmonic generation is another nonlinear effect that can be successfully described through real-time propagation schemes in both finite [162] and periodic [163] systems. Real-time TDDFT has also been employed to investigate phenomena beyond the perturbative regime, such as pump-probe experiments [164], charge-transfer dynamics [165], and others [166–168].

In this chapter, we consider the non-perturbative optical response due to an impulsive electric field $\mathcal{E}^{\mu}(t) = K^{\mu}\delta(t)$. In order to study it, we extend the range of applicability of the real-time propagation scheme of Sec. 3.6.1 to field amplitudes K^{μ} of arbitrarily intensities. As the intensity of the perturbation is increased and the nonlinear response becomes relevant, the absorption cross section will contain absorption terms coming from excited states. Excited-state absorption allows transitions to states which cannot be reached starting from the ground state. In addition, excited-state absorption contains information about transition matrix elements between excited states. Thus, the study of the nonlinear absorption cross section allows to access excited-state properties which are not contained in the linear

absorption cross section.

Excited-state absorption is also considered the key mechanism in several nonlinear phenomena. Among them, optical limiting consists in the strong attenuation of transmitted light as the input fluence exceeds a threshold value [169–171]. The optical limiting behavior can be investigated by studying the optical response to the same kind of perturbations we consider in this chapter within TDDFT [172]. While the results in Ref. [172] were mainly numerical, here we develop an analytical study of the nonlinear cross section. Therefore, this chapter provides us with analytical insights about nonlinear cross sections for optical limiting phenomena derived through TDDFT.

6.1 Theory

6.1.1 General considerations

We consider a system of N interacting electrons subject to a time-dependent classical electric field. The Hamiltonian of such a system is

$$\hat{H}(t) = \hat{H}_0 + \hat{H}'(t) \ . \tag{6.1.1}$$

The first term of Eq. (6.1.1) is $\hat{H}_0 = \hat{T} + \hat{V}_{en} + \hat{W}$, where $\hat{T}$ is the kinetic energy operator, $\hat{V}_{en}$ the nuclear potential, and $\hat{W}$ the electron-electron repulsion. $\hat{H}'(t)$ represents the interaction between the electrons and a semiclassical time-dependent electric field. Spin-magnetic field coupling is neglected. Since the wavelength of the radiation in the region of interest for optical absorption is much larger than the interatomic distances, the dependence of the electric field on the spatial coordinates can be dropped, and $\hat{H}'(t)$ can be written in the dipole approximation as

$$\hat{H}'(t) = -\hat{d}^{\mu}\mathcal{E}^{\mu}(t) \ , \tag{6.1.2}$$

where $\hat{d}^{\mu} = \sum_{i=1}^{N} \hat{x}_i^{\mu}$ is the electric dipole operator and $\hat{x}_i^{\mu}$ is the μ component of the position operator of the i-th electron, where $\mu = 1, 2, 3$. Sum over repeated indices is implied. The square modulus of a vector will be indicated with the following notation: $K^{\mu}K^{\mu} \equiv K^2$. We define the Fourier transform $\tilde{f}(\omega)$ of a time-dependent function $f(t)$ as follows:

$$\tilde{f}(\omega) = \int_{-\infty}^{+\infty} dt \ f(t)e^{i\omega t}. \tag{6.1.3}$$

Therefore, the inverse Fourier transform is

$$f(t) = \frac{1}{2\pi}\int_{-\infty}^{+\infty} d\omega \ \tilde{f}(\omega)e^{-i\omega t}. \tag{6.1.4}$$

6.1.2 Absorption cross section in the non-perturbative regime

In this section, we recall how the absorption cross section of a quantum system can be described in a non-perturbative way. The absorption cross section is defined as

the ratio between the absorbed energy E_{abs} and the incoming energy per unit area I_{in} at each frequency ω:

$$\sigma(\omega) = \frac{E_{abs}(\omega)}{I_{in}(\omega)} \ . \tag{6.1.5}$$

The total energy absorbed by the system is

$$\Delta E = \int_{-\infty}^{+\infty} \frac{dE(t)}{dt}\, dt = \int_{-\infty}^{+\infty} \frac{d}{dt} \langle \Psi(t)|\hat{H}(t)|\Psi(t)\rangle \ dt \ , \tag{6.1.6}$$

where $E(t) = \langle \Psi(t)|\hat{H}(t)|\Psi(t)\rangle$ is the total energy at time t. By applying the Ehrenfest theorem to the integrand of Eq. (6.1.6), we obtain

$$\frac{d}{dt} \langle \Psi(t)|\hat{H}(t)|\Psi(t)\rangle = \left\langle \Psi(t) \left| \frac{\partial \hat{H}(t)}{\partial t} \right| \Psi(t) \right\rangle = -d^{\mu}(t) \cdot \frac{d\mathcal{E}^{\mu}(t)}{dt} \ . \tag{6.1.7}$$

Substituting Eq. (6.1.7) into Eq. (6.1.6), we have

$$\Delta E = -\int_{-\infty}^{+\infty} dt \ d^{\mu}(t) \cdot \frac{d\mathcal{E}^{\mu}(t)}{dt}. \tag{6.1.8}$$

By using the Plancherel theorem, we changee from time to the frequency domain

$$\Delta E = -\frac{i}{2\pi} \int_{-\infty}^{+\infty} d\omega \ \omega \tilde{d}^{\mu}(\omega) \cdot \tilde{\mathcal{E}}^{\mu *}(\omega), \tag{6.1.9}$$

where $\tilde{d}^{\mu}(\omega)$ and $\tilde{\mathcal{E}}^{\mu}(\omega)$ are the Fourier transforms of $d^{\mu}(t)$ and $\mathcal{E}^{\mu}(t)$, respectively. In Eq. (6.1.9), we used the following property of Fourier transforms: $\mathcal{F}[df(t)/dt] = -i\omega \tilde{f}(\omega)$, where $\mathcal{F}[\ldots]$ is the Fourier transform operator.
Now we separate the integral into positive and negative frequencies

$$\Delta E = -\frac{i}{2\pi} \int_{0}^{+\infty} d\omega \ \omega \tilde{d}^{\mu}(\omega) \cdot \tilde{\mathcal{E}}^{\mu *}(\omega) - \frac{i}{2\pi} \int_{-\infty}^{0} d\omega \ \omega \tilde{d}^{\mu}(\omega) \cdot \tilde{\mathcal{E}}^{\mu *}(\omega). \tag{6.1.10}$$

Since both $d^{\mu}(t)$ and $\mathcal{E}^{\mu}(t)$ are real quantities, their complex conjugates fulfill the relations $\tilde{d}^{\mu}(-\omega) = \tilde{d}^{\mu *}(\omega)$ and $\tilde{\mathcal{E}}(-\omega) = \tilde{\mathcal{E}}^{\mu *}(\omega)$. Thus, we can sum the positive-and-negative frequency contributions in Eq. (6.1.10) by making the variable substitution $\omega' = -\omega$ in the second integral of Eq. (6.1.10),

$$\Delta E = \frac{1}{\pi} \int_{0}^{\infty} \omega \, \mathrm{Im} \left[\tilde{d}^{\mu}(\omega) \cdot \tilde{\mathcal{E}}^{\mu *}(\omega) \right] \ d\omega \ . \tag{6.1.11}$$

The integrand is the energy absorbed at each frequency ω

$$E_{abs}(\omega) = \frac{1}{\pi} \omega \, \mathrm{Im} \left[\tilde{d}^{\mu}(\omega) \cdot \tilde{\mathcal{E}}^{\mu *}(\omega) \right] \ . \tag{6.1.12}$$

It is useful to stress that $E_{abs}(\omega)$ is defined only for $\omega > 0$, since $E_{abs}(\omega)$ contains contributions from both absorption and emission terms coming from ω and $-\omega$. The incident energy per unit area in given by [173]

$$I_{in}(\omega) = \frac{c}{4\pi^2}|\tilde{\mathcal{E}}(\omega)|^2 \ . \tag{6.1.13}$$

Inserting Eq. (6.1.12) and (6.1.13) into Eq. (6.1.5) leads to

$$\sigma(\omega) = \frac{4\pi\omega}{c}\frac{\mathrm{Im}\left[\tilde{d}^{\mu}(\omega)\cdot\tilde{\mathcal{E}}^{\mu *}(\omega)\right]}{|\tilde{\mathcal{E}}(\omega)|^2} \ . \tag{6.1.14}$$

Eq. (6.1.14) is derived without any assumption about the intensity of the perturbation. Nevertheless, the absorption process described by $\tilde{d}^{\mu}(\omega)$ in Eq. (6.1.14) behaves differently if the response of the system is linear or not with respect to the external field. If the dependence of $\tilde{d}^{\mu}$ on $\tilde{\mathcal{E}}^{\mu}$ is linear, then we can write $\tilde{d}^{\mu}(\omega) = \alpha^{\mu\nu}(\omega)\tilde{\mathcal{E}}^{\nu}(\omega)$, where $\alpha^{\mu\nu}(\omega)$ is the dynamical polarizability tensor. Therefore, in this case, both the numerator and denominator of Eq. (6.1.14) are proportional to $|\tilde{\mathcal{E}}(\omega)|^2$, and $\sigma(\omega)$ is proportional to $\mathrm{Im}[\alpha(\omega)]$. The absorption cross section is then an intrinsic property of the system, independent of the specific form of the perturbation. Due to this linearity, the absorption of a field $\mathcal{E}^{\mu}(t)$ can be expressed as the sum of the absorption of each of the Fourier components of the electric field taken separately. However, if the system response is non-linear in $\tilde{\mathcal{E}}^{\mu}$, $\tilde{d}^{\mu}(\omega)$ may depend also on the components of the electric field at different frequencies $\tilde{\mathcal{E}}^{\mu}(\omega' \neq \omega)$. In this case $\sigma(\omega)$ depends on $\tilde{\mathcal{E}}^{\mu}(\omega' \neq \omega)$ and it is not possible to express the absorption of a field $\mathcal{E}^{\mu}(t)$ into the sum of absorptions of each Fourier components of $\mathcal{E}^{\mu}(t)$. Namely, the absorption at each frequency ω is a functional of the specific shape of the incoming field $\mathcal{E}^{\mu}(t)$.

6.1.3 The case of an impulsive perturbation

Let us now examine the case of an extremely short pulse in the limit

$$\mathcal{E}^{\mu}(t) = K^{\mu}\delta(t) \ , \tag{6.1.15}$$

where $\delta(t)$ is the Dirac delta at $t = 0$. Without making any particular assumption about its intensity $|K|^2$. Here, we consider the absorption process as occurring at equilibrium, i.e. we suppose the system is in its ground state for $t < 0$

$$|\Psi(t<0)\rangle = |\Psi_0\rangle\, e^{-iE_0 t}. \tag{6.1.16}$$

For a description of out-of-equilibrium absorption processes, as is the case in time-resolved absorption spectroscopy, further analysis is required [174]. For $t > 0$, the solution of the time-dependent Schrödinger equation for the system described by $\hat{H}(t)$ in Eq. (6.1.1) can be studied by projecting the time-dependent wavefunction $|\Psi(t)\rangle$ onto the eigenstates of $\hat{H}_0$, $\{|\Psi_i\rangle\}$. In this way we obtain

$$|\Psi(t>0)\rangle = \sum_{i=0}^{+\infty} c_i\, |\Psi_i\rangle\, e^{-iE_i t} \ , \tag{6.1.17}$$

where the coefficients c_i are given by

$$c_i = \langle \Psi_i | e^{-i\hat{d}^\mu K^\mu} | \Psi_0 \rangle \ , \tag{6.1.18}$$

and $\{E_i\}$ are the eigenvalues of $\hat{H}_0$. Due to the instantaneous nature of the perturbation the c_i coefficients are time-independent. The time-dependent dipole moment $d^\mu(t) = \langle \Psi(t) | \hat{d}^\mu | \Psi(t) \rangle$ for such a system is

$$d^\mu(t) = \theta(t) \sum_{i,j=0}^{+\infty} c_i^* c_j d_{ij}^\mu e^{-i\omega_{ji}t} + \theta(-t) d_{00}^\mu \ , \tag{6.1.19}$$

where $\theta(t)$ is the Heaviside theta function, $d_{ij}^\mu = \langle \Psi_i | \hat{d}^\mu | \Psi_j \rangle$ are the dipole matrix elements and $\omega_{ji} = E_j - E_i$. In Eq. (6.1.19), the system may have a ground state dipole moment d_{00}^μ different from zero. The sum over the indices i and j in Eq. (6.1.19) starts from $i, j = 0$ (i.e. at the ground state of the system) and runs over all the excited-state indices of the unperturbed system.

$\tilde{d}^\mu(\omega)$ is the key ingredient to obtain the absorption cross section from Eq. (6.1.14). By Fourier transforming Eq. (6.1.19) and substituting the result in Eq. (6.1.14), we obtain

$$\begin{aligned} \sigma(\omega) = \frac{4\pi^2}{c|K|^2} \sum_{i,j>i} \Big[& \langle \Psi_0 | \cos\left(\hat{d}^\mu K^\mu\right) | \Psi_i \rangle \ \langle \Psi_i | \hat{d}^\mu K^\mu | \Psi_j \rangle \ \langle \Psi_j | \sin\left(\hat{d}^\mu K^\mu\right) | \Psi_0 \rangle \\ - & \langle \Psi_0 | \sin\left(\hat{d}^\mu K^\mu\right) | \Psi_i \rangle \ \langle \Psi_i | \hat{d}^\mu K^\mu | \Psi_j \rangle \ \langle \Psi_j | \cos\left(\hat{d}^\mu K^\mu\right) | \Psi_0 \rangle \Big] \omega_{ji} \delta(\omega_{ji} - \omega). \end{aligned} \tag{6.1.20}$$

The demonstration of Eq. (6.1.20) is reported in Appx. 6.A. The cross section is derived with the assumption that the system is centrosymmetric, therefore $d_{00}^\mu = 0$. Eq. (6.1.20) can be used to describe an ensemble of molecules randomly oriented with respect to the incoming-field polarization, e.g. molecules in a gas phase. In fact, the ensemble-averaged optical response is always centrosymmetric despite the symmetry properties of the single molecules.

In order to highlight the nonlinear contributions of the cross section, we extract from Eq. (6.1.20) the first-order term in the perturbation, $\sigma^{(1)}(\omega)$, and compare $\sigma(\omega)$ with $\sigma^{(1)}(\omega)$. The linear cross section can be obtained by approximating the matrix elements of Eq. (6.1.20) up to first order in K^μ (the amplitude of the electric field), $\sin\left(\hat{d}^\mu K^\mu\right) \approx d^\mu K^\mu$ and $\cos\left(d^\mu K^\mu\right) \approx 1$. The resulting cross section is

$$\sigma^{(1)}(\omega) = \frac{4\pi^2 \omega}{c|K|^2} \sum_{j=0}^{+\infty} \left| \langle \Psi_0 | \hat{d}^\mu K^\mu | \Psi_j \rangle \right|^2 \delta(\omega - \omega_{j0}) \ . \tag{6.1.21}$$

Eq. (6.1.21) provides a good approximation for Eq. (6.1.20) if $|K| \ll 1/|R|$, where $|R|$ is the size of the system [61]. Since for molecular systems, $|R| \approx 1 - 100$ a.u., a value of $|K| \approx 10^{-3}\text{bohr}^{-1}$ is usually employed to trigger the linear response only [61]. While in the linear regime the resonances in the cross section are found only at $\omega = \omega_{j0}$, which corresponds to the difference between the energy of an excited state Ψ_j and the energy of the ground state Ψ_0, in Eq. (6.1.20) resonances $\omega = \omega_{ji}$ occur

where the energy ω of the incoming light equals the energy difference ω_{ji} between any pair of eigenstates Ψ_j and Ψ_i of the unperturbed Hamiltonian $\hat{H}_0$.
Eq. (6.1.20) and Eq. (6.1.21) share the same dipole parity selection rule since they include the same matrix elements $\langle\Psi_i|\hat{d}^\mu K^\mu|\Psi_j\rangle$ [N.B. in Eq. (6.1.21), $i=0$]. Therefore, dipole-forbidden excitations correspond to

$$\langle\Psi_i|\hat{d}^\mu K^\mu|\Psi_j\rangle = 0 \ , \qquad i,j = 0,\dots,+\infty \tag{6.1.22}$$

both in the linear and nonlinear regime. In Eq. (6.1.20), due to the presence of additional matrix elements, new selection rules arise

$$\langle\Psi_0|\cos\left(\hat{d}^\mu K^\mu\right)|\Psi_i\rangle = \langle\Psi_i|\cos\left(\hat{d}^\mu K^\mu\right)|\Psi_0\rangle = 0 \ , \qquad i = 0,\dots,+\infty \ , \tag{6.1.23}$$

$$\langle\Psi_j|\sin\left(\hat{d}^\mu K^\mu\right)|\Psi_0\rangle = \langle\Psi_j|\sin\left(\hat{d}^\mu K^\mu\right)|\Psi_0\rangle = 0 \ , \qquad j = 0,\dots,+\infty \ . \tag{6.1.24}$$

In Eq.s (6.1.23) and (6.1.24), bra and ket can be interchanged since $\Psi_i \in$ Re and $\hat{d}^\mu$ is diagonal in real space. We note that the selection rules in Eq. (6.1.23) and (6.1.24) have a different nature with respect to the one in Eq. (6.1.22). The selection rule in Eq. (6.1.22) selects if a transition $i \to j$ is allowed or not, while Eq.s (6.1.23) and (6.1.24) select if a state i or j can participate in the absorption process. In addition, $\sigma(\omega)$ in Eq. (6.1.20) satisfies the sum rule

$$\int_0^{+\infty} d\omega\sigma(\omega) = \frac{2\pi^2 N}{c} \ , \tag{6.1.25}$$

where N is the number of electrons. We note that the right hand side of Eq. (6.1.25) does not depend on K^μ and therefore it is valid both in the linear and nonlinear regime.
In Fig. 6.1.a we present a sketch of the excitations involved in the linear and nonlinear absorption processes in the impulsive limit. While in the linear regime only absorption from the ground state is allowed (black arrows), in the nonlinear regime also transitions between excited states are possible (red arrows). This condition is physically obtained for example when one or more excited states of the unperturbed system are populated by a laser. The absorption cross section contains precious information about excited-state properties: the peak positions are related to excitation energies, the peak intensities are related to transition matrix elements. States with the same symmetries as the ground state cannot be populated in the linear regime due to the dipole selection rule in Eq. (6.1.22). These states can be instead populated in the nonlinear regime, through excited-state absorption. In addition, the nonlinear cross section includes information about transition matrix elements between excited states, which are not included in the linear cross section. We will discuss this point in more detail in Sec. 6.2. The Hamiltonian in Eq. (6.1.1) does not contain terms allowing for spin-flips, therefore, assuming the ground state is a spin singlet S_0, both the expressions in Eq. (6.1.20) and (6.1.21) allow transitions between states belonging to the singlet manifold (S_1, S_2,...). In order to study excited-state properties of states with different multiplicity from the ground state, it is necessary to explicitly include the spin degrees of freedom in $\hat{H}'(t)$. We refer for example to the work of Oliveira *et al.* [175] for a study of the triplet excitation spectra in the linear regime.

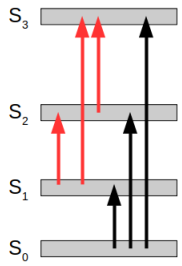

FIGURE 6.1: Sketch of the nonlinear excitations (red arrows) described by Eq. (6.1.20). The linear excitations given by Eq. (6.1.21) starting from the ground state S_0 are marked by black arrows.

6.2 Applications

We now adopt the analytical scheme presented in the previous section to calculate the nonlinear absorption properties of a 1D model system composed of two interacting electrons trapped in a square potential well with infinitely dept walls (1DW). The effect of an electric field impulse [see Eq. (6.1.2)] both in the linear and nonlinear regime is analysed in Sec. 6.2.1, which allows to better clarify the physical meaning of the equations derived in the previous section.

1D model systems are commonly employed as case studies to validate approximations, e.g. in the field of non-linear time-dependent phenomena [164,176] and density functional approximations [177–180], both in density-functional theory (DFT) and time-dependent density functional theory (TDDFT). The main reason is that 1D models can be exactly solved by mapping the 1D Hamiltonian of N interacting electrons into an N-dimensional Hamiltonian for a single electron [179,180].
The unperturbed Hamiltonian of the 1DW is

$$\hat{H}_0 = \sum_{i=1}^{2}\left[-\frac{1}{2}\frac{\partial^2}{\partial x_i^2} + v_{ext}(x_i)\right] + \frac{1}{\sqrt{1+(x_1-x_2)^2}}\,, \tag{6.2.1}$$

where the first term contains the kinetic energy and the external potential. The external potential is

$$v_{ext}(x_i) = \begin{cases} 0 & -L/2 < x_i < L/2 \\ \infty & \text{otherwise} \end{cases}\,, \tag{6.2.2}$$

where we set $L = 5.0$ bohr. The second term in Eq. (6.2.1) is the soft Coulomb interaction between the two electrons. The Coulomb interaction is softened to avoid the Coulomb singularity at $x_1 = x_2$ [181].

Let us now analyze the symmetries of $\hat{H}_0$, which will determine the allowed and forbidden transitions in the absorption process. $\hat{H}_0$ is symmetric under particle interchange $x_1 \leftrightarrow x_2$, thus we can chose the spatial component of the wavefunction $\psi_i(x_1, x_2)$ to be either symmetric or antisymmetric with respect to the exchange of the spatial coordinates. As the total wavefunction $\Psi_i(x_1, s_1, x_2, s_2) = \psi_i(x_1, x_2)\chi_i(s_1, s_2)$

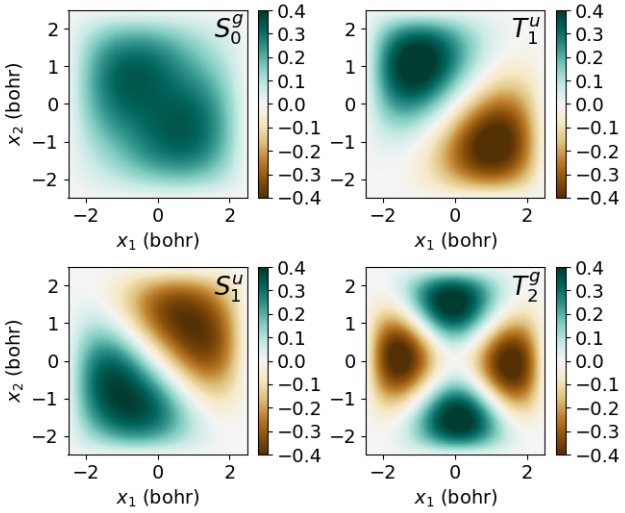

FIGURE 6.2: Eigenstates of $\hat{H}_0$ [see Eq. (6.1.2)] for a 1D potential well confining two electrons (1DW). The states are labelled with the following notation: $M_i^{g/u}$; where M indicates the spin state (singlet S or triplet T), i the order in energy within the spin channel and g/u the parity of with respect to inversion of the coordinates. Colorbar units are bohr^{-1}.

must be antysimmetric, the parity of $\psi(x_1, x_2)$ determines the parity of the spin component of the wavefunction $\chi_i(s_1, s_2)$. If $\psi_i(x_1, x_2)$ is symmetric under exchange of the coordinates, $\chi_i(s_1, s_2)$ must be a singlet (antisymmetric) state and viceversa for the triplet state. We label i-th singlet and triplet states with S_i and T_i respectively. $\hat{H}_0$ has also spatial inversion symmetry, $\hat{H}_0(-x_1, -x_2) = \hat{H}_0(x_1, x_2)$, and we can chose the eigenstates of $\hat{H}_0$ to be either symmetric or antisymmetric under such inversion. The superscripts g (*gerade*) or u (*ungerade*) label the parity of the wavefunction. Tab. 6.1 reports the ground and first five energy levels of each spin channel in which the ground state is denoted by S_0^g and the first excited state is a triplet (T_1^u). The wavefunctions are plotted in Fig. 6.2.
Due to the selection rules expressed by Eq.s (6.1.22), the only allowed transitions are between *gerade* and *ungerade* states. In addition the spin selection rule is $\Delta S = 0$, as the perturbed Hamiltonian is spin-independent. Thus, allowed transitions are only $S_i^g \to S_j^u$ and $S_i^u \to S_j^g$. We recall that Eq.s (6.1.22) is valid both in the linear and nonlinear regime.

6.2.1 Nonlinear absorption spectrum of the 1DW

In order to calculate the absorption spectrum, we consider the following interacting term of the Hamiltonian

$$\hat{H}'(t) = -\hat{d}\mathcal{E}(t), \tag{6.2.3}$$

where $\hat{d} = \hat{x}_1 + \hat{x}_2$ and $\mathcal{E}(t) = K\delta(t)$. Eq. (6.2.3) is the 1D counterpart of Eq. (6.1.2) in the case of an electric field impulse. $\hat{d}$ and $\mathcal{E}(t)$ are no longer vectors since

State	Energy (H)	State	Energy (H)
S_0^g	1.09		
S_1^u	1.76	T_1^u	1.47
S_2^g	2.17	T_2^g	2.53
S_3^g	2.72	T_3^u	3.05
S_4^u	3.26	T_4^u	3.95
S_5^u	4.05	T_5^g	4.49

TABLE 6.1: Eigenvalues of $\hat{H}_0$ [see Eq. (6.1.2)] of a 1D potential well containing two electrons (1DW). State notation is explained in the caption of Fig. 6.2.

the system is 1D. After the impulse is applied to the ground state (S_0^g), the time-dependent wavefunction is propagated by solving the Schrödinger equation. The time-dependent polarization is calculated through the time-dependent wavefunction as $d(t) = \langle \Psi(t)|\hat{d}|\Psi(t)\rangle$ and its Fourier transform $\tilde{d}(\omega)$ enters in the absorption cross section:

$$\sigma(\omega) = \frac{4\pi\omega}{c}\frac{\mathrm{Im}[\tilde{d}(\omega)]}{K} \ , \tag{6.2.4}$$

which is the 1D counterpart of Eq. (6.1.14) in the case of an electric field impulse. We recall that Eq. (6.2.4) is valid both in the linear and nonlinear regimes.

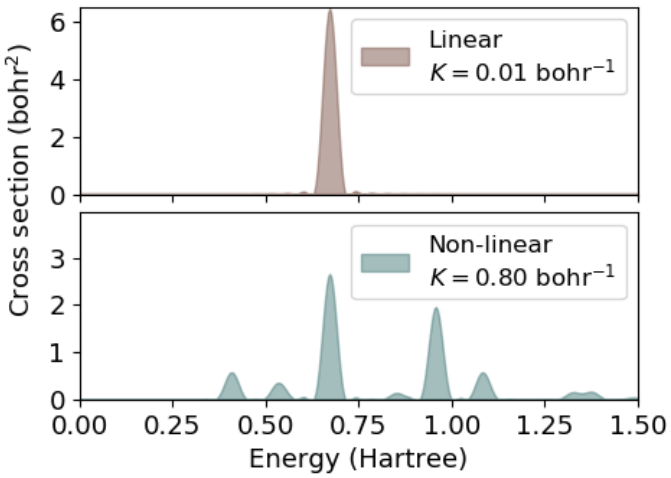

FIGURE 6.3: Comparison of the linear and nonlinear absorption spectra of a 1D square potential well containing two electrons (1DW) subject to different electric field impulses [see Eq. (6.1.2)]. The linear absorption spectrum (upper panel) is obtained applying an impulsive electric field with intensity $K = 0.01$ bohr^{-1}. The nonlinear absorption spectrum (lower panel) is obtained by applying an electric field with intensity $K = 0.80$ bohr^{-1}.

In Fig. 6.3, we show the linear and nonlinear absorption spectra of the 1DW obtained by applying an electric field impulse of $K = 0.01$ bohr^{-1} (upper panel) and $K = 0.80$ bohr^{-1} (lower panel), respectively. The linear spectrum shows one peak at 0.67 Hartree, corresponding to the $S_0^g \rightarrow S_1^u$ transition. The nonlinear absorption cross section shows instead several excitations. In fact, the spectral weight is spread over the range 0.4-1.4 Hartree, instead of being grouped at ≈ 0.7 Hartree. The peaks are located both at lower and higher energies with respect to the linear excitation. The main peak of the nonlinear spectrum is at the same energy as the linear one, since it corresponds to the same excitation $S_0^g \rightarrow S_1^u$, but with approximately one half of its spectral weight.

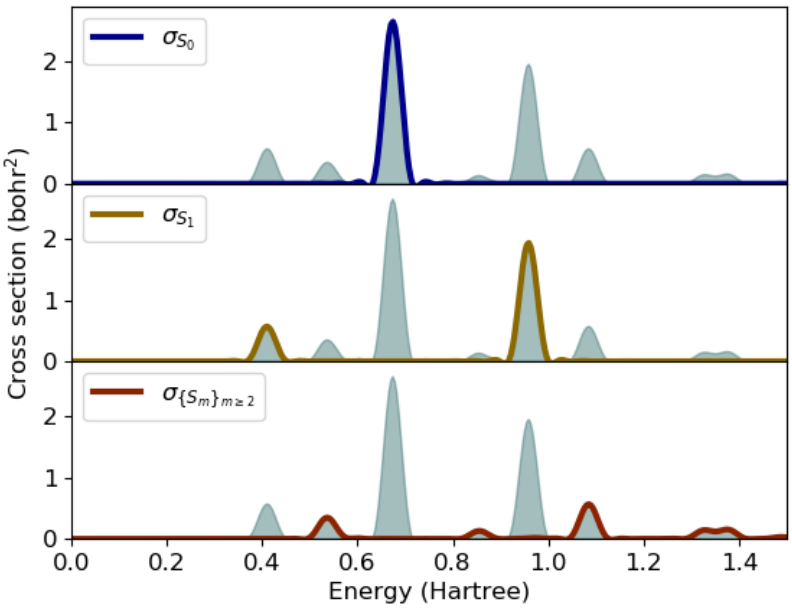

FIGURE 6.4: Nonlinear absorption cross section of a 1D square potential well containing two electrons (1DW) perturbed by an electric field impulse [see Eq. (6.1.15)] of $K = 0.80$ a.u.. The cross section is split into ground state absorption (blue curve), first excited state absorption (yellow curve) and absorption from higher excited states (red curve).

In order to analyze the transitions involved in the nonlinear cross section shown in the lower panel of Fig. 6.3, we split it into three components (see Fig. 6.4): absorption from the ground state $[\sigma_{S_0}(\omega)]$, from the first excited state $[\sigma_{S_1}(\omega)]$ and the remainder $[\sigma_{\{S_m\}}(\omega)$ with $m \geq 2]$. The ground-state cross section $\sigma_{S_0}(\omega)$ includes the same transition $S_0^g \rightarrow S_1^u$ as the linear cross section in the top panel of Fig. 6.3. The new peaks in the spectrum result from excited state absorption. The two peaks at 0.41 and 0.96 Hartree, shown in the middle panel of Fig. 6.4, arise from absorption from the first-excited-state and correspond respectively to the transitions $S_1^u \rightarrow S_2^g$ and $S_1^u \rightarrow S_3^g$. The absorption from the first excited-state (S_1^u) involves *gerade* excited-states, which are not accessible through the linear-regime

cross section implying that, in order to get information about the *gerade* manifold of excited-states, it is required to consider the *nonlinear* absorption cross section, instead of the linear one. The remaining peaks (lower panel in Fig. 6.4) have their origin in higher-order excited-state absorption. $\sigma_{\{S_m\}}(\omega)$ (we remeber $m \geq 2$) is composed by several low intensity excitations spread out over the frequency range $0.4 < \omega < 1.4$ Hartree. The peak with higher intensity is located at 1.09 Hartree and corresponds to the transition $S_2^g \to S_4^u$.

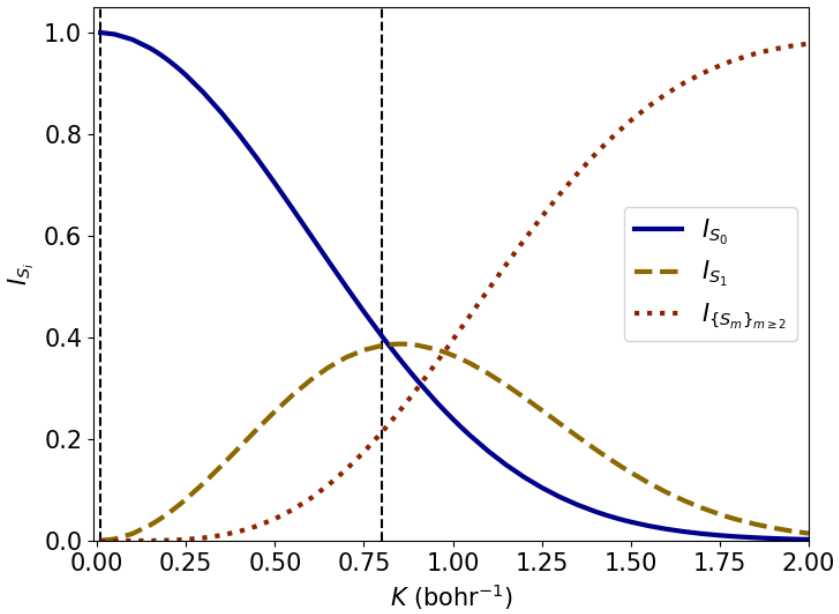

FIGURE 6.5: Normalized weights [see Eq. (6.2.5)] of the three components of the absorption cross section given in Fig. 6.4 as a function of the strength of the electric field impulse K. Dashed vertical lines correspond to the values of K used in Fig. 6.3.

Finally, in Fig. 6.5 we show the weight of the above-discussed three different contributions of the nonlinear cross section (highlighted in Fig. 6.4) as a function of the strength of the electric field impulse, K. We define the normalized weight of a component of the cross section as

$$I_{S_i} = \frac{c}{4\pi^2} \int_0^{+\infty} d\omega \; \sigma_{S_i}(\omega) \; . \tag{6.2.5}$$

The solid line in Fig. 6.5 corresponds to the weight of the ground-state cross section I_{S_0}. We note that $I_{S_0} \approx 1$ for $K \approx 0$, which confirms that there is only ground-state absorption in the linear regime, as expected from the linearized expression of the cross section in Eq. (6.1.21). I_{S_0} decreases monotonically as K increases: the response of the system becomes nonlinear and excited-state absorption becomes relevant. For $K > 1.44$ bohr^{-1}, we have $I_{S_0} < 0.05$ and we therefore consider negligible ground-state absorption. The dashed curve corresponds to the weight of the first-excited-state

cross section I_{S_1}. It starts from zero at $K \approx 0$, reaching its maximum at $K = 0.85$ Hartree, and then decreasing monotonically. The dotted curve, corresponding to the higher-order excited state absorption $I_{\{S_m\}}$, where $m \geq 2$. $I_{\{S_m\}}$ also starts from zero at $K \approx 0$ increasing monotonically up its saturation value, one, for high values of K. For high impulses ($K > 1.76$ bohr^{-1}), the only non-negligible component of the cross section is I_{S_m}. We finally note that for the K value selected in the lower panel of Fig. 6.3 the ground-state and first-excited-state cross sections have similar weight, while the higher-order cross-section weight is lower (see dashed vertical line in Fig. 6.5).

6.3 Computational details

We carried out all our calculations with the OCTOPUS code [182–184] that solves the Schrödinger equations (time dependent and time independent) on a regular spatial grid with Dirichlet boundary conditions. We select a grid spacing of $g = 0.015$ bohr. x_1 and x_2 range from -2.5 to 2.5 bohr [see Eq. (6.2.2)]. In the calculation of the absorption spectra, the electric-field impulse is performed using the Yabana-Bertsch scheme [61]. Time-dependent wavefunctions are propagated up to $T_{max} = 150$ Hartree^{-1}, employing a time step of $dt = 0.002$ Hartree^{-1}. The resulting cross sections show an intrinsic broadening of 0.04 Hartree due to the finite length of the propagation.
The components of the cross section are obtained from Eq. (6.1.20). Numerically, the double sums in Eq. (6.1.20) are evaluated up to the first 100 eigenstates of the unperturbed Hamiltonian $\hat{H}_0$. The convergence of the cross sections have been verified by evaluating the sum rule in Eq. (6.1.25). Dirac deltas in Eq. (6.1.20) are broadened in order to match the peak width of the cross sections obtained from the solution of the time-dependent Schrödinger equations.
The integrals in the calculation of the normalized weights of the cross section component [see Eq. (6.2.5)] are performed up to 10.0 Hartree.

6.4 Conclusions and outlooks

We have studied the optical absorption properties of a many-electron system subject to an impulsive electric field in the non-perturbative regime. We have studied the absorption properties obtainable through the real-time propagation scheme described in Sec. 3.6.1 in the nonlinear regime. Due to the Dirac-delta time dependence of the perturbation, we have been able to express the absorption cross section $\sigma(\omega)$ in terms of the eigenstates of $\hat{H}_0$. Within this decomposition, we have demonstrated that, as the response of the system becomes nonlinear, excited states start to absorb thus allowing to populate states not reachable from the ground state due to dipole selection rules. We have shown that the study of the nonlinear absorption cross section is a useful tool to get information about excited-state properties which are not accessible through the linear absorption cross section.
As an application of this scheme, we have studied the linear and nonlinear absorption cross sections of a 1D model system composed by two interacting electrons trapped in a 1D potential well (1DW). We have shown that the nonlinear absorption cross section contains information about *gerade* excited states, which remains dark in the

nonlinear regime.

The work presented in this chapter supports the importance of pioneering TDDFT applications concerning nonlinear optical properties, such as the work by Cocchi *et al.* [172], which has pointed out TDDFT as an ideal framework to study the optical limiting behavior of macrocyclic molecules. While the results reported by Cocchi *et al.* were mainly numerical, in this chapter we have provided an analytical derivation of the nonlinear cross section and its properties. Moreover, we have carried out numerically exact calculations on model systems useful to investigate its limitations due either to the numerical problems or functional approximations.

6.A Derivation of equation (6.1.20)

Here, we derive an expression for the absorption cross section $\sigma(\omega)$ in the case of an incoming impulsive electric field [see Eq. (6.1.15)]. First, we calculate the Fourier transform of the time-dependent dipole moment

$$d^{\mu}(t) = \theta(t) \sum_{i,j=0}^{+\infty} c_i^* c_j d_{ij}^{\mu} e^{-i\omega_{ji}t} + \theta(-t) d_{00}^{\mu}, \tag{6.A.1}$$

that will be then inserted into Eq. (6.1.12) to get $E_{abs}(\omega)$. In the end, the absorption cross section is obtained as the ratio $\sigma(\omega) = E_{abs}(\omega)/I_{in}(\omega)$. The c_i coefficients are defined in Eq. (6.1.18).
In order to compute $\tilde{d^{\mu}}(\omega)$, we consider the spectral representation of the Heaviside theta function:

$$\theta(t) = \frac{i}{2\pi} \lim_{\epsilon \to 0^+} \int_{-\infty}^{+\infty} d\omega \frac{e^{-i\omega t}}{\omega + i\epsilon}, \tag{6.A.2}$$

thus

$$\theta(-t) = \frac{-i}{2\pi} \lim_{\epsilon \to 0^+} \int_{-\infty}^{+\infty} d\omega \frac{e^{-i\omega t}}{\omega - i\epsilon}. \tag{6.A.3}$$

Substituting Eq. (6.A.2) and Eq. (6.A.3) into Eq. (6.A.1)

$$\begin{aligned} d^{\mu}(t) &= \frac{i}{2\pi} \lim_{\epsilon \to 0^+} \int_{-\infty}^{+\infty} d\omega \frac{e^{-i\omega t}}{\omega + i\epsilon} \sum_{i,j=0}^{+\infty} c_i^* c_j d_{ij}^{\mu} e^{-i\omega_{ji}t} + \frac{-i}{2\pi} \lim_{\epsilon \to 0^+} \int_{-\infty}^{+\infty} d\omega \frac{e^{-i\omega t}}{\omega - i\epsilon} d_{00}^{\mu} \\ &= \frac{i}{2\pi} \lim_{\epsilon \to 0^+} \sum_{i,j=0}^{+\infty} c_i^* c_j d_{ij}^{\mu} \int_{-\infty}^{+\infty} d\omega \frac{e^{-i(\omega+\omega_{ji})t}}{\omega + i\epsilon} - \frac{i}{2\pi} d_{00}^{\mu} \lim_{\epsilon \to 0^+} \int_{-\infty}^{+\infty} d\omega \frac{e^{-i\omega t}}{\omega - i\epsilon}. \end{aligned} \tag{6.A.4}$$

We now make the variable substitution $\omega' = \omega + \omega_{ji}$ to the first integral in the right hand side

$$d^{\mu}(t) = \frac{i}{2\pi} \lim_{\epsilon \to 0^+} \sum_{i,j=0}^{+\infty} c_i^* c_j d_{ij}^{\mu} \int_{-\infty}^{+\infty} d\omega \frac{e^{-i\omega t}}{\omega - \omega_{ji} + i\epsilon} - \frac{i}{2\pi} d_{00}^{\mu} \lim_{\epsilon \to 0^+} \int_{-\infty}^{+\infty} d\omega \frac{e^{-i\omega t}}{\omega - i\epsilon}, \tag{6.A.5}$$

and insert the identity relation $d^{\mu}_{00} = \sum_{i,j=0}^{+\infty} c_i^* c_j d^{\mu}_{ij}$ into Eq. (6.A.5). Thus,

$$d^{\mu}(t) = \lim_{\epsilon \to 0^+} \frac{1}{2\pi} \int_{-\infty}^{+\infty} d\omega \sum_{i,j=0}^{+\infty} c_i^* c_j d^{\mu}_{ij} \left(\frac{i}{\omega - \omega_{ji} + i\epsilon} - \frac{i}{\omega - i\epsilon} \right) e^{-i\omega t}. \tag{6.A.6}$$

If we compare Eq. (6.A.6) with the spectral decomposition of the dipole moment

$$d^{\mu}(t) = \frac{1}{2\pi} \int_{-\infty}^{+\infty} d\omega \tilde{d}^{\mu}(\omega) e^{-i\omega t}, \tag{6.A.7}$$

we find

$$\tilde{d}^{\mu}(\omega) = i \lim_{\epsilon \to 0^+} \sum_{i,j=0}^{+\infty} c_i^* c_j d^{\mu}_{ij} \left(\frac{1}{\omega - \omega_{ji} + i\epsilon} - \frac{1}{\omega - i\epsilon} \right). \tag{6.A.8}$$

Let us now proceed in the calculation of the absorbed energy per unit frequency given by Eq. (6.1.12), where $\tilde{d}^{\mu}(\omega)$ is given by Eq. (6.A.8) and $\tilde{\mathcal{E}}^{\mu}(\omega) = K^{\mu}$

$$\begin{aligned} E_{abs}(\omega) &= \frac{1}{\pi} \omega \, \mathrm{Im} \left[\tilde{d}^{\mu}(\omega) K^{\mu} \right] \\ &= \lim_{\epsilon \to 0^+} \frac{1}{\pi} \mathrm{Im} \left[i \sum_{i,j=0}^{+\infty} c_i^* c_j d^{\mu}_{ij} K^{\mu} \left(\frac{\omega}{\omega - \omega_{ji} + i\epsilon} - \frac{\omega}{\omega - i\epsilon} \right) \right] \\ &= \lim_{\epsilon \to 0^+} \frac{1}{\pi} \mathrm{Re} \left[\sum_{i,j=0}^{+\infty} c_i^* c_j d^{\mu}_{ij} K^{\mu} \left(\frac{\omega}{\omega - \omega_{ji} + i\epsilon} - \frac{\omega}{\omega - i\epsilon} \right) \right]. \end{aligned} \tag{6.A.9}$$

In the second term inside the round brackets of Eq. (6.A.9), we have

$$\lim_{\epsilon \to 0^+} \frac{\omega}{\omega - i\epsilon} = 1. \tag{6.A.10}$$

By simplifying the expression within round brackets and using Eq. (6.A.10), we obtain

$$\lim_{\epsilon \to 0^+} \frac{\omega}{\omega - \omega_{ji} + i\epsilon} - 1 = \lim_{\epsilon \to 0^+} \frac{\omega_{ji} + i\epsilon}{\omega - \omega_{ji} + i\epsilon} = \lim_{\epsilon \to 0^+} \frac{\omega_{ji}}{\omega - \omega_{ji} + i\epsilon} \tag{6.A.11}$$

where, we dropped the small imaginary part in the numerator. By inserting Eq. (6.A.11) into Eq. (6.A.9), we have

$$E_{abs}(\omega) = \lim_{\epsilon \to 0^+} \frac{1}{\pi} \mathrm{Re} \left[\sum_{i,j=0}^{+\infty} c_i^* c_j d^{\mu}_{ij} K^{\mu} \frac{\omega_{ji}}{\omega - \omega_{ji} + i\epsilon} \right]. \tag{6.A.12}$$

At this point it is useful to split the double sum over i and j into three parts

$$\sum_{i,j=0}^{+\infty} = \sum_{i,j>i}^{+\infty} + \sum_{i,j=i}^{+\infty} + \sum_{i,j<i}^{+\infty}. \tag{6.A.13}$$

The second sum in the right hand side of Eq. (6.A.13) is null due to the presence of ω_{ji}. Thus,

$$E_{abs}(\omega) = \lim_{\epsilon\to 0^+} \frac{1}{\pi} \mathrm{Re}\left[\sum_{i,j>i}^{+\infty} c_i^* c_j d_{ij}^\mu K^\mu \frac{\omega_{ji}}{\omega - \omega_{ji} + i\epsilon} + \sum_{i,j<i}^{+\infty} c_i^* c_j d_{ij}^\mu K^\mu \frac{\omega_{ji}}{\omega - \omega_{ji} + i\epsilon}\right]. \quad (6.A.14)$$

Next, we make the substitution $i \to j$ and $j \to i$ in the second term in the right hand side of Eq. (6.A.14) and use $\omega_{ij} = -\omega_{ji}$ and $d_{ij}^\mu = d_{ji}^\mu$ to write

$$E_{abs}(\omega) = \lim_{\epsilon\to 0^+} \frac{1}{\pi} \sum_{i,j>i}^{+\infty} \mathrm{Re}\left[c_i^* c_j d_{ij}^\mu K^\mu \frac{\omega_{ji}}{\omega - \omega_{ji} + i\epsilon} - c_i c_j^* d_{ij}^\mu K^\mu \frac{\omega_{ji}}{\omega + \omega_{ji} + i\epsilon}\right]. \quad (6.A.15)$$

Let us now explicitly consider the real part in Eq. (6.A.15)

$$\begin{aligned} E_{abs}(\omega) = \frac{1}{\pi} \lim_{\epsilon\to 0^+} \sum_{i,j=i}^{+\infty} \Bigg[& \mathrm{Re}(c_i^* c_j) d_{ij}^\mu K^\mu \omega_{ji} \,\mathrm{Re}\left(\frac{1}{\omega - \omega_{ji} + i\epsilon}\right) \\ & - \mathrm{Re}(c_i c_j^*) d_{ij}^\mu K^\mu \omega_{ji} \,\mathrm{Re}\left(\frac{1}{\omega + \omega_{ji} + i\epsilon}\right) - \mathrm{Im}(c_i^* c_j) d_{ij}^\mu K^\mu \omega_{ji} \,\mathrm{Im}\left(\frac{1}{\omega - \omega_{ji} + i\epsilon}\right) \\ & + \mathrm{Im}(c_i c_j^*) d_{ij}^\mu K^\mu \omega_{ji} \,\mathrm{Im}\left(\frac{1}{\omega + \omega_{ji} + i\epsilon}\right)\Bigg]. \end{aligned} \quad (6.A.16)$$

In the following we will use the following identities:

$$\mathrm{Re}(c_i c_j^*) = \mathrm{Re}(c_i^* c_j), \quad (6.A.17)$$

$$\mathrm{Im}(c_i c_j^*) = -\mathrm{Im}(c_i^* c_j), \quad (6.A.18)$$

$$\mathrm{Re}\left(\frac{1}{\omega \pm \omega_{ji} + i\epsilon}\right) = \frac{(\omega \pm \omega_{ji})}{(\omega \pm \omega_{ji})^2 + \epsilon^2}, \quad (6.A.19)$$

$$\mathrm{Im}\left(\frac{1}{\omega \pm \omega_{ji} + i\epsilon}\right) = -\frac{\epsilon}{(\omega \pm \omega_{ji})^2 + \epsilon^2}. \quad (6.A.20)$$

Substituting Eq.s (6.A.17)-(6.A.20) into Eq. (6.A.16), we have

$$\begin{aligned} E_{abs}(\omega) = \frac{1}{\pi} \lim_{\epsilon\to 0^+} \sum_{i,j>i} \Bigg[& \mathrm{Re}(c_i^* c_j) d_{ij}^\mu K^\mu \omega_{ji} \left(\frac{\omega - \omega_{ji}}{(\omega - \omega_{ji})^2 + \epsilon^2} - \frac{\omega + \omega_{ji}}{(\omega + \omega_{ji})^2 + \epsilon^2}\right) \\ & + \mathrm{Im}(c_i^* c_j) d_{ij}^\mu K^\mu \omega_{ji} \left(\frac{\epsilon}{(\omega - \omega_{ji})^2 + \epsilon^2} - \frac{\epsilon}{(\omega + \omega_{ji})^2 + \epsilon^2}\right)\Bigg]. \end{aligned} \quad (6.A.21)$$

The second term in the right hand side of Eq. (6.A.21) contains the difference of two Lorentzians, that become Dirac deltas in the limit $\epsilon \to 0^+$

$$\lim_{\epsilon\to 0^+} \frac{1}{\pi} \frac{\epsilon}{(\omega_{ji} \pm \omega)^2 + \epsilon^2} = \delta(\omega_{ji} \pm \omega). \quad (6.A.22)$$

We note that $\omega_{ji} > 0$, as $j > i$. Thus, in $\delta(\omega_{ji} - \omega)$ resonances are located at $\omega > 0$, while in $\delta(\omega_{ji} + \omega)$ resonances are located at $\omega < 0$. We are interested in $E_{abs}(\omega)$ for $\omega > 0$, as the contribution coming from negative frequencies was already included by taking the imaginary part part [see the derivation of $\sigma(\omega)$ in the main section]. Thus, we may remove the resonances at negative frequencies and write

$$E_{abs}(\omega) = \sum_{i,j>i} \left[\lim_{\epsilon \to 0^+} \mathrm{Re}(c_i^* c_j) d_{ij}^{\mu} K^{\mu} \left(\frac{\omega_{ji}(\omega - \omega_{ji})}{(\omega - \omega_{ji})^2 + \epsilon^2} - \frac{\omega_{ji}(\omega + \omega_{ji})}{(\omega + \omega_{ji})^2 + \epsilon^2} \right) + \mathrm{Im}(c_i^* c_j) d_{ij}^{\mu} K^{\mu} \omega_{ji} \delta(\omega_{ji} - \omega) \right] . \quad (6.A.23)$$

Let us now explicitly calculate the real part of the product $c_i^* c_j$. By using the expression of the c_i coefficients in Eq. (6.1.18), we write

$$\mathrm{Re}(c_i^* c_j) = \langle \Psi_0 | \cos\left(\hat{d}^{\mu} K^{\mu}\right) | \Psi_i \rangle \langle \Psi_j | \cos\left(\hat{d}^{\mu} K^{\mu}\right) | \Psi_0 \rangle + \langle \Psi_0 | \sin\left(\hat{d}^{\mu} K^{\mu}\right) | \Psi_i \rangle \langle \Psi_j | \sin\left(\hat{d}^{\mu} K^{\mu}\right) | \Psi_0 \rangle , \quad (6.A.24)$$

$$\mathrm{Im}(c_i^* c_j) = \langle \Psi_0 | \cos\left(\hat{d}^{\mu} K^{\mu}\right) | \Psi_i \rangle \langle \Psi_j | \sin\left(\hat{d}^{\mu} K^{\mu}\right) | \Psi_0 \rangle - \langle \Psi_0 | \sin\left(\hat{d}^{\mu} K^{\mu}\right) | \Psi_i \rangle \langle \Psi_j | \cos\left(\hat{d}^{\mu} K^{\mu}\right) | \Psi_0 \rangle . \quad (6.A.25)$$

We now suppose that the system is centrosymmetric. In this case, the eigenstates $\{\Psi_i\}$ show *gerade* or *ungerade* parity under inversion of the coordinates. Let us indicate the parity of the wavefunction with the following notation: $\Psi_i = \Psi_i^{g_i}$, where $g_i = g$ means that the wavefunction is even under inversion of the coordinates and $g_i = u$ the opposite. For such a system, the following matrix elements

$$\langle \Psi_0 | \cos\left(\hat{d}^{\mu} K^{\mu}\right) | \Psi_i \rangle \neq 0 \quad \text{if} \quad g_0 = g_i, \quad (6.A.26)$$

$$\langle \Psi_0 | \sin\left(\hat{d}^{\mu} K^{\mu}\right) | \Psi_i \rangle \neq 0 \quad \text{if} \quad g_0 \neq g_i, \quad (6.A.27)$$

$$\langle \Psi_0 | \hat{d}^{\mu} K^{\mu} | \Psi_i \rangle \neq 0 \quad \text{if} \quad g_0 \neq g_i. \quad (6.A.28)$$

Looking at the first term in the right hand side of Eq. (6.A.23), where the real part of the coefficients is expressed through Eq. (6.A.24), we construct the selection rules from a combination of the conditions in Eq. (6.A.26), (6.A.27) and (6.A.28)

$$\langle \Psi_0 | \cos\left(\hat{d}^{\mu} K^{\mu}\right) | \Psi_i \rangle \langle \Psi_i | \hat{d}^{\mu} K^{\mu} | \Psi_j \rangle \langle \Psi_j | \cos\left(\hat{d}^{\mu} K^{\mu}\right) | \Psi_0 \rangle \neq 0 \quad \text{if} \quad g_0 = g_i, g_i \neq g_j, g_j = g_0$$

$$\langle \Psi_0 | \sin\left(\hat{d}^{\mu} K^{\mu}\right) | \Psi_i \rangle \langle \Psi_i | \hat{d}^{\mu} K^{\mu} | \Psi_j \rangle \langle \Psi_j | \sin\left(\hat{d}^{\mu} K^{\mu}\right) | \Psi_0 \rangle . \neq 0 \quad \text{if} \quad g_0 \neq g_i, g_i \neq g_j, g_j \neq g_0$$

There are no possible combinations of *gerade* and *ungerade* wavefunctions that result in matrix elements different from zero. Thus, if the system is centrosymmetric, $\mathrm{Re}(c_i^* c_j) = 0$ and

$$E_{abs}(\omega) = \sum_{i,j>i} \left[\mathrm{Im}(c_i^* c_j) d_{ij}^{\mu} K^{\mu} \omega_{ji} \delta(\omega_{ji} - \omega) \right] . \quad (6.A.29)$$

By substituting Eq. (6.A.25) into Eq. (6.A.29), we have

$$E_{abs}(\omega) = \sum_{i,j>i} \Big[\langle\Psi_0|\cos\left(\hat{d}^\mu K^\mu\right)|\Psi_i\rangle \ \langle\Psi_i|\hat{d}^\mu K^\mu|\Psi_j\rangle \ \langle\Psi_j|\sin\left(\hat{d}^\mu K^\mu\right)|\Psi_0\rangle$$
$$- \ \langle\Psi_0|\sin\left(\hat{d}^\mu K^\mu\right)|\Psi_i\rangle \ \langle\Psi_i|\hat{d}^\mu K^\mu|\Psi_j\rangle \ \langle\Psi_j|\cos\left(\hat{d}^\mu K^\mu\right)|\Psi_0\rangle\Big] \ \omega_{ji}\delta(\omega_{ji}-\omega). \quad (6.A.30)$$

Finally, we substitute the absorbed energy per unit frequency $E_{abs}(\omega)$ and $I_{in}(\omega) = c/4\pi^2|K|^2$ into the definition of the absorption cross section [see Eq. (6.1.14)

$$\sigma(\omega) = \frac{E_{abs}(\omega)}{I_{in}(\omega)} = \frac{4\pi^2}{c|K|^2} \sum_{i,j>i} \Big[\langle\Psi_0|\cos\left(\hat{d}^\mu K^\mu\right)|\Psi_i\rangle \ \langle\Psi_i|\hat{d}^\mu K^\mu|\Psi_j\rangle \ \langle\Psi_j|\sin\left(\hat{d}^\mu K^\mu\right)|\Psi_0\rangle$$
$$- \ \langle\Psi_0|\sin\left(\hat{d}^\mu K^\mu\right)|\Psi_i\rangle \ \langle\Psi_i|\hat{d}^\mu K^\mu|\Psi_j\rangle \ \langle\Psi_j|\cos\left(\hat{d}^\mu K^\mu\right)|\Psi_0\rangle\Big] \ \omega_{ji}\delta(\omega_{ji}-\omega). \quad (6.A.31)$$

Chapter 7

Concluding remarks

In this Ph.D. thesis, I have investigated new strategies for the calculation of charged and neutral excitations within density-functional approaches. I have presented three new contributions.

First, I have shown how to obtain the fundamental gap of low-dimensional quantum dots with good accuracy at the computational cost of just one self-consistent calculation. This procedure involves the evaluation of the discontinuity of the exchange potential – expressed within the optimized effective method – with quantities obtained from a ground-state calculation at the level of the local-density approximation. This method has been applied to harmonic quantum dots with different electron numbers and strengths of confinement. In the exchange-only limit, the comparison with the Krieger-Li-Iafrate approximation is remarkably good, with a mean relative absolute error of 4%. A straightforward inclusion of correlation leads to a mean relative absolute error of 14% in comparison with benchmark results from exact diagonalization.
It would be interesting to explore if our conclusions can apply also to other classes of confined nanostructures with experimental relevance, such as two-dimensional quantum rings or three-dimensional parabolically confined quantum dots (Hooke atoms).
In addition, the proposed method can be generalized to explicitly include also the discontinuity of the correlation potential. This can be done by replacing the exact-exchange approximation with an orbital functional approximation that explicitly includes correlation, e.g., through the fluctuation-dissipation theorem. This procedure should increase accuracy when correlation effects become important, i.e., at low number of trapped electrons and low confinement strengths.

Second, I have constructed an exchange-correlation potential approximation in the spirit of the GLLB [145] and GLLB-SC [144] potentials for two-dimensional systems. The newly created 2DGLLB potential shows a non-vanishing contribution for the exchange-correlation correction to the Kohn-Sham gap – derived in the first-part of this work – both for finite and periodic two-dimensional systems. Thus, the 2DGLLB approximation can be usefully employed for the description of the fundamental gap in low-dimensional nanostructures. Although the procedure involves single-particle orbitals, the computational cost is comparable with the cost of standard DFT calculations. I started by applying the 2DGLLB approximation in the evaluation of the fundamental gap of the same two-dimensional quantum dots considered in the first part of this PhD thesis, in the exchange-only limit. The results

are very close to the KLI benchmark, with a mean relative absolute error of 3%. Next, I have considered the case of artificial graphene, to which a Kekulé distortion has been applied in order to open a finite band gap at Dirac points. The correction to the Kohn-Sham gap given by the 2DGLLB approximation greatly affects the conduction band with respect to 2DLDA results, which shows instead a vanishing gap correction. The 2DGLLB fundamental gap is approximately 4 times lager than that of the 2DLDA. This is consistent with results obtained in the literature for three-dimensional periodic systems.
For three-dimensional semiconductor solids the GLLB-SC potential gives similar results for the fundamental gap than the accurate GW approximation. It would be interesting to investigate if the same happens for two-dimensional nanostructures; however, to the best of our knowledge, GW approaches have not yet been yet applied to two-dimensional artificial graphene.

The results of the first and second parts make possible the accurate calculation of the fundamental gap of two-dimensional nanostructures at a low computational cost, both for finite and periodic systems, in a unified framework.

In the third part, I have considered neutral excitations and studied the optical absorption properties of a many-electron system subject to an *impulsive* electric field beyond the perturbative regime, i.e. for arbitrary incoming field intensities. I have shown that the corresponding absorption cross section in the nonlinear regime has absorption terms coming from excited states. Excited-state absorption allows to populate states which cannot be reached in the linear regime starting from the ground state. Thus, the study of the nonlinear absorption cross section can give information about excited-state properties which are not accessible through the analysis of the absorption cross section in the linear regime.
As an example, I have considered the linear and nonlinear absorption cross sections of a 1D model system composed by two interacting electrons trapped in a 1D potential well with infinite walls. The study of the excitations included in the cross sections reveals that *gerade* excited states, which are dark in the linear regime, are populated in the nonlinear regime due to excited-state absorption.
As an outlook of this work, the proposed analytical scheme may be used to provide information for real-time TDDFT applications concerning nonlinear optical properties. For example, Cocchi *et al.* [172] have investigated the optical limiting behavior of macrocyclic molecules by applying increasing electric field impulses by means of TDDFT methods. Thus, our conclusions directly applies to the cross sections obtained numerically in Ref. [172]. Furthermore, our numerically exact calculations on model systems may provide benchmark results to investigate limitations in actual applications either to numerical problems or functional approximations.
In addition, it is known from the literature that optical limiting phenomena involve excitations of triplet states. Along this line, contributions of the nonlinear triplet excitation energies may be computed by extending the proposed analysis to external impulses which are spin-dependent.

Bibliography

[1] R. M. Martin, L. Reining, and D. M. Ceperley, *Interacting Electrons: Theory and Computational Approaches*. Cambridge University Press, 2016.

[2] W. M. C. Foulkes, L. Mitas, R. J. Needs, and G. Rajagopal, "Quantum monte carlo simulations of solids," *Rev. Mod. Phys.*, vol. 73, pp. 33–83, 2001.

[3] W. G. Aulbur, L. Jnsson, and J. W. Wilkins, "Quasiparticle calculations in solids," in *Solid State Physics* (H. Ehrenreich and F. Spaepen, eds.), vol. 54, pp. 1 – 218, Academic Press, 2000.

[4] A. Georges, G. Kotliar, W. Krauth, and M. J. Rozenberg, "Dynamical mean-field theory of strongly correlated fermion systems and the limit of infinite dimensions," *Rev. Mod. Phys.*, vol. 68, pp. 13–125, 1996.

[5] M. D. Reiner and E. K. U. Gross, *Density functional theory. An approach to the quantum many-body problem*. Reading, MA: Addison-Wesley, 1994.

[6] R. Parr and W. Yang, *Density-Functional Theory of Atoms and Molecules*. International Series of Monographs on Chemistry, Oxford University Press, USA, 1994.

[7] J. Kohanoff, *Electronic structure calculations for solids and molecules: theory and computational methods*. Cambridge: Cambridge University Press, 2006.

[8] E. Engel and R. M. Dreizler, *Density functional theory: an advanced course*. Berlin: Springer Science & Business Media, 2011.

[9] C. Fiolhais, F. Nogueira, and M. Marques, *A Primer in Density Functional Theory*. Lecture Notes in Physics, Springer, Berlin, 2008.

[10] M. A. Marques, N. T. Maitra, F. M. Nogueira, E. K. U. Gross, and A. Rubio, *Fundamentals of Time-Dependent Density Functional Theory*. Lecture Notes in Physics book series, Springer, Berlin, Heidelberg, 2012.

[11] C. A. Ullrich, *Time-dependent density-functional theory: concepts and applications*. Oxford: Oxford University Press, 2011.

[12] A. J. Cohen, P. Mori-Snchez, and W. Yang, "Challenges for density functional theory," *Chem. Rev.*, vol. 112, no. 1, pp. 289–320, 2012.

[13] N. Q. Su and X. Xu, "Development of new density functional approximations," *Annu. Rev. Phys. Chem.*, vol. 68, no. 1, pp. 155–182, 2017.

[14] T. Gould and S. Pittalis, "Density-driven correlations in many-electron ensembles: Theory and application for excited states," *Phys. Rev. Lett.*, vol. 123, p. 016401, 2019.

[15] S. Huefner, *Photoemission Spectroscopy: Principles and Applictions.* Springer-Verlag, Berlin, 2003.

[16] M. Cardona and L. Ley, *Photoemission in Solids I.* Springer-Verlag, Berlin, 1992.

[17] J. W. Rabalais, *Principles of ultraviolet photoelectron spectroscopy.* New York: Wiley, 1977.

[18] E. Illenberger and J. Momigny, *Photoemission in Solids I.* Springer-Verlag, Berlin, 1978.

[19] I. V. Hertel and W. Radloff, "Ultrafast dynamics in isolated molecules and molecular clusters," *Rep. Prog. Phys.*, vol. 69, no. 6, pp. 1897–2003, 2006.

[20] F. Krausz and M. Ivanov, "Attosecond physics," *Rev. Mod. Phys.*, vol. 81, pp. 163–234, 2009.

[21] R. W. Boyd, *Nonlinear Optics, Third Edition.* Orlando, FL, USA: Academic Press, Inc., 3rd ed., 2008.

[22] M. S. Kodikara, R. Stranger, and M. G. Humphrey, "Computational studies of the nonlinear optical properties of organometallic complexes," *Coord. Chem. Rev.*, vol. 375, pp. 389–409, 2018.

[23] V. Fock, "Näherungsmethode zur lösung des quantenmechanischen mehrkörperproblems," *Z. Phys.*, vol. 61, no. 1, pp. 126–148, 1930.

[24] J. C. Slater, "Note on Hartree's method," *Phys. Rev.*, vol. 35, pp. 210–211, 1930.

[25] P. Hohenberg and W. Kohn, "Inhomogeneous electron gas," *Phys. Rev.*, vol. 136, pp. B864–B871, 1964.

[26] G. R. Stewart, "Heavy-fermion systems," *Rev. Mod. Phys.*, vol. 56, pp. 755–787, 1984.

[27] W. Jones and N. H. March, *Theoretical solid state physics, Vol. I.* John Wiley and Sons, New York, 1976.

[28] M. Levy, "Electron densities in search of Hamiltonians," *Phys. Rev. A*, vol. 26, pp. 1200–1208, Sep 1982.

[29] M. Levy, "Universal variational functionals of electron densities, first-order density matrices, and natural spin-orbitals and solution of the v-representability problem," *Proc. Natl. Acad. Sci.*, vol. 76, no. 12, pp. 6062–6065, 1979.

[30] E. H. Lieb, "Density functionals for Coulomb systems," *Int. J. Quantum Chem.*, vol. 24, no. 3, pp. 243–277, 1983.

[31] T. L. Gilbert, "Hohenberg-Kohn theorem for nonlocal external potentials," *Phys. Rev. B*, vol. 12, pp. 2111–2120, 1975.

[32] W. Kohn and L. J. Sham, "Self-consistent equations including exchange and correlation effects," *Phys. Rev.*, vol. 140, pp. A1133–A1138, 1965.

[33] J. T. Chayes, L. Chayes, and M. B. Ruskai, "Density functional approach to quantum lattice systems," *J. Stat. Phys.*, vol. 38, no. 3, pp. 497–518, 1985.

[34] P. E. Lammert, "Well-behaved coarse-grained model of density-functional theory," *Phys. Rev. A*, vol. 82, p. 012109, 2010.

[35] S. Kvaal, U. Ekstrm, A. M. Teale, and T. Helgaker, "Differentiable but exact formulation of density-functional theory," *J. Chem. Phys.*, vol. 140, no. 18, p. 18A518, 2014.

[36] D. M. Ceperley and B. J. Alder, "Ground state of the electron gas by a stochastic method," *Phys. Rev. Lett.*, vol. 45, pp. 566–569, 1980.

[37] J. P. Perdew and S. Kurth, *Density Functionals for Non-relativistic Coulomb Systems in the New Century.* Springer, Berlin, Heidelberg, 2003. In: Fiolhais C., Nogueira F., Marques M.A.L. (eds) A Primer in Density Functional Theory. Lecture Notes in Physics, vol 620. .

[38] A. D. Becke, "Density-functional exchange-energy approximation with correct asymptotic behavior," *Phys. Rev. A*, vol. 38, no. 6, pp. 3098–3100, 1988.

[39] J. P. Perdew and Y. Wang, "Accurate and simple analytic representation of the electron-gas correlation energy," *Phys. Rev. B*, vol. 45, pp. 13244–13249, 1992.

[40] J. P. Perdew, K. Burke, and M. Ernzerhof, "Generalized gradient approximation made simple," *Phys. Rev. Lett.*, vol. 77, pp. 3865–3868, 1996.

[41] C. Lee, W. Yang, and R. G. Parr, "Development of the Colle-Salvetti correlation-energy formula into a functional of the electron density," *Phys. Rev. B*, vol. 37, no. 2, pp. 785–789, 1988.

[42] A. D. Becke, "Density-functional thermochemistry. III. the role of exact exchange," *J. Chem. Phys.*, vol. 98, no. 7, p. 5648, 1993.

[43] P. J. Stephens, F. J. Devlin, C. F. Chabalowski, and M. J. Frisch, "*Ab Initio* calculation of vibrational absorption and circular dichroism spectra using density functional force fields," *J. Phys. Chem.*, vol. 98, no. 45, pp. 11623–11627, 1994.

[44] R. Sharp and G. Horton, "A variational approach to the unipotential many-electron problem," *Phys. Rev. A*, vol. 90, p. 317, 1953.

[45] J. D. Talman and W. F. Shadwick, "Optimized effective atomic central potential," *Phys. Rev. A*, vol. 14, no. 1, p. 36, 1976.

[46] S. Kümmel and L. Kronik, "Orbital-dependent density functionals: Theory and applications," *Rev. Mod. Phys.*, vol. 80, no. 1, pp. 3–60, 2008.

[47] J. B. Krieger, Y. Li, and G. J. Iafrate, "Construction and application of an accurate local spin-polarized Kohn-Sham potential with integer discontinuity: Exchange-only theory," *Phys. Rev. A*, vol. 45, no. 1, pp. 101–126, 1992.

[48] O. Gritsenko, R. van Leeuwen, E. van Lenthe, and E. J. Baerends, "Self-consistent approximation to the Kohn-Sham exchange potential," *Phys. Rev. A*, vol. 51, no. 3, p. 1944, 1995.

[49] J. P. Perdew, R. G. Parr, M. Levy, and J. L. Balduz, "Density-functional theory for fractional particle number: Derivative discontinuities of the energy," *Phys. Rev. Lett.*, vol. 49, pp. 1691–1694, 1982.

[50] J. P. Perdew and M. Levy, "Physical content of the exact Kohn-Sham orbital energies: Band gaps and derivative discontinuities," *Phys. Rev. Lett.*, vol. 51, pp. 1884–1887, 1983.

[51] L. J. Sham and M. Schlüter, "Density-functional theory of the band gap," *Phys. Rev. B*, vol. 32, pp. 3883–3889, 1985.

[52] E. Kraisler and L. Kronik, "Fundamental gaps with approximate density functionals: The derivative discontinuity revealed from ensemble considerations," *J. Chem. Phys.*, vol. 140, no. 18, p. 18A540, 2014.

[53] E. Runge and E. K. U. Gross, "Density-functional theory for time-dependent systems," *Phys. Rev. Lett.*, vol. 52, pp. 997–1000, 1984.

[54] S. Botti, A. Schindlmayr, R. D. Sole, and L. Reining, "Time-dependent density-functional theory for extended systems," *Rep. Prog. Phys.*, vol. 70, no. 3, pp. 357–407, 2007.

[55] N. T. Maitra, I. Souza, and K. Burke, "Current-density functional theory of the response of solids," *Phys. Rev. B*, vol. 68, p. 045109, 2003.

[56] G. Vignale, "Mapping from current densities to vector potentials in time-dependent current density functional theory," *Phys. Rev. B*, vol. 70, p. 201102, 2004.

[57] R. van Leeuwen, "Mapping from densities to potentials in time-dependent density-functional theory," *Phys. Rev. Lett.*, vol. 82, pp. 3863–3866, 1999.

[58] N. T. Maitra, T. N. Todorov, C. Woodward, and K. Burke, "Density-potential mapping in time-dependent density-functional theory," *Phys. Rev. A*, vol. 81, p. 042525, 2010.

[59] M. Ruggenthaler, M. Penz, and R. van Leeuwen, "Existence, uniqueness, and construction of the density-potential mapping in time-dependent density-functional theory," *J. of Phys. Condens. Matter*, vol. 27, no. 20, p. 203202, 2015.

[60] N. T. Maitra, K. Burke, and C. Woodward, "Memory in time-dependent density functional theory," *Phys. Rev. Lett.*, vol. 89, p. 023002, 2002.

[61] K. Yabana and G. F. Bertsch, "Time-dependent local-density approximation in real time," *Phys. Rev. B*, vol. 54, pp. 4484–4487, 1996.

[62] M. E. Casida, *Time-Dependent Density Functional Response Theory for Molecules*, pp. 155–192. World Scientific, 1995.

[63] S. M. Reimann and M. Manninen, "Electronic structure of quantum dots," *Rev. Mod. Phys.*, vol. 74, pp. 1283–1342, 2002.

[64] L. P. Kouwenhoven, D. G. Austing, and S. Tarucha, "Few-electron quantum dots," *Rep. Prog. Phys.*, vol. 64, no. 6, pp. 701–736, 2001.

[65] Y. Meir, N. S. Wingreen, and P. A. Lee, "Transport through a strongly interacting electron system: Theory of periodic conductance oscillations," *Phys. Rev. Lett.*, vol. 66, pp. 3048–3051, 1991.

[66] A. Guandalini, C. A. Rozzi, E. Räsänen, and S. Pittalis, "Fundamental gaps of quantum dots on the cheap," *Phys. Rev. B*, vol. 99, p. 125140, 2019.

[67] M. Levy, J. P. Perdew, and V. Sahni, "Exact differential equation for the density and ionization energy of a many-particle system," *Phys. Rev. A*, vol. 30, pp. 2745–2748, 1984.

[68] C. O. Almbladh and A. C. Pedroza, "Density-functional exchange-correlation potentials and orbital eigenvalues for light atoms," *Phys. Rev. A*, vol. 29, pp. 2322–2330, 1984.

[69] C. O. Almbladh and U. von Barth, "Exact results for the charge and spin densities, exchange-correlation potentials, and density-functional eigenvalues," *Phys. Rev. B*, vol. 31, pp. 3231–3244, 1985.

[70] J. P. Perdew and M. Levy, "Comment on "significance of the highest occupied Kohn-Sham eigenvalue"," *Phys. Rev. B*, vol. 56, pp. 16021–16028, 1997.

[71] T. Gould and J. Toulouse, "Kohn-Sham potentials in exact density-functional theory at noninteger electron numbers," *Phys. Rev. A*, vol. 90, p. 050502, 2014.

[72] T. Gould and J. F. Dobson, "The flexible nature of exchange, correlation, and Hartree physics: Resolving "delocalization errors" in a "correlation free" density functional," *J. Chem. Phys.*, vol. 138, no. 1, p. 014103, 2013.

[73] E. Kraisler and L. Kronik, "Piecewise linearity of approximate density functionals revisited: Implications for frontier orbital energies," *Phys. Rev. Lett.*, vol. 110, p. 126403, 2013.

[74] M. Levy and F. Zahariev, "Ground-state energy as a simple sum of orbital energies in Kohn-Sham theory: A shift in perspective through a shift in potential," *Phys. Rev. Lett.*, vol. 113, p. 113002, 2014.

[75] B. Senjean and E. Fromager, "Unified formulation of fundamental and optical gap problems in density-functional theory for ensembles," *Phys. Rev. A*, vol. 98, p. 022513, 2018.

[76] K. Capelle, M. Borgh, K. Kärkkäinen, and S. M. Reimann, "Energy gaps and interaction blockade in confined quantum systems," *Phys. Rev. Lett.*, vol. 99, p. 010402, 2007.

[77] R. W. Godby, M. Schlüter, and L. J. Sham, "Self-energy operators and exchange-correlation potentials in semiconductors," *Phys. Rev. B*, vol. 37, pp. 10159–10175, 1988.

[78] F. Aryasetiawan and O. Gunnarsson, "The GW method," *Rep. Prog. Phys.*, vol. 61, no. 3, p. 237, 1998.

[79] G. Onida, L. Reining, and A. Rubio, "Electronic excitations: density-functional versus many-body Green's-function approaches," *Rev. Mod. Phys.*, vol. 74, pp. 601–659, 2002.

[80] M. Grüning, A. Marini, and A. Rubio, "Density functionals from many-body perturbation theory: The band gap for semiconductors and insulators," *J. Chem. Phys.*, vol. 124, no. 15, p. 154108, 2006.

[81] A. Görling, "Exchange-correlation potentials with proper discontinuities for physically meaningful Kohn-Sham eigenvalues and band structures," *Phys. Rev. B*, vol. 91, p. 245120, 2015.

[82] M. Rontani, C. Cavazzoni, D. Bellucci, and G. Goldoni, "Full configuration interaction approach to the few-electron problem in artificial atoms," *J. of Chem. Phys.*, vol. 124, no. 12, p. 124102, 2006.

[83] V. U. Nazarov and G. Vignale, "Optics of semiconductors from meta-generalized-gradient-approximation-based time-dependent density-functional theory," *Phys. Rev. Lett.*, vol. 107, p. 216402, 2011.

[84] F. G. Eich and M. Hellgren, "Derivative discontinuity and exchange-correlation potential of meta-GGAs in density-functional theory," *J. Chem. Phys.*, vol. 141, no. 22, p. 224107, 2014.

[85] Z. H. Yang, H. Peng, J. Sun, and J. P. Perdew, "More realistic band gaps from meta-generalized gradient approximations: Only in a generalized Kohn-Sham scheme," *Phys. Rev. B*, vol. 93, p. 205205, 2016.

[86] O. Gritsenko, R. van Leeuwen, E. van Lenthe, and E. J. Baerends, "Self-consistent approximation to the Kohn-Sham exchange potential," *Phys. Rev. A*, vol. 51, pp. 1944–1954, 1995.

[87] A. D. Becke and E. R. Johnson, "A simple effective potential for exchange," *J. Chem. Phys.*, vol. 124, no. 22, p. 221101, 2006.

[88] F. Tran and P. Blaha, "Accurate band gaps of semiconductors and insulators with a semilocal exchange-correlation potential," *Phys. Rev. Lett.*, vol. 102, p. 226401, 2009.

[89] M. Kuisma, J. Ojanen, J. Enkovaara, and T. T. Rantala, "Kohn-Sham potential with discontinuity for band gap materials," *Phys. Rev. B*, vol. 82, p. 115106, 2010.

[90] H. Jiang, "Band gaps from the Tran-Blaha modified Becke-Johnson approach: A systematic investigation," *J. Chem. Phys.*, vol. 138, no. 13, p. 134115, 2013.

[91] R. Armiento and S. Kümmel, "Orbital localization, charge transfer, and band gaps in semilocal density-functional theory," *Phys. Rev. Lett.*, vol. 111, p. 036402, 2013.

[92] T. F. T. Cerqueira, M. J. T. Oliveira, and M. A. L. Marques, "Benchmarking the AK13 exchange functional: Ionization potentials and electron affinities," *J. Chem. Theory Comput.*, vol. 10, no. 12, pp. 5625–5629, 2014.

[93] I. E. Castelli, T. Olsen, S. Datta, D. D. Landis, S. Dahl, K. S. Thygesen, and K. W. Jacobsen, "Computational screening of perovskite metal oxides for optimal solar light capture," *Energy Environ. Sci.*, vol. 5, pp. 5814–5819, 2012.

[94] J. Heyd, G. E. Scuseria, and M. Ernzerhof, "Hybrid functionals based on a screened Coulomb potential," *J. Chem. Phys.*, vol. 118, no. 18, pp. 8207–8215, 2003.

[95] J. Heyd, G. E. Scuseria, and M. Ernzerhof, "Erratum: "Hybrid functionals based on a screened Coulomb potential" [J. Chem. Phys. 118, 8207 (2003)]," *J. Chem. Phys.*, vol. 124, no. 21, p. 219906, 2006.

[96] T. Stein, H. Eisenberg, L. Kronik, and R. Baer, "Fundamental gaps in finite systems from eigenvalues of a generalized Kohn-Sham method," *Phys. Rev. Lett.*, vol. 105, p. 266802, 2010.

[97] L. Kronik, T. Stein, S. Refaely-Abramson, and R. Baer, "Excitation gaps of finite-sized systems from optimally tuned range-separated hybrid functionals," *J. Chem. Theory Comput.*, vol. 8, no. 5, pp. 1515–1531, 2012.

[98] C. Franchini, "Hybrid functionals applied to perovskites," *J. Phys. Condens. Matter*, vol. 26, no. 25, p. 253202, 2014.

[99] J. P. Perdew, W. Yang, K. Burke, Z. Yang, E. K. U. Gross, M. Scheffler, G. E. Scuseria, T. M. Henderson, I. Y. Zhang, A. Ruzsinszky, H. Peng, J. Sun, E. Trushin, and A. Görling, "Understanding band gaps of solids in generalized Kohn-Sham theory," *PNAS*, vol. 114, no. 11, pp. 2801–2806, 2017.

[100] J.-D. Chai and P.-T. Chen, "Restoration of the derivative discontinuity in Kohn-Sham density functional theory: An efficient scheme for energy gap correction," *Phys. Rev. Lett.*, vol. 110, p. 033002, 2013.

[101] E. J. Baerends, "From the Kohn-Sham band gap to the fundamental gap in solids. An integer electron approach," *Phys. Chem. Chem. Phys.*, vol. 19, pp. 15639–15656, 2017.

[102] U. von Barth and L. Hedin, "A local exchange-correlation potential for the spin polarized case. I," *J. Phys. C*, vol. 5, no. 13, p. 1629, 1972.

[103] J. P. Perdew, *What do the Kohn-Sham Orbital Energies Mean? How do Atoms Dissociate?*, pp. 265–308. Boston, MA: Springer US, 1985.

[104] A. Görling and M. Levy, "Hardness of molecules and the band gap of solids within the Kohn-Sham formalism: A perturbation-scaling approach," *Phys. Rev. A*, vol. 52, pp. 4493–4499, 1995.

[105] R. T. Sharp and G. K. Horton, "A variational approach to the unipotential many-electron problem," *Phys. Rev.*, vol. 90, pp. 317–317, 1953.

[106] J. D. Talman and W. F. Shadwick, "Optimized effective atomic central potential," *Phys. Rev. A*, vol. 14, pp. 36–40, 1976.

[107] T. Grabo and E. Gross, "Density-functional theory using an optimized exchange-correlation potential," *Chem. Phys. Lett.*, vol. 240, no. 1, pp. 141 – 150, 1995.

[108] T. Grabo, T. Kreibich, and E. K. U. Gross, *Optimized Effective Potential for Atoms and Molecules*, pp. 27–50. Dordrecht: Springer Netherlands, 1997.

[109] S. Kümmel and L. Kronik, "Orbital-dependent density functionals: Theory and applications," *Rev. Mod. Phys.*, vol. 80, pp. 3–60, 2008.

[110] J. Krieger, Y. Li, and G. Iafrate, "Derivation and application of an accurate Kohn-Sham potential with integer discontinuity," *Phys. Lett. A*, vol. 146, no. 5, pp. 256 – 260, 1990.

[111] J. B. Krieger, Y. Li, and G. J. Iafrate, "Construction and application of an accurate local spin-polarized Kohn-Sham potential with integer discontinuity: Exchange-only theory," *Phys. Rev. A*, vol. 45, pp. 101–126, 1992.

[112] S. Pittalis, E. Räsänen, N. Helbig, and E. K. U. Gross, "Exchange-energy functionals for finite two-dimensional systems," *Phys. Rev. B*, vol. 76, p. 235314, 2007.

[113] E. Räsänen, S. Pittalis, C. R. Proetto, and E. K. U. Gross, "Electronic exchange in quantum rings: Beyond the local-density approximation," *Phys. Rev. B*, vol. 79, p. 121305, 2009.

[114] A. K. Rajagopal and J. C. Kimball, "Correlations in a two-dimensional electron system," *Phys. Rev. B*, vol. 15, pp. 2819–2825, 1977.

[115] B. Tanatar and D. M. Ceperley, "Ground state of the two-dimensional electron gas," *Phys. Rev. B*, vol. 39, pp. 5005–5016, 1989.

[116] C. Attaccalite, S. Moroni, P. Gori-Giorgi, and G. B. Bachelet, "Correlation energy and spin polarization in the 2D electron gas," *Phys. Rev. Lett.*, vol. 88, p. 256601, 2002.

[117] Effective atomic units: effective Bohr length $a_0^* = (\epsilon/m^*)a_0$; effective Hartree energy $E_h^* = (m^*/\epsilon^2)E_h$.

[118] X. Andrade, D. Strubbe, U. De Giovannini, A. H. Larsen, M. J. T. Oliveira, J. Alberdi-Rodriguez, A. Varas, I. Theophilou, N. Helbig, M. J. Verstraete, L. Stella, F. Nogueira, A. Aspuru-Guzik, A. Castro, M. A. L. Marques, and A. Rubio, "Real-space grids and the Octopus code as tools for the development of new simulation approaches for electronic systems," *Phys. Chem. Chem. Phys.*, vol. 17, pp. 31371–31396, 2015.

[119] A. Castro, H. Appel, M. Oliveira, C. A. Rozzi, X. Andrade, F. Lorenzen, M. A. L. Marques, E. K. U. Gross, and A. Rubio, "Octopus: a tool for the application of time-dependent density functional theory," *Phys. status solidi B*, vol. 243, no. 11, pp. 2465–2488, 2006.

[120] M. A. Marques, A. Castro, G. F. Bertsch, and A. Rubio, "Octopus: a first-principles tool for excited electronion dynamics," *Comput. Phys. Commun.*, vol. 151, no. 1, pp. 60 – 78, 2003.

[121] F. Yuan, S. J. Novario, N. M. Parzuchowski, S. Reimann, S. K. Bogner, and M. Hjorth-Jensen, "Addition and removal energies of circular quantum dots," *J. Chem. Phys.*, vol. 147, no. 16, p. 164109, 2017.

[122] M. Polini, F. Guinea, M. Lewenstein, H. C. Manoharan, and V. Pellegrini, "Artificial honeycomb lattices for electrons, atoms and photons," *Nat. Nanotechnol.*, vol. 8, no. 11, p. 625, 2013.

[123] Y.-H. Kim, I.-H. Lee, S. Nagaraja, J.-P. Leburton, R. Q. Hood, and R. M. Martin, "Two-dimensional limit of exchange-correlation energy functional approximations," *Phys. Rev. B*, vol. 61, pp. 5202–5211, 2000.

[124] L. Pollack and J. P. Perdew, "Evaluating density functional performance for the quasi-two-dimensional electron gas," *J. Phys. Condens. Matter*, vol. 12, no. 7, pp. 1239–1252, 2000.

[125] S. Pittalis, E. Räsänen, and M. A. L. Marques, "Local correlation functional for electrons in two dimensions," *Phys. Rev. B*, vol. 78, p. 195322, 2008.

[126] S. Pittalis, E. Räsänen, J. G. Vilhena, and M. A. L. Marques, "Density gradients for the exchange energy of electrons in two dimensions," *Phys. Rev. A*, vol. 79, no. 1, p. 12503, 2009.

[127] S. Pittalis, E. Räsänen, C. R. Proetto, and E. K. U. Gross, "Correlation energy of finite two-dimensional systems: Toward nonempirical and universal modeling," *Phys. Rev. B*, vol. 79, no. 8, p. 85316, 2009.

[128] S. Pittalis, E. Räsänen, and E. K. U. Gross, "Gaussian approximations for the exchange-energy functional of current-carrying states: Applications to two-dimensional systems," *Phys. Rev. A*, vol. 80, p. 032515, 2009.

[129] S. Pittalis and E. Räsänen, "Orbital-free energy functional for electrons in two dimensions," *Phys. Rev. B*, vol. 80, p. 165112, 2009.

[130] E. Rsnen and S. Pittalis, "Exchange and correlation energy functionals for two-dimensional open-shell systems," *Physica E*, vol. 42, no. 4, pp. 1232 – 1235, 2010.

[131] S. Pittalis and E. Räsänen, "Laplacian-level density functionals for the exchange-correlation energy of low-dimensional nanostructures," *Phys. Rev. B*, vol. 82, no. 16, pp. 1–8, 2010.

[132] E. Räsänen, S. Pittalis, and C. R. Proetto, "Parameter-free density functional for the correlation energy in two dimensions," *Phys. Rev. B*, vol. 81, p. 195103, 2010.

[133] S. Pittalis and E. Räsänen, "Exchange-correlation potential with a proper long-range behavior for harmonically confined electron droplets," *Phys. Rev. B*, vol. 82, p. 195124, 2010.

[134] S. Pittalis, E. Räsänen, and C. R. Proetto, "Becke-Johnson-type exchange potential for two-dimensional systems," *Phys. Rev. B*, vol. 81, no. 11, pp. 1–7, 2010.

[135] J. G. Vilhena, E. Räsänen, M. A. L. Marques, and S. Pittalis, "Construction of the B88 exchange-energy functional in two dimensions," *J. Chem. Theory Comput.*, vol. 10, no. 5, pp. 1837–1842, 2014.

[136] S. Jana and P. Samal, "Exploration of near the origin and the asymptotic behaviors of the Kohn-Sham kinetic energy density for two-dimensional quantum dot systems with parabolic confinement," *J. Chem. Phys.*, vol. 148, no. 2, p. 024111, 2018.

[137] S. Jana and P. Samal, "Exploration of near the origin and the asymptotic behaviors of the Kohn-Sham kinetic energy density for two-dimensional quantum dot systems with parabolic confinement," *J. Chem. Phys.*, vol. 148, no. 2, p. 024111, 2018.

[138] A. Patra, S. Jana, and P. Samal, "A parameter-free semilocal exchange energy functional for two-dimensional quantum systems," *J. Phys. Chem. A*, vol. 122, no. 13, pp. 3455–3461, 2018.

[139] A. Patra and P. Samal, "Colle-Salvetti type correlation functionals for two-dimensional quantum dot systems," *Chem. Phys. Lett.*, vol. 720, pp. 70 – 75, 2019.

[140] A. Patra, S. Jana, and P. Samal, "Inhomogeneity induced and appropriately parameterized semilocal exchange and correlation energy functionals in two-dimensions," *J. Chem. Phys.*, vol. 148, no. 13, p. 134117, 2018.

[141] S. Jana and P. Samal, "Semilocal exchange energy functional for two-dimensional quantum systems: A step beyond generalized gradient approximations," *J. Phys. Chem. A*, vol. 121, no. 25, pp. 4804–4811, 2017.

[142] S. Jana, A. Patra, and P. Samal, "Gradient approximated exchange energy functionals with improved performances for two-dimensional quantum dot systems," *Physica E*, vol. 97, pp. 268 – 276, 2018.

[143] F. Tran, J. Doumont, L. Kalantari, A. W. Huran, M. A. L. Marques, and P. Blaha, "Semilocal exchange-correlation potentials for solid-state calculations: Current status and future directions," *J. Appl. Phys.*, vol. 126, no. 11, p. 110902, 2019.

[144] M. Kuisma, J. Ojanen, J. Enkovaara, and T. T. Rantala, "Kohn-Sham potential with discontinuity for band gap materials," *Phys. Rev. B*, vol. 82, no. 11, pp. 1–7, 2010.

[145] O. Gritsenko, R. van Leeuwen, E. Van Lenthe, and E. J. Baerends, "Self-consistent approximation to the Kohn-Sham exchange potential," *Phys. Rev. A*, vol. 51, no. 3, pp. 1944–1954, 1995.

[146] K. K. Gomes, W. Mar, W. Ko, F. Guinea, and H. C. Manoharan, "Designer Dirac fermions and topological phases in molecular graphene," *Nature*, vol. 483, pp. 306–310, 2012.

[147] L. Tarruell, D. Greif, T. Uehlinger, G. Jotzu, and T. Esslinger, "Creating, moving and merging Dirac points with a Fermi gas in a tunable honeycomb lattice," *Nature*, vol. 483, pp. 302–305, 2012.

[148] S. Paavilainen, M. Ropo, J. Nieminen, J. Akola, and E. Rsnen, "Coexisting honeycomb and Kagome characteristics in the electronic band structure of molecular graphene," *Nano Lett.*, vol. 16, no. 6, pp. 3519–3523, 2016.

[149] C.-H. Park and S. G. Louie, "Making massless Dirac fermions from a patterned two-dimensional electron gas," *Nano Lett.*, vol. 9, no. 5, pp. 1793–1797, 2009.

[150] M. Gibertini, A. Singha, V. Pellegrini, M. Polini, G. Vignale, A. Pinczuk, L. N. Pfeiffer, and K. W. West, "Engineering artificial graphene in a two-dimensional electron gas," *Phys. Rev. B*, vol. 79, p. 241406, 2009.

[151] A. Singha, M. Gibertini, B. Karmakar, S. Yuan, M. Polini, G. Vignale, M. I. Katsnelson, A. Pinczuk, L. N. Pfeiffer, K. W. West, and V. Pellegrini, "Two-dimensional Mott-Hubbard electrons in an artificial honeycomb lattice," *Science*, vol. 332, no. 6034, pp. 1176–1179, 2011.

[152] E. Räsänen, C. A. Rozzi, S. Pittalis, and G. Vignale, "Electron-electron interactions in artificial graphene," *Phys. Rev. Lett.*, vol. 108, no. 24, pp. 2–5, 2012.

[153] I. Kylänpä, F. Berardi, E. Räsänen, P. Garcìa-Gonzàlez, C. A. Rozzi, and A. Rubio, "Stability of the Dirac cone in artificial graphene formed in quantum wells: A computational many-electron study," *New J. Phys.*, vol. 18, no. 8, 2016.

[154] C. F. Hirjibehedin, A. Pinczuk, B. S. Dennis, L. N. Pfeiffer, and K. W. West, "Evidence of electron correlations in plasmon dispersions of ultralow density two-dimensional electron systems," *Phys. Rev. B*, vol. 65, p. 161309, 2002.

[155] C. F. Hirjibehedin, I. Dujovne, A. Pinczuk, B. S. Dennis, L. N. Pfeiffer, and K. W. West, "Splitting of long-wavelength modes of the fractional quantum hall liquid at $\nu = 1/3$," *Phys. Rev. Lett.*, vol. 95, p. 066803, 2005.

[156] C. P. García, V. Pellegrini, A. Pinczuk, M. Rontani, G. Goldoni, E. Molinari, B. S. Dennis, L. N. Pfeiffer, and K. W. West, "Evidence of correlation in spin excitations of few-electron quantum dots," *Phys. Rev. Lett.*, vol. 95, p. 266806, 2005.

[157] J. D. Pack and H. J. Monkhorst, ""Special points for Brillouin-zone integrations"—a reply," *Phys. Rev. B*, vol. 16, pp. 1748–1749, 1977.

[158] J. J. Goings, P. J. Lestrange, and X. Li, "Real-time time-dependent electronic structure theory," *Wiley Interdiscip. Rev. Comput. Mol. Sci.*, vol. 8, no. 1, pp. 1–19, 2018.

[159] Y. Takimoto, F. D. Vila, and J. J. Rehr, "Real-time time-dependent density functional theory approach for frequency-dependent nonlinear optical response in photonic molecules," *J. Chem. Phys.*, vol. 127, no. 15, 2007.

[160] C. Attaccalite and M. Grüning, "Nonlinear optics from an *ab initio* approach by means of the dynamical berry phase: Application to second- and third-harmonic generation in semiconductors," *Phys. Rev. B*, vol. 88, no. 23, pp. 1–10, 2013.

[161] M. Uemoto, Y. Kuwabara, S. A. Sato, and K. Yabana, "Nonlinear polarization evolution using time-dependent density functional theory," *J. Chem. Phys.*, vol. 150, no. 9, p. 094101, 2019.

[162] A. Castro, A. Rubio, and E. K. U. Gross, "Enhancing and controlling single-atom high-harmonic generation spectra: a time-dependent density-functional scheme," *Eur. Phys. J. B*, vol. 88, no. 8, p. 191, 2015.

[163] N. Tancogne-Dejean and A. Rubio, "Atomic-like high-harmonic generation from two-dimensional materials," *Sci. Adv.*, vol. 4, no. 2, 2018.

[164] U. De Giovannini, G. Brunetto, A. Castro, J. Walkenhorst, and A. Rubio, "Simulating pump-probe photoelectron and absorption spectroscopy on the attosecond timescale with time-dependent density functional theory," *ChemPhysChem*, vol. 14, no. 7, pp. 1363–1376, 2013.

[165] S. M. Falke, C. A. Rozzi, D. Brida, M. Maiuri, M. Amato, E. Sommer, A. De Sio, A. Rubio, G. Cerullo, E. Molinari, and C. Lienau, "Coherent ultrafast charge transfer in an organic photovoltaic blend," *Science*, vol. 344, no. 6187, pp. 1001–1005, 2014.

[166] S. Yamada, M. Noda, K. Nobusada, and K. Yabana, "Time-dependent density functional theory for interaction of ultrashort light pulse with thin materials," *Phys. Rev. B*, vol. 98, p. 245147, 2018.

[167] A. Yamada and K. Yabana, "Multiscale time-dependent density functional theory for a unified description of ultrafast dynamics: Pulsed light, electron, and lattice motions in crystalline solids," *Phys. Rev. B*, vol. 99, p. 245103, 2019.

[168] H. O. Wijewardane and C. A. Ullrich, "Real-time electron dynamics with exact-exchange time-dependent density-functional theory," *Phys. Rev. Lett.*, vol. 100, no. 5, pp. 1–4, 2008.

[169] D. Dini, M. J. Calvete, and M. Hanack, "Nonlinear optical materials for the smart filtering of optical radiation," *Chem. Rev.*, vol. 116, no. 22, pp. 13043–13233, 2016.

[170] Y.-P. Sun and J. E. Riggs, "Organic and inorganic optical limiting materials. From fullerenes to nanoparticles," *Int. Rev. Phys. Chem.*, vol. 18, no. 1, pp. 43–90, 1999.

[171] L. W. Tutt and T. F. Boggess, "A review of optical limiting mechanisms and devices using organics, fullerenes, semiconductors and other materials," *Prog. Quant. Electron.*, vol. 17, no. 4, pp. 299 – 338, 1993.

[172] C. Cocchi, D. Prezzi, A. Ruini, E. Molinari, and C. A. Rozzi, "*Ab initio* simulation of optical limiting: The case of metal-free phthalocyanine," *Phys. Rev. Lett.*, vol. 112, no. 19, pp. 1–5, 2014.

[173] J. D. Jackson, *Classical electrodynamics*. New York: Wiley, 3rd ed., 1999.

[174] E. Perfetto and G. Stefanucci, "Some exact properties of the nonequilibrium response function for transient photoabsorption," *Phys. Rev. A*, vol. 91, p. 033416, 2015.

[175] M. J. T. Oliveira, A. Castro, M. A. L. Marques, and A. Rubio, "On the use of Neumann's principle for the calculation of the polarizability tensor of nanostructures," *J. Nanosci. Nanotechnol.*, vol. 8, no. 7, pp. 3392–3398, 2008.

[176] M. Lein, E. K. U. Gross, and V. Engel, "On the mechanism of strong-field double photoionization in the helium atom," *J. Phys. B*, vol. 33, no. 3, pp. 433–442, 2000.

[177] J. I. Fuks, L. Lacombe, S. E. B. Nielsen, and N. T. Maitra, "Exploring non-adiabatic approximations to the exchangecorrelation functional of TDDFT," *Phys. Chem. Chem. Phys.*, vol. 20, pp. 26145–26160, 2018.

[178] P. Elliott and N. T. Maitra, "Propagation of initially excited states in time-dependent density-functional theory," *Phys. Rev. A*, vol. 85, no. 5, pp. 1–11, 2012.

[179] N. Helbig, J. Fuks, I. Tokatly, H. Appel, E. Gross, and A. Rubio, "Time-dependent density-functional and reduced density-matrix methods for few electrons: Exact versus adiabatic approximations," *Salud Uninorte*, vol. 29, no. 2, pp. 288–297, 2013.

[180] N. Helbig, J. I. Fuks, M. Casula, M. J. Verstraete, M. A. Marques, I. V. Tokatly, and A. Rubio, "Density functional theory beyond the linear regime: Validating an adiabatic local density approximation," *Phys. Rev. A*, vol. 83, no. 3, pp. 1–5, 2011.

[181] Q. Su and J. H. Eberly, "Model atom for multiphoton physics," *Phys. Rev. A*, vol. 44, pp. 5997–6008, 1991.

[182] X. Andrade, D. Strubbe, U. De Giovannini, A. H. Larsen, M. J. T. Oliveira, J. Alberdi-Rodriguez, A. Varas, I. Theophilou, N. Helbig, M. J. Verstraete, L. Stella, F. Nogueira, A. Aspuru-Guzik, A. Castro, M. A. L. Marques, and A. Rubio, "Real-space grids and the Octopus code as tools for the development of new simulation approaches for electronic systems," *Phys. Chem. Chem. Phys.*, vol. 17, pp. 31371–31396, 2015.

[183] A. Castro, H. Appel, M. Oliveira, C. A. Rozzi, X. Andrade, F. Lorenzen, M. A. L. Marques, E. K. U. Gross, and A. Rubio, "Octopus: a tool for the application of time-dependent density functional theory," *Phys. status solidi B*, vol. 243, no. 11, pp. 2465–2488, 2006.

[184] M. A. Marques, A. Castro, G. F. Bertsch, and A. Rubio, "Octopus: a first-principles tool for excited electronion dynamics," *Comput. Phys. Commun.*, vol. 151, no. 1, pp. 60 – 78, 2003.